COMPARATIVE ANALYSIS OF THE SELF- AND CO-ASSEMBLY OF TYPE-I AND TYPE-III COLLAGEN

A Dissertation

by

ESMA ERYILMAZ

Submitted to the Office of Graduate and Professional Studies of
Texas A&M University
in partial fulfillment of the requirements for the degree of

DOCTOR OF PHILOSOPHY

Chair of Committee,	Winfried Teizer
Committee Members,	Hans Schuessler
	Helmut G. Katzgraber
	Wonmuk Hwang
Head of Department,	George R. Welch

December 2015

Major Subject: Physics

ABSTRACT

Collagen represents the most abundant protein family in the human body which forms 30% of the total protein. Among different types, type-I and type-III are the two most abundant, respectively, in the heterotypic fibril structure. Although many tissues in the human body have a heterotypic form of co-assembled two or more types of collagens, not much is known concerning the heterotypic assembly of two or more types of collagens. Therefore, the purpose of this study is to investigate the characteristics of the co-assembly process of the two main types of collagen.

Collagen, which is a major component of an Extracellular Matrix (ECM) protein, also has a self-assembly ability *in vitro*, and the resulting matrices are used as scaffolds for cell-biological applications, templates for microelectronic applications, coating materials for non-biological surfaces for enhanced bio-compatibility. The assembly process is, so far, mostly monitored turbidimetrically in solution. In this study, by using atomic force microscopy(AFM), custom image analysis, and kinetic modeling, we study the homotypic and the heterotypic assembly of type-I and type-III collagen on muscovite and phlogopite mica surfaces with varying concentrations and ratios of the two collagen types. We found that when assembled individually, type-I collagen nucleates and assembles faster than type-III, and forms thicker fibrils. When the two collagens co-assemble, the fibril thickness and growth rate decrease as the fraction of type-III collagen increases. However, the fibril nucleation rate depends non-monotonically on the type-III fraction, being the highest for an intermediate mixture of types-I and III collagens. These results can be understood based on their amino acid composition, where type-I collagen, being more hydrophobic, nucleates fibrils fast and grows in both longitudinal and lateral directions. In con-

trast, the more hydrophilic character of type-III collagen limits the lateral growth of fibrils, which in turn makes more monomers available to nucleate additional fibrils. These results demonstrate how subtle differences in physico-chemical properties of similar molecules can be used to fine-tune their assembly behavior.

DEDICATION

To my mom and dad..

NOMENCLATURE

ECM	Extracellular Matrix
AFM	Atomic Force Microscopy
VDW	Van der Waals
DLVO	Derjaguin - Landau - Verwey - Overbeek
DL	Double Layer
PB	Poisson Boltzmann
FFT	Fast Fourier Transform
OLE	Orientational Linear Epitaxy
IEP	Isoelectric Point
SP	Polystyrene
SFM	Scanning Force Microscopy
CAFE	Computer-Aided Feature Extraction Program
SFA	Surface Force Apparatus

TABLE OF CONTENTS

Page

ABSTRACT ii

DEDICATION iv

NOMENCLATURE v

TABLE OF CONTENTS vi

LIST OF FIGURES ix

LIST OF TABLES xviii

1. INTRODUCTION 1

1.1 Overview 1
1.1.1 Biotechnological aspect 2
1.1.2 Biomedical aspect 3
1.2 Aim and Outline of the Dissertation 5

2. BACKGROUND 8

2.1 Collagen Family and Structure 8
2.1.1 Fibrillar collagen 9
2.1.2 Type-I and type-III collagen 10
2.2 Self-Assembly of Collagen 11

3. INTERMOLECULAR FORCES THAT DRIVE THE SELF-ASSEMBLY OF COLLAGEN 15

3.1 Introduction 15
3.2 Non-Covalent Interactions Between Surfaces 16
3.2.1 Van der Waals (VDW) forces 16
3.2.2 Electrostatic forces 18
3.2.3 DLVO theory 19
3.3 Water-Mediated Forces 20
3.3.1 Hydration forces 20
3.3.2 Hydrophilic effect 21

3.3.3 Hydrophobic forces . . . 21
3.4 Application of DLVO Theory to Collagen-Mica System . . . 23
3.4.1 Debye length of the collagen buffer . . . 23
3.4.2 Surface potential of the collagen molecule . . . 24
3.5 DLVO Interaction Between Collagen and Mica at the Contact Distance 28
3.6 Collagen-Collagen Interaction Away from the Mica Surface . . . 31
3.6.1 Effect of the solution pH on the DL force . . . 32
3.6.2 Effect of [KCl] on the DL force . . . 35
3.7 Discussion . . . 38

4. SEQUENCE LEVEL ANALYSES OF THE INTERACTION FORCES INVOLVED IN THE SELF- AND CO-ASSEMBLY OF TYPE-I AND TYPE-III COLLAGEN . . . 40

4.1 Introduction . . . 40
4.2 Python Analyses . . . 40
4.2.1 Interaction forces between the collagen molecules in 1D: electrostatic, hydrophobic, and polar interactions . . . 41
4.2.2 Distribution of proline and hydroxyproline . . . 44
4.3 Results . . . 48

5. EXPERIMENT . . . 50

5.1 Materials and Methods . . . 50
5.1.1 Materials . . . 50
5.1.2 Sample preparation . . . 51
5.1.3 Atomic force microscopy (AFM) imaging and image processing 51
5.1.4 Data analysis . . . 52
5.2 Atomic Force Microscopy . . . 53

6. SURFACE PATTERNING VIA SELF ASSEMBLY OF COLLAGEN . . . 57

6.1 Epitaxially Guided Self-Assembly . . . 57
6.2 Time and K^+ Ion Dependent Self-Assembly of Collagen . . . 57
6.2.1 Assembly on muscovite mica . . . 57
6.2.2 Assembly on phlogopite mica . . . 59
6.3 Structure of Muscovite and Phlogopite Mica . . . 60
6.4 Model Systems to Investigate The Homotypic/Heterotypic Assembly Process . . . 66
6.5 Discussion . . . 68

7. CO-ASSEMBLY OF TYPE-I AND TYPE-III COLLAGEN . . . 72

7.1 Introduction . . . 72

7.2 Monomer Analysis 73
7.3 Primary Structure of Type-I and Type-III Collagen 74
7.4 Homotypic Self-Assembly 75
7.4.1 Homotypic assembly on muscovite mica 75
7.4.2 Homotypic assembly on phlogopite mica 79
7.5 Heterotypic Self-Assembly 82
7.5.1 Heterotypic assembly on muscovite mica 82
7.5.2 Heterotypic assembly on phlogopite mica 86
7.6 Discussion 89

8. ADDITIONAL DATA AND PRACTICAL CONSIDERATIONS 95

8.1 Obstacles in AFM Study of Biological Samples 95
8.1.1 AFM related artifacts 95
8.1.2 Buffer solution or protein related defects 97
8.1.3 Substrate related defects 99
8.2 Additional Experimental Observations 106

9. SUMMARY AND OUTLOOK 116

REFERENCES 121

APPENDIX A. PYTHON CODES 145

LIST OF FIGURES

FIGURE Page

2.1 Procollagen molecule [1]. 10

2.2 Monomer molecule of type-I collagen, Tropocollagen [1]. 12

2.3 a) AFM image of the characteristic D-periodic spacing 67 nm on type-I collagen fibril from the sample of 5 μg/ml concentration upon 1 h incubation. b) Illustration of D-period as suggested in Petruska model [2] as a combination of gap and overlap region on the fibril. 13

3.1 Atom-atom pair VDW energy. 16

3.2 Electrostatic potential distribution of mica in electrolyte solution in terms of the distance from the surface. 25

3.3 The net interaction forces between collagen and mica resulted in a monotonic attractive force with the contribution of the attractive VDW and electrostatic force. The pure attraction at long distance could be the explanation of adsorption on mica. 27

3.4 The DLVO energy between collagen and mica in terms of the separation between them. 28

3.5 Illustration of the collagen-mica interaction near the surface indicating double attraction by the VDW and the DL force. 30

3.6 The interaction force as a combination of 'VDW+100*DL' between collagen molecules in terms of the surface separations. Even 100-fold increase on the repulsive DL force did not change the characteristic of the net force from a pure attraction showing the relative weakness of the electrostatic DL interaction. 31

3.7 Illustration of collagen-collagen interaction away from the surface showing the repulsive Dl and the attractive VDW forces. 33

3.8 The influence of the surface potential of collagen on the interaction force. The interaction force is given as a combination of 'VDW+100*DL' as in Figure 3.6. The inset shows the DLVO force of the surface potential of 9 mV as the sum of 'VDW+DL'. The units of the inset are the same as the main graph. Zeta potential measurements are taken from an experimental study [3]. 34

3.9 DL interaction force-distance curve between two collagen molecules showing how the long range electric DL force can be stronger depending on the concentration of KCl and might change the characteristic of the net DLVO force. 36

3.10 The effect of the KCl concentration on the DLVO force between collagen-collagen interaction. Although, a clear increase has been calculated with increasing KCl concentration shown in Figure 3.9, very small change on the DLVO force has been seen because of the relatively small magnitude of DL force between collagen molecules compared to VWD. 37

4.1 The part of our program which counts the electrostatic interaction between type-I molecules at 0D arrangement that means perfectly arrayed. 43

4.2 Illustration of number of amino acid for each residue considered for (a) electrostatic and (b) hydrophobic and polar interaction. $\alpha 1$ and $\alpha 2$ represent the same sequence for homotypic interaction and different sequences for heterotypic interactions. 45

4.3 The histogram of interaction forces involved in self- and co-assembly of type-I and type-III collagen. a) The electrostatic, b) The hydrophobic, c) The polar, and d) The total interaction between like and unlike molecules. 45

4.4 The part of the script which replaces amino acids except glycine and proline with X, to check the consistency of G-P-X motif of alpha chain. Note that the figure is cropped from the main program so that the sequence of aa1I continues. 46

4.5 A sample code which splits the amino acid sequence into triplet elements. Note that the sequence used is just a small fraction of the actual amino acid line. 47

4.6 Histogram of GPP intensity of alpha1(I) and alpha1(III) chain. The vertical axis represents the frequency of GPP element and the horizontal axis shows the number of GPP through the whole sequence. . 47

5.1 Image-J window when installed (Scientific image analysis software). . . . 53

5.2 The original AFM image of mixture(3:1) sample opened with Image-J (left) and 8-bit type of image of the original scan to start the image processing with an adjusted threshold of the original AFM image (right) 53

5.3 The final image after processing used for analysis (left). The result and the summary tables produced by Image-J after particle analysis tool applied (right). 54

5.4 The general principle and components of AFM. The laser is focused on the cantilever and the changes in the angle of the reflected beam is detected by photosensitive detector. 56

6.1 Effect of K^+ ion on the assembly mechanism of type-I collagen on muscovite mica surface: All images are with 5 $\mu g/ml$ collagen in a buffer solution containing of 30 mM Na_2HPO_4, 10 mM KH_2PO_4 and (a, b) 100 mM KCl, (c, d) 200 mM KCl at pH 7. (a, c) Assembly morphology of 30 min, and (b, d) 2 h of the incubation. 61

6.2 Effect of K^+ ion on on the assembly of type-I collagen on phlogopite mica: All images are with 5 $\mu g/ml$ collagen in a buffer solution containing of 30 mM Na_2HPO_4, 10 mM KH_2PO_4 and (a, b) 100 mM KCl, (c, d) 200 mM KCl at pH 7. (a, c) Assembly morphology at 30 min, (b, d) 2 h incubation time. 62

6.3 Collagen matrices fabricated by the self-assembly of 5 $\mu g/ml$ type-I collagen at 1 h deposition on (a) muscovite and (b) phlogopite mica in a buffer solution consisting of 30 mM Na_2HPO_4, 10 mM KH_2PO_4, and 200 mM KCl at physiological pH (pH 7). Under the appropriate condition, collagen molecules result in triaxial pattern on phlogopite and highly unidirectional alignment on muscovite mica pointing out the surface topography of the underlying lattice of the substrates. Color scale corresponds to a vertical range of (a) 5.33 nm and (b) 12.06 nm. The insets are Fast Fourier Transform (FFT) data of the images. (c-d) Histogram analysis of image (a) and (b), respectively, on the gray scale. 63

6.4 Orientational distribution of collagen network of Figure 6.3 showing a dominant unidirectional alignment at -34^0 for muscovite and three peaks at $-28^0, 1^0$ and -33^0 for phlogopite mica. 64

6.5 Schematic representation of muscovite (a, b) and phlogopite mica atomic structure (c, d). Muscovite contains aluminium in the center layer, while phlogopite has magnesium. The insets show different orientation of the OH groups in the two lattices. Proximity and position of OH group to K^+ atom in phlogopite reduces the affinity of collagen. Atoms are vertically aligned in phlogopite compared to muscovite mica. (a, c) View from the a axis of the unit cell. (b, d) View from above the cleavage plane (ab plane. Only top layer including K, O, Si/Al are shown for clarity. In (b), the OH group is also shown to indicate its direction of tilt (transparent grey arrow) [4]. 65

6.6 Stochastic simulation of four types of OLE networks that have been experimentally observed: **a.** Triaxial [14,16,26], **b.** biaxial [7,9], **c.**regtangular [1,2,11], and **d.** random [21-24, 8]. **a,b** form on hexagonal lattices, notably on mica. **c** forms on cubic lattices such as KCl. **d** forms when the orientational bias not strong. 68

6.7 Analysis of a triaxial collagen network. (a) AFM scan of concentration of 5 $\mu g/ml$ after 5 h deposition on phlogopite mica. (b) Corresponding in silico network extracted via CAFE (Computer-Aided Feature Extraction program). Filaments are individually recognized and coloured randomly. (c) Filament angle distribution. Angle θ is measured relative to the horizontal direction in (a) [5]. 71

7.1 AFM topography images of monomer molecules at the concentration of 0.3 $\mu g/ml$ type-I and type-III collagen at 85 s of the deposition on muscovite mica. The images exhibit a color scale corresponding to a vertical range of 3 nm. 74

7.2 Concentration dependent homotypic self-assembly of type-I (a,c,e) and type-III (b,d,f) collagen at 2 min of the deposition. (a-b) 2 $\mu g/ml$, (c-d) 4 $\mu g/ml$, (e,f) 5 $\mu g/ml$ concentration of collagen in the buffer solution consisting of 30 mM Na_2HPO_4, 10 mM KH_2PO_4, and 200 mM KCl at physiological pH (pH 7). The images exhibit a color scale corresponding to a vertical range of (a,b,c,d) 2 nm and (e,f) 5 nm. . . 77

7.3 AFM topography images of homotypic self-assembly of type-I and type-III collagen at the concentration of 5 $\mu g/ml$ at 1 h deposition on phlogopite mica. The images exhibit a color scale corresponding to a vertical range of (a,b) 7 nm and (c,d) 4 nm. The surface area of the fibrils are (a) 67.52 μm^2 and (c) 36.57 μm^2 measured by image-J. e) The orientational distribution of fibrils on panel (a) and panel (c). . . 81

7.4 Effect of type-III on the self-assembly of type-I. All images are with 0.5 $\mu g/ml$ final concentration and 30 min deposition. The small area scan in the case of type-III shows low level of assembly with very low z-scale of the sample covered by type-III monomers in panel (e). All images have a color scale corresponding to a vertical range of 2 nm after flattening. 82

7.5 The number of fibrils formed on the sample sets of heterotypic assembly of 0.5 $\mu g/ml$ collagen, shown in Figure 7.4. Enhanced nucleation was observed for the mixture(3:1) sample (Type-I:Type-III=3:1), shown in Figure 7.4a. 83

7.6 Nucleation analysis for co-assembly of type-(I+III). (a,b,c,d) Corresponding in silico network extracted via CAFE for topography image of (e,f,g,h) type-I, mixture(1:1), mixture(1:3) and mixture(3:1) respectively. All images are with 0.5 $\mu g/ml$ final concentration and 30 min deposition. The color scale is 3 nm for (e) and 4 nm for (f,g,h). . . . 84

7.7 AFM topography images of type-III collagen at 0.5 $\mu g/ml$ at (a) 30 min and (b) 90 min of the deposition on muscovite mica. The images exhibit a color scale corresponding to a vertical range of (a)1.5 and (b) 2 nm. (c-d) The line section of the image (a) and (b), respectively. 87

7.8 AFM topography of the homotypic self-assembly of type-I and type-III collagen at the concentration of 5 $\mu g/ml$ at 1 h deposition on phlogopite mica. The resulting network of collagen fibrils revealed a regulatory effect of type-III collagen on the fibril length distribution of the heterotypic self-assembly network. The images exhibit a color scale corresponding to a vertical range of (a,c) 10 nm and (b) 15 nm. 88

7.9 Snapshots of the intermediate steps of image analysis program Image-J applied to Figure 7.3. (a,d) The original AFM scan. (b,e) Filtered image (colored red) of the original by color thresholding tool. (c,f) The final version of the selected fibrils (by yellow) to measure the surface area of each type. 94

8.1 Double tip effect. a) AFM image of type-I collagen fibrils. The color scale corresponds to 15 nm. Bruker Dimension Icon AFM was operated. b) Line section between the point C and D verifying characteristic D-period of a collagen fibril. c) Profile plot from the point A to the point B shown on the image exhibits double tip effect on the recorded topography data. 96

8.2 Noise effect on topography signal. 5 $\mu g/ml$ concentration of type-III collagen was deposited for 30 min on muscovite mica in the presence of 200 mM KCl. a,b) AFM image. Z-scale is 6 nm for both images. AFM Nanoscope IIIa was performed. c) Plot profile for the line shown in panel b. The x-axis represents distance along the line and the y-axis is the vertically averaged pixel intensity. 97

8.3 (a,b) Different area scans of 5 $\mu g/ml$ of the mixture(1:1) sample of type-I and type-III collagen deposited for 1 h in the presence of 200 mM KCl. Z-scale of the images are 30 nm. AFM Nanoscope IIIa was operated. c) Profile plot for the line from point A to point B taken from the panel b. The x-axis represents distance along the line and the y-axis is the vertically averaged pixel intensity. 98

8.4 The network of 5 $\mu g/ml$ of type-III collagen deposited for 30 min (for the top row images) and 1 h (for the bottom row images) on phlogopite mice, after 10 sec centrifuge in the presence 150 mM KCl. AFM CP-II was operated The orientational distribution of the image (b1). 100

8.5 5 $\mu g/ml$ of type-III collagen was deposited after 10 sec centrifuge on phlogopite mica for 37 min in the presence of 150 M KCl. The bad condition of mica breaks the consistent pattern formation. A thick layer of cleavage could be a possible solution. Z-scale is 20.57 nm (a) and 14.98 nm (b). AFM CP-II was operated. (c) 8-Bit version of the nonuniform part of panel (b). (d) The plot profile of the line shown in panel (c). 101

8.6 a)AFM Topography image of 5 $\mu g/ml$ concentration of mixture(1:3) sample deposited for 1 h on phlogopite mica in the presence of 200 mM KCl. The topography results showed a tilted structure of the surface which makes difficult to analyse fibrils on the surface. If additional cleavage does not solve the problem, the mica could be mounted on another metal disk. The color scale corresponds to 10 nm. Bruker Dimension Icon AFM was operated. b) The orientational distribution of image a) showing one dominant three direction of growth fibrils. . 102

8.7 (a,b)5 $\mu g/ml$ of type-III collagen deposited for 3.15 h on phlogopite mica in the presence of 150 M KCl after 10 sec centrifuge. AFM CP-II was operated. (c) Model system to illustrate fibril formation on mica and fibril formation on a collagen layer onto mica (d). 103

8.8 Analysis of collagen network formed at 2.5 $\mu g/ml$ concentration of type-I collagen. a) AFM image, z-scale is 12 nm. Bruker Dimension Icon AFM was operated. b) Orientational distribution of the network obtained by image-j and c) by CAFE [5]. 105

8.9 5 $\mu g/ml$ concentration of type-III collagen was deposited for 30 min on phlogopite mica in the presence of 200 M KCl. Type-III collagen is in the process of assembly on the mica surface. At 2 h of the deposition, the growing was observed in an appropriate triangular shape. Z scale is 10 nm for panel(a), and 7 nm for panel(b). AFM Nanoscope IIIa was operated for the images. 107

8.10 5 $\mu g/ml$ type-I collagen deposited for 30 min. The corresponding orientational distribution of fibrils. Z-scale is 18.03 nm for panel(a), and 197.66 nm for panel(b). AFM CP-II was operated. 108

8.11 5 $\mu g/ml$ of type-I collagen was deposited for 30 min for the upper images and 1 h for the bottom images on phlogopite mice after 10 sec centrifuge, in the presence of 50 mM glycine and 150 mM KCl. The fibril formation process is observed in details at 30 min of deposition and the characteristic d-periodic structure is shown in the bottom left image. AFM CP-II was operated. 109

8.12 5 $\mu g/ml$ of type-III collagen was deposited after 10 sec centrifuge on muscovite mica for 80 sec in the presence of 150 M KCl. AFM CP-II was operated. 109

8.13 5 $\mu g/ml$ of type-III collagen was deposited on muscovite mica for 1 h in the presence of 150 M KCl. High level of dirts and junks on the surface make impossible to find a clean area. The experiment should repeat with a higher level of protection from dirts like sealing of the sample right after deposition till scanning. AFM CP-II was operated. 110

8.14 0.1 $\mu g/ml$ of type-I collagen was deposited on muscovite mica for 2 min in the presence of 200 mM KCl. Too low concentration to observe the monomer molecules. AFM CP-II was operated. 110

8.15 5 $\mu g/ml$ of type-III collagen was deposited after 10 sec centrifuge on muscovite mica for 1 h in in the presence of 150 M KCl. The reason of the observed pattern is unclear. It could be a bad mica or old electrolyte or a composition of the two. We found that the electrolytes should be renewed at least once a month. AFM CP-II was operated. 111

8.16 0.1 $\mu g/ml$ concentration of type-III collagen was deposited on muscovite mica for 90 sec in the presence of 200 M KCl. The type-III molecules were quite dim. We reconstituted the type-III aliquot and obtained a better results. AFM CP-II was operated. 111

8.17 0.4 $\mu g/ml$ concentration of type-III was deposited on muscovite mica for 90 sec in the presence of 200 M KCl. During the reconstitution process of type-III collagen, we used liquid nitrogen for some of the aliquots to figure out which method is the best to keep protein in its natural shape/properties. The observed structure of the sample showed that liquid nitrogen broke down the nature of the molecules and the sample surface was fully covered with the crystallized structure of type-III molecules. Thus, we eliminated this type of reconstitution of type-III collagen. AFM CP-II was operated. 112

8.18 5 $\mu g/ml$ concentration of type-III molecule was deposited on phlogopite mica for 20 min in the presence of 200 mM KCl. The sample surface was fully covered with collagen molecules without any fibrils yet. Type-III molecules are in the lag phase. The collagen network is observed as the one that is close to the early incubation at 1.30 min. AFM CP-II was operated. 112

8.19 5 $\mu g/ml$ concentration of type-III molecule was deposited for 3.45 h on phlogopite mica in the presence of 200 M KCl. Although the self-assembly of type-III molecules was observed on the surface, the resulting topography is not trustable, because the sample surface did not show an homogeneous appearance, which is probably due to the bad condition of mica. Some region among fibrils was found to be without collagen molecules as seen in the left image, some is full of type-III molecules as the right image. AFM CP-II was operated. . . . 113

8.20 5 $\mu g/ml$ concentration of type-I molecule was deposited for 30 min on phlogopite mica in the presence of 200 M KCl. Variety of problems are seen on the sample. Cracked surface of phlogopite mica is one of them. If the thickness of crack is about 10 $\mathring{A}$, further cleaving might solve the problem. The aggregates of small mass could be collagen molecules. We have found that type-I collagen has a shelf-life of 3 months at 4^0C. After reconstitution of type-I working solutionmolecules from the stock solution, we have obtain an expected pattern on phlogopite mica. AFM CP-II was operated. 113

8.21 5 $\mu g/ml$ concentration of type-I molecule was deposited for 30 min on phlogopite mica in the presence of 200 M KCl. The sample surface did not show almost any growing, but small collagen molecules did cover almost the entire surface. Even 2 h deposition did not result in an assembly. The sample solution might be not mixed well and uneven amount of electrolyte or collagen would be taken for deposition. The sample solution would be re-prepared. AFM CP-II was operated. . . 114

8.22 5 $\mu g/ml$ concentration of type-I molecule was deposited for 2 h on phlogopite mica in the presence of 100 M KCl. Multiple layers of fibrils are observed on the substrate. AFM CP-II was operated. . . . 114

8.23 5 $\mu g/ml$ type-I collagen was deposited after 10 sec centrifuge on phlogopite mice for 5 h, in the presence of 50 mM glycine and 150 mM KCl. At the end of 5 h deposition, we found no liquid on the mica surface, since the sample was left to the laboratory environment which caused the sample solution on the surface to evaporate. We figured out that for depositions more than 1 h, the sample should be protected in a moisture chamber, because the evaporation prevented the assembly process from its natural way. AFM CP-II was operated for the images. 115

LIST OF TABLES

TABLE Page

3.1 Measured zeta potential of soluble collagen as reported in Li's study[3] 33

4.1 The scores calculated by our program for each and the total interaction between type-I, type-III, and type-I:type-III molecules. 44

7.1 The top table shows the characteristic properties of type-I and type-III collagen in terms of side-chains specific to each amino acid. Type-I collagen is a heterotrimer consisting of two $\alpha 1(I)$ (COL1A1) chains and one $\alpha 2(I)$ (COL1A2) chain, whereas type-III collagen is a homotrimer of $\alpha 1(III)$ (COL3A1) chain. The numbers in parenthesis represents the number of amino acids in telopeptides. a.a stands for amino acid. The bottom table shows the net molecular properties of each type of collagen. For the number of hydrophobic amino acid, we considered Val, Leu, Ile, Met, Phe, Trp, Cys [6]. For polar amino acids, we considered Gln, Asn, His, Ser, Thr, and Tyr. 76

7.2 Possible scenarios in terms of the presence of telopeptides in the collagen molecule of type-I and type-III. Asterisk (*) represents the existence of telopeptide ends in the monomer molecule. 91

1. INTRODUCTION

1.1 Overview

Macromolecular self-assembly is a promising way of fabricating ordered structures with interesting mechanical [7] and optical [8] properties. Learning how to produce highly organized structures and how to mediate the organization provide technological and application wise opportunities at both macroscale and nanoscale [9, 10, 11]. Grzybowski and his colleagues generated an assembly by manipulating electric dipoles of the spheres (1.58 mm or 3.18 mm in diameter) and vibrating a container at a certain frequency. Doing so, they obtained ordered structures such as hexagonal or square arrays [11]. Stupp and his team also showed an ordered structure, periodicity and orientation of triblock molecules with a molar mass of about 200 kDa [9].

In many cases, assembly is achieved on solid substrates. The resulting matrix is used for different purposes such as coating non-biological surfaces for enhanced biocompatibility and creating nanopatterned biomaterials for cell biological, biomedical, and biotechnological applications [12, 13, 14, 15]. Experimentally, solid surfaces also allow researcher to monitor the assembly process, as the resulting two-dimensional structures can be imaged via scanning probe microscopy, notably AFM. Biofunctionalization of surfaces with proteins provides opportunities to understand thousands of experiments which characterize the interaction between a coated surface and a specific molecule, drug, or nanoparticles which are covered by proteins in the physiological environment [16]. Such patterned surface can also be utilized for cell attachment, orientation and migration [17, 13, 12]. It is expected that the biofunctionalized surfaces coating with functional materials may be programmable in the

future to manipulate complex biological processes.

The extracellular matrix (ECM) in metazoan organisms provides structural integrity and mediate cellular signaling [18]. It is increasingly recognized that the ECM is a *biological alloy*, whose functions are determined not by individual constituent molecules, but more collectively by their assemblies [19, 20]. In this way, structural and functional diversity of different tissue types can be achieved with a limited number of components that assemble in different proportions and suprastructures. Co-assembly of different ECM molecules also has potential in tissue engineering applications for generating matrices of tailored properties [21, 22, 23, 24, 25].

Among the constituents of the ECM, collagen is predominant, forming 30% of the total protein mass in human body [26]. Currently there are 28 different collagen types known [26, 27]. By combining with other molecules such as proteoglycans and minerals, collagen provides enormous diversity in tissue types, such as bone, tendon, blood vessel, cornea, and skin [28]. Among them, fibrillar collagens including types-I, II, III, and V are dominant. Their assembly into fibrils and fibrillar networks have been intensely studied [21, 29, 30, 31]. Collagen is also used for a wide range of biomedical and biotechnological applications, including templates for fabricating nanowires [32], coating material for non-biological surfaces for enhanced bio-compatibility [33, 34, 12], surface patterning [35, 36], and for drug delivery [37].

1.1.1 Biotechnological aspect

Collagen is one of the most important materials for fabricating functionalized surfaces [34, 12]. Although there are different techniques to produce aligned network of collagen fibrils, such as use of magnetic field [38], hydrodynamic flow [39], dip-pen nanolithography [40], and traction forces generated by cell [41], most of these methods

do not allow to control the assembly process. Neither do they help to investigate dynamics of the self-assembly. Instead, hierarchical self-assembly of collagen in vitro from nanoscale of collagen monomers to milimeter scale of collagen bundles [42] provides a precise control with fine-tuning of environmental conditions.

ECM, which is the non-cellular component of tissues, is substantially composed of collagen molecules. The mechanical strength, stability and resilience of tissues are provided by this biological framework. Understanding the dynamics of ECM, where collagen type-I and type-III are the most abundant constituents, is also important for implant integration in tissue engineering and cell biological applications [12, 43, 44, 45]. A variety of functions such as gene expression, cell division, differentiation, proliferation, migration, and orientation are determined, organized and/or regulated by its tissue specific composition and morphology [46, 12, 47, 48, 49, 50, 51, 52, 53, 54]. Cells are embedded in the ECM whose composition and architecture provide signal for cellular processes. To understand the communication between cells and ECM, more effort should be put into the study of ECM, mostly formed by the two major components, type-I and type-III collagen [21, 55].

1.1.2 Biomedical aspect

Collagen also plays an important role in various human diseases such as tumor suppression, Ehler-Danlos syndrome type-IV [56, 57, 58], ovary and colon cancer [59, 60, 61], and aneurysms [62, 63, 64]. The relative amount of type-III to type-I collagen and/or their mutations are found to be related to these diseases. Also in both colon and breast carcinoma tissue, it is shown that the modified matrix structure due to the distribution change of type-I and type-III content may promote invasion by means of negatively affected self-assembly process of the two types of collagen

[65]. Therefore, to understand the principles and the conditions for the self-assembly of collagen type-I and type-III is crucial for medical and technical applications.

Ehlers-Danlos syndrome type IV(EDS IV), which is the most severe, vascular type of EDS, is an hereditary connective tissue disorder caused by mutations in COL3A1 which encodes alpha-1 chain of procollagen type-III [66, 56]. In vascular EDS, the skin is thinner and softer. It is easily bruising and translucent with visible vessels [56]. Most patients encounter arterial, digestive and uterine complications with rupture and dissections of large vessels. The reduced amount of type-III in vessel walls increases fragility and made surgical repair hard to manage [67, 68]. Also, due to the vascular rupture, pregnancy may even cause maternal mortality especially during last months women suffering from EDS type IV [66, 69]. Since type-III content is high in the walls of digestive tract, patients with EDS type IV have severe digestive complications [57, 58].

The ovary and colon cancer are other relevant diseases. It was reported that there is a relation between the increasing production of type-I and type-III collagen and the degree of malignancy, since their synthesis is very slow in normal ovarian tissue [59, 60]. Also in both colon and breast carcinoma tissues, it was shown that the modified matrix structure due to the change of distribution of type-I and type-III content may promote invasion by means of negatively affected self-assembling process [65]. Another interesting finding is that although the total collagen amount decreased, the procollagen expression of type-I and type-III collagen increased in gastrointestinal malignant tumor [61].

Aneurysms is an abnormal widening of an artery or vein, resulting from a localized weakness on the walls of the vessel. Some patients with aneurysms showed a decrease and even lack of type-III collagen [63, 64, 62]. In wound healing process, increasing amount of type-III to type-I and smaller diameter of fibrils were reported

by Fleischmajer [70].

In addition to diseases, heterotypic fibrils of type-I and type-III collagen were observed to affect cell growth and DNA synthesis. When cells are cultured on the hybrid fibrils of both types, cell growth and DNA synthesis were simulated [71], while only type-I fibrils coated dishes suppressed those processes [72].

1.2 Aim and Outline of the Dissertation

Compared to the assembly of a single collagen type, co-assembly of multiple types is far less understood. A basic question in heterotypic collagen assembly is the dependence of the fibril morphology and growth kinetics on the ratio of the component collagens, in particular, between types-I and III that are respectively the two most abundant collagen types in tissues [73].

The ultimate aim of this work is to explore the heterotypic self-assembly mechanism of type-I and type-III collagen. Many collagen based tissues have a hybrid/heterotypic structure of the two types in animals. To understand the heterotypic process will provide a better understanding of the structural organization and the properties of tissues. That will build a bridge between the structure and the mechanics of tissues. To achieve this aim, the self-assembly of type-I collagen on mica, which is the most studied and the most abundant type, is investigated in terms of the electrolyte concentration and the assembly time in this study. A recent work from our lab performed a set of experiment using AFM. The topography images taken from different stages of the self-assembly process of type-I collagen showed that the assembly on the solid surface mica follow a pathway in the order of surface adsorption of the collagen molecules, surface diffusion, nucleation and then growth of the collagen fibrils [4]. To understand these stages and the following sections better,

Section 2 presents some background information about ECM protein collagen, its structure and family. The properties of the most abundant two types of collagen, type-I and type-III which form the significant amount of ECM, and an introduction to the self-assembly mechanism of collagen are also covered in Section 2.

In **Section 3**, we describe the three main types of non-covalent forces accompanying the self-assembly process, van der Waals forces (VDW), electric double-layer (DL) interaction, and water-mediated forces and discuss the range of those interactions. In addition to the theoretical investigation of the system, we performed a computational analysis using a programming language, Python in **Section 4**. Following the theoretical approaches to the assembly process, the experimental details including the materials, methods and experimental conditions are provided in **Section 5**.

Before starting to investigate the heterotypic self-assembly of type-I and type-III, type-I collagen is used as a coating material to produce a patterned surface with resultant fibrillar network. The unidirectional and triangular patterns produced in **Section 6** via the self-assembly of type-I collagen are the two templates that we used for the next steps of the project. For this part of the research, the influence of the substrate on the resulting network structure of the self-assembly is investigated by using the two types of mica which are muscovite and phlogopite.

We start the co-assembly section, **Section 7**, with a successfully produced unidirectionally aligned and a triangular shaped network of collagen fibrils on muscovite and phlogopite mica, respectively. Whether type-III can self-assemble and can form fibril is examined in this section, since there has not been an observation of type-III assembly before. By starting with very low concentration, 0.1 μg/ml, the monomer molecules of type-III was investigated at very early incubation time and compared with type-I monomers. Then, by increasing the concentration and the deposition time, the homotypic self-assembly of both type-I and type-III were investigated and

a different assembly rate meaning a different net driven force was revealed in this section. A basic question in heterotypic collagen assembly is the dependence of the fibril morphology and growth kinetics on the ratio of the component collagens, in particular, between types-I and III. To our knowledge, there has not been an investigation of the heterotypic assembly of type-I and type-III collagen on a solid substrate either at nano scale (at the nucleation level) or at micrometer scale with the advantage of high resolution Atomic Force Microscopy (AFM). This part of the thesis, **Section 7**, investigates and discusses the role of type-III collagen on the type-I assembly, the heterotypic self-assembly, at the nucleation and the growth level. **Section 8** is dedicated to some of the possible difficulties encountered during the study, practical considerations and possible solutions.

The last part of the thesis, **Section 9** presents the summary and outlook of our research.

2. BACKGROUND

2.1 Collagen Family and Structure

Collagen molecule represents the most abundant (30%) structural material in the human body and the largest component of the ECM providing strength, stability and elasticity to organisms [45, 74, 75]. It comprises a big family with at least 28 different types [76, 77]. Each of them has a characteristic structural and functional properties to enhance biomechanical and interfibrillar communication in the related part of the body. Several reviews have been published on this superfamily [45, 27].

Collagen fibrils are the major constituents of many tissues such as skin, tendon, bone, cornea, and cartilage. Many properties of the tissues are derived from the structural organization of collagen molecules within a fibril and the topography of fibrils. The presence of different types in a single fibril is also prerequisite for specific, structural tissue properties such as fibril size and interfibrillar communication. Many soft tissues and internal organs such as skin, cornea, vessel walls, liver and kidney consist of the most abundant two types of fibril forming collagen, type-I and type-III, in the form of heterotypic fibril structure. Despite of the widespread existence of the heterotypic fibril in the body, not much information has been obtained so far regarding the heterotypic self-assembly mechanism of the two types [21, 78, 79]. The aim of this investigation is to examine how cooperation of type-III collagen with type-I affects the co-assembly process, the fibril size and the length distribution of the resulting network structure.

Fibrils in collagen-based tissues are structured in a significantly complex manner, and that is essential for the tissue network. Collagen-based tissues are build up hierarchically from the lowest level triple helical collagen molecule, tropocollagen

(400 kDa), with a length of 300 nm and a diameter of about 1.5 nm up to milimeter scale collagen fibers [42]. Each monomer molecule, tropocollagen, is made of three polypeptide chains, which form long, fibrillar triple helix (see Figure 2.1). Tropocollagen first assembles into fibrils (∼10-300nm) and fibers (∼1-20 μm) via lateral association. Fibers then assemble into bundles, such as tendons, with diameters of up to 500 μm [80]. With its highly organized structure, collagen is the main constituent of tissues not only bearing stress but also storing, transforming and dissipating the elastic energy. The physical, mechanical and functional properties of different collagen tissues are directly related to resulting network structure of the self-assembly process.

2.1.1 Fibrillar collagen

Significant amount of total collagen in the body (approximately 90%) is represented by fibrillar collagen [81]. They constitute the majority of the ECM and provide the structural framework and the mechanical strength of tissues [80]. They are synthesized from a precursor molecule called procollagen which contains globular domains (N(amino)- and C(carboxy)- terminal propeptide) at both ends, as shown in Figure 2.1. Between these N- and C- terminal propeptide and the long, straight, triple helical domain, there are short non-helical parts, called telopeptides, with the sites fundamental for proper functioning of the self-assembly and the molecular cross-linking [82, 83, 84].

After completing this large precursor in the cell, it is secreted out of the cell for extracellular processing. During this process, the propeptide ends are cleaved by specific enzymes and then the mature collagen monomer is produced and is ready for the self-assembly process.

Among the fibrillar collagens, type-I is the primary element of the fibrillar tissue

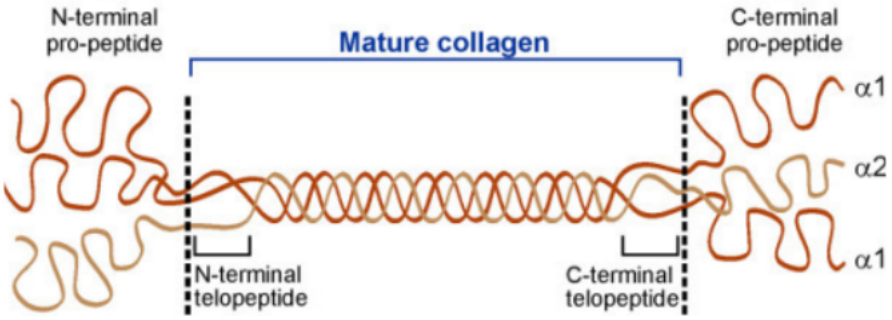

Figure 2.1: Procollagen molecule [1].

structure. Type-I rich fibrils contain a significant amount of type-III collagen which is the second most abundant type in the body [73]. Therefore, the self-assembly mechanism of the mixture of the two types, which we call the heterotypic assembly, is important for tissue biological and mechanical properties. In this research, we investigated the self-assembly of type-I and type-III collagen on a solid surface mica.

2.1.2 Type-I and type-III collagen

Type-I collagen is the largest fraction of the fibrillar collagens with more than 70% abundance [85] depending on tissues, and it is the best studied type of collagen. It presents in both soft and hard connective tissues including bone, cornea, tendon, ligament, and skin [84, 86, 87, 88, 89, 90]. Type-I collagen was found to possess a rod-like structure with very little flexibility [91]. There are many reports in the literature about the Young modulus (elastic modulus) of type-I collagen, and the results show a wide range depending on the status of fibril as hydrated [92, 93], dried [94, 93] or cross linked [95]. To study the mechanical properties of type-I fibrils, Yang performed a micromechanical bending experiment with AFM tip-less cantilever and

obtained Young modulus of 5.4 GPa for native and 14.7 GPa for gluteraldehyde cross linked collagen [96]. Another effort by nanoindentation method for Young modulus of rat tail tendon, which is mostly formed by type-I collagen, resulted in 5 to 11 GPa [97]. For primary structure, type-I is a heterotrimer of two α1(I) and one α2(I) amino acid chains which differs from α1(I) chain in amino acid sequence [90]. It is mostly found in a heterotypic form with type-III [98] and/or type-V collagen [19] and with some molecules such as proteoglycans [99] in a tissue.

Type-III collagen is the second most abundant type of collagen found in soft connective tissues such as blood vessel walls, skin, muscle, placenta and in a variety of internal organs. Type-III collagen has a homotrimer of three α1(III) chains. It has a slightly longer triple helical length than type-I collagen does [100, 101]. It is associated with the tissues with smaller and regulated fibril diameters, such as cornea and skin [102, 103, 104]. Fibrils in those tissues have the heterotypic form of type-I with type-III in a wide distribution of the ratio of the two types depending on different parameters such as age, types of tissue, or being healthy or damaged [105]. Presence of type-III is also a marked feature of damaged tissues undergoing a healing process [105]. Therefore, as one of the key parameters affecting the co-assembly mechanism that is the resulting network structure and its mechanical properties, the ratio influence of type-III on the self assembly of type-I had been investigated in this study.

2.2 Self-Assembly of Collagen

Collagen fibril formation is a self-assembly process. Collagen molecules hierarchically self-assemble into nano, micro and macro scale structures depending on their physiological function in tissues. With its highly organized structura, collagen is the main constituent of tissues, that is not only bearing stress but also storing, trans-

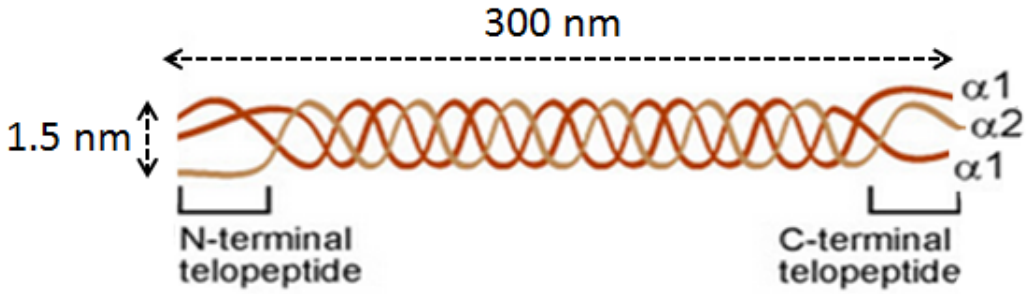

Figure 2.2: Monomer molecule of type-I collagen, Tropocollagen [1].

forming and dissipating elastic energy. A collagen fibril has 67 nm repetitive binding pattern on its fibril surface consisting of overlap and gab region, as its characteristic signature, called D-period. According to that, a collagen molecule has a length of $4.4 \times D$. It can be observed by using electron microscopy [106] or AFM [107] as seen in Figure 2.3 from our sample of 5 μg/ml concentration of type-I collagen upon 1 h deposition. Formation of D-period indicates that the collagen fibrils are in the structure of a native-like [85]. This distinct and regular spacing was explained by Hodhe and Petruska [2]. In the model, the phenomena is explained with five collagen molecules deposited side by side and parallel in a fibril and arranged in a staggered like structure as illustrated in Figure 2.3b.

The self-assembly of collagen molecules into fibrils, fibers, and bundles is a very complex mechanism. Although a significant amount of knowledge has been obtained about collagen type-I structure, even its homotypic self-assembly mechanism has still not understood completely and has questions to be answered. The assembly mechanism was found to be an entropy-driven process for the homotypic system [108]. At neutral pH, a combination of hydrophobic forces, hydrogen bonding and electrostatic interaction between adjacent molecules results in the formation of col-

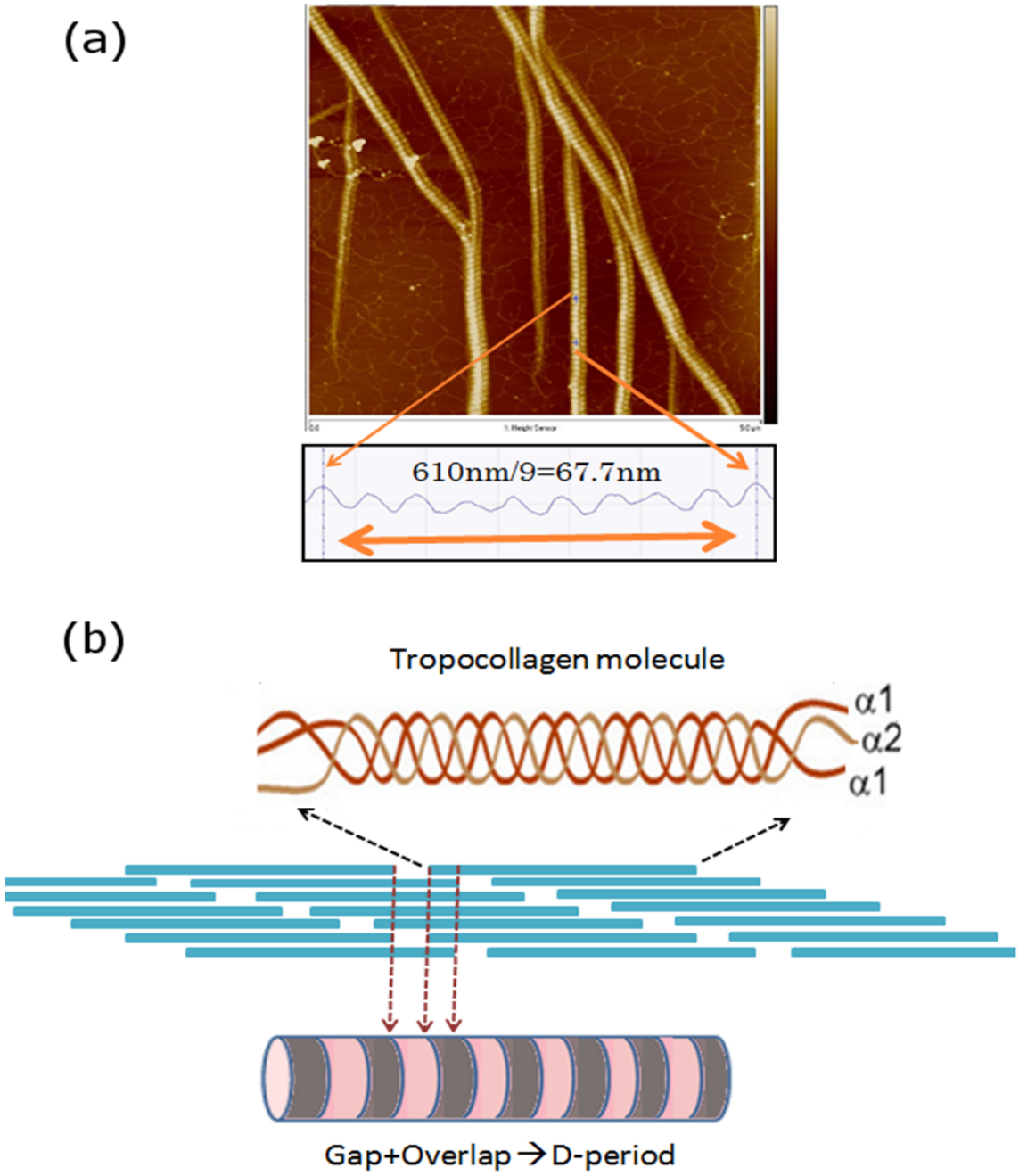

Figure 2.3: a) AFM image of the characteristic D-periodic spacing 67 nm on type-I collagen fibril from the sample of 5 μg/ml concentration upon 1 h incubation. b) Illustration of D-period as suggested in Petruska model [2] as a combination of gap and overlap region on the fibril.

lagen fibrils with the characteristic D-periodic spacing [109, 110, 111]. The amino acid sequence of $\alpha(I)$-chain was analysed to explain D-periodic structure of collagen fibrils [112]. Each amino acid pair containing positive and negative charge and hydrophobic side chains were given a score of one while one molecule passed trough the other molecule and the rest of the pair combinations were given a score of zero. Although they simplified the triple helix of collagen-I to homotypic which does not include more hydrophobic $\alpha II(I)$-chain, the result showed that D-spacing configuration is energetically more favourable. The plot of the number of interaction versus the number of stagger showed peaks at 0D, 1D, 2D, 3D, and 4D, with decreased number of interaction as the number of stagger was increased.

Recently, AFM with very high resolution has been utilized to investigate the self-assembly mechanism in details. As the mechanical properties of tissues are directly related to the structure of fibril network and how the collagen units are arranged during the assembly process, we are interested in the interaction forces accompanying the self-assembly mechanism of both homotypic and heterotypic system of type-I and type-III collagen.

3. INTERMOLECULAR FORCES THAT DRIVE THE SELF-ASSEMBLY OF COLLAGEN

3.1 Introduction

Interactions/Bonds in materials are generally categorized into two classes which have different interaction environments, covalent and non-covalent. Covalent forces refer to chemical bonds within the individual molecule or compound. Non-covalent interactions, on the other hand, are those that occur between molecules. They are weaker than the covalent bonds, as heating the system alters the physical properties first rather than its chemical structures such as a change the state of substances from solid to liquid, before any change in its atomic or molecular structure.

Non-Covalent interactions can be classified into two categories as specific and non-specific interactions. Certain molecules may have a strong structural and/or orientational fit which lead them to form an extremely strong, but non-covalent bond. Such interactions are called specific interaction, and forces that drive the interaction are called specific forces. Unlike specific forces, non-specific interactions are those which arise between many atoms, molecules or surfaces irrespective of their geometry or orientation. The major physical forces such as van der Waals, electrostatic, hydrogen bonding, or hydrophobic/hydrophilic forces fall into this category. In this study, we will be interested in non-specific physical interactions/bonds, not chemical or covalent bonds.

The driving force for the self-assembly process of biomolecules is a combination of various types of physical forces. The major contributions to the net force, which are van der Waals force (VDW), Double Layer (DL) electrostatic force, and water-mediated forces as hydrophobic and hydrophilic, will be analysed in this research.

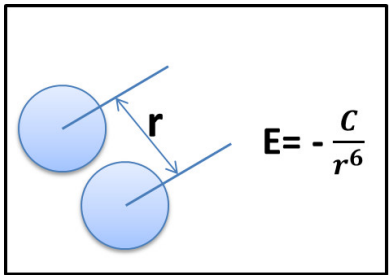

Figure 3.1: Atom-atom pair VDW energy.

3.2 Non-Covalent Interactions Between Surfaces

In this section, we will explore the two main long range interaction forces that drive the self-assembly of collagen on the solid surface mica; van der Waals and electric double layer forces. The sum of the two interactions is explained by Derjaguin - Landau - Verwey - Overbeek abbreviated to DLVO theory [113] which will be focused more in the following sections.

3.2.1 Van der Waals (VDW) forces

VDW force is a long-range interaction and always present between all atoms and molecules including totally neutral or non-polar structures. It is originally electrodynamic based interaction which arises from a temporary or a permanent electrical dipole moment of molecules. VDW force is attractive for similar materials, such as the same type of collagen molecules, but can also be repulsive in the case of dissimilar materials. It consists of three distinct types of forces known as the orientation/Keesom force, the induction/Debye force and the dispersion/London force interacting between dipole-dipole molecules, polar-nonpolar molecule and neutral

atoms or nonpolar molecules, respectively.

The VDW energy is generally defined in terms of Hamakar constant A, $A = \pi^2 C \rho_1 \rho_2$ where ρ_1 and ρ_2 are the number of atoms per unit volume in the two bodies and C is the coefficient in the atom-atom pair potential illustrated in Figure 3.1. For proteins interacting in salt solution, Marra reported the Hamakar constant A between $(1.0 - 1.5) * 10^{-20}$ J [114].

To calculate the total VDW energy of the self-assembly of a molecule on a solid surface, the substrate-molecule and molecule-molecule interaction should be considered at the same time. To first approximation, collagen and mica can be considered as a cylinder of radius R and length l and a flat surface, respectively. The VDW interaction energy of a collagen molecule near mica surface can be expressed as [115]

$$\begin{aligned} E^{VDW} &= E_{cc}^{VDW}(D_c, D_m) + E_{cm}^{VDW}(D_c, D_m) \\ &= \frac{-A_c}{12\sqrt{2}} D_c^{\frac{-3}{2}} \sqrt{\frac{R}{2}} - \frac{A_m}{12\sqrt{2}} D_m^{\frac{-3}{2}} \sqrt{R}. \end{aligned} \tag{3.1}$$

The first term represents the VDW interaction with another collagen and the second term represents that between collagen-mica. The VDW interaction between similar surfaces like the first term is always attractive. The sum of the two negative VDW term gives the final VDW energy. D_c and D_m are the distance between collagen-collagen and collagen-mica. A_c and A_m are the corresponding Hamakar constant. Experimentally, to distinguish them from each other and measure them individually are not possible as they exist in the system at the same time and they are affected from the surrounding environment simultaneously. When the surface charges are screened, the only long-range force left is VDW interaction. For collagen-mica system which has different the isoelectric points (IEP)of interacting surfaces, to obtain neutral/screened surfaces is not simple. If the self-assembly occurs at the IEP of

collagen, at pH 9.3, we can eliminate the electrostatic interaction between collagen molecules. However, the previous findings showed that mica surface is negatively charged at all pH [116], meaning that there will be an electrostatic interaction all the time. The relative change of the long range forces can still be useful to elucidate the system. When the self-assembly monitors at different pH values, the resulting difference of each case would be caused by mostly electrostatic interactions that will be explained in the following sections, as the VDW force is insensitive to change on the solution.

3.2.2 Electrostatic forces

The other major long-range force between surfaces in aqueous solution, including neutral surfaces, is the electric double layer (DL) force. Opposite to the VDW, the electric force is always repulsive between similarly charged surfaces and can be attractive for some cases of asymmetric surfaces depending on the solution pH. For example, two surfaces with a different IEP value may charge oppositely at the pH below the IEP of one surface, but above the other surface resulting in an attractive electric DL force. DL interaction energy is an exponential function of the characteristic Debye length of the solution,

$$W^{es}(r) \simeq W_0^{es} e^{-\kappa r} \tag{3.2}$$

where W_0^{es} is the surface potential that depends on the geometry, size, and the electric charge of the surface and also the condition of the buffer solution. κ^{-1} in Eqn (3.2) is the Debye length.

The DL interaction energy between two parallel collagens and a collagen and

mica, by assuming the two surface as a cylinder and a flat surface, can be given [115]

$$\begin{aligned} E^{DL} &= E_{cc}^{DL}(D_c, D_m) + E_{cm}^{DL}(D_c, D_m) \\ &= \kappa^{\frac{1}{2}} Z_{cc} \sqrt{\frac{R}{4\pi}} e^{-\kappa D_c} - \kappa^{\frac{1}{2}} Z_{cm} \sqrt{\frac{R}{2\pi}} e^{-\kappa D_m} \end{aligned} \tag{3.3}$$

where κ is the inverse of the Debye length given by Eqn (3.5). Z_{cc} and Z_{cm} is the interaction constant of the electrostatic DL force between collagen-collagen and collagen-mica, respectively. The first term represents the repulsive DL interaction energy between collagen-collagen and the second term represents that between collagen-mica which is associated with the attractive electrostatic force between negatively charged mica surface and a positively charged collagen molecule. Although the two terms in the Eqn (3.3) look similar, the interaction constants are different as explained below.

3.2.3 DLVO theory

In an aqueous solution, the net interaction usually involves both the VDW and the electrostatic DL forces together. The two forces depends different distance dependence, as one is a power law and the other one is an exponential. At small separations, the VDW interaction is dominant and it is almost insensitive to changes in the electrolyte solution. However, the DL force strongly depends on the condition of the buffer solution. The effect of these two forces is expressed by **DLVO theory** (Derjaguin - Landau - Vervey - Overbeek theory). Therefore, plotting the two forces together as shown in Figure 3.6 and Figure 3.3 is a common way to describe the net force of the system. The result can be attractive, repulsive or a combination of the two, depending on the relative strength of the two main forces.

DLVO Theory has been widely studied since last a few decades for different sys-

tems. It is consistent with experiments [117, 118, 119] at long separations. At short distances, however, DLVO theory is not enough to explain the net interaction between surfaces [120, 121, 122]. Therefore, additional forces should act on the system at this short distances which we called water-mediated/hydration forces that will be mentioned in the following section.

3.3 Water-Mediated Forces

3.3.1 Hydration forces

Hydration. When an ion is dissolved in water (highly polar solvent), the surrounding water molecules reorient themselves to the ion due to the strong ion-dipole interaction. Reorganized group of water molecule around the ion is called 'Hydration shell'. The postulated role of the hydration shell is to generate the hydration force [122].

The existence of hydration force is investigated in our group by Ravikumar in three different biological filament systems, hydrated (collagen), dry non-polar and dry polar interfaces. A weakly oscillating hydration force was found and the hydration shell is formed in all cases regardless of the type of the surface such as different types of surface residues. The magnitude and other details of the interaction depend on the surface properties [122]. This suggests that the hydration shell and the resulting hydration force exist almost always regardless of the structural and physical condition of the molecule. An oscillatory short-range force varying between attraction and repulsion with a characteristic dimension of solvent molecule is seen between any two rigid surfaces as they approach each other in liquid. Theoretical understanding of the oscillatory force is provided by a variety of papers [123, 124, 115, 125]. The weakly oscillating hydration force arises from coalescence and depletion of the hydration

shells as two filaments approach [122].

Water-mediated/hydration forces play crucial roles in biomolecular interactions and assemblies. They can be divided into hydrophilic and hydrophobic interactions.

3.3.2 Hydrophilic effect

Molecules with polar structure is called hydrophilic, means water-loving. They can share hydrogen bonds with water and easily dissolve in water. If solvent and solute molecules have a strong interaction/bond, such as polar hydrophilic molecule and water, there occurs a protective hydration layer which prevent the molecules from coming closer each other more than a certain distance which depends on the solvent molecule dimension. Therefore, a repulsive hydration force occurs for hydrophilic molecules in liquid. This repulsive primary hydration shell (short-range repulsive force) around ionic groups or polymer chains or macromolecules causes a reduction in the strength of adhesion (the interaction energy at D=3 $\mathring{A}$, the interface of water molecules at contact).

3.3.3 Hydrophobic forces

Hydrophobicity, which literally means water-hating, reflects the tendency of substances to avoid water contact. Those molecules posses non-polar, stable structure (zero dipole moment), and they are not willing to interact with polar water molecules. They rather prefer to contact with each other, hydrophobic attraction, to minimize contact with water molecules. They are referred as hydrophobic, oil-like substances. Therefore, they are not soluble in water.

Hydration force between two hydrophobic molecules or hydrophobic groups on the surface is monotonically attractive. Proteins as a chain of amino acids can have

both hydrophobic and hydrophilic side chains. Such types of compounds are called amphiphilic. However, a common criteria used in surface science for hydrophobicity/hydrophilicity of a surface is to determine the contact angle θ of water or other appropriate liquid on it. If the water angle is in the range of $75^0 - 90^0$, it is considered as partially hydrophobic, or strongly/fully hydrophobic if it is in the range of $100^0 - 115^0$.

Knowledge about the hydration force is basically empirical and specific to the system interested. One study found that hydrophobic interaction has different behaviours at below and above 10 nm. Experiments showed that at separations $D < 10$ nm, the hydrophobic force only weakly depends on the solution conditions such as concentration, ionic strength [121]. Thus, the unaffected interaction by the 'screening of ions' in solution indicates non-electrostatic nature of hydrophobic interaction at this range. However, at separations $D > 10$ nm, the attraction is affected by changing the solution condition till to the separation of 80 nm in some on the experiments reported in the literature [126, 127]. Based on another experimental force measurement, the hydrophobic interaction in the range of 4-10 nm between hydrophobic surfaces in water, can be roughly defined with an exponential function given by

$$E(D) = -2\gamma_i e^{-D/\lambda_0}, \text{per unit area} \tag{3.4}$$

where λ_0=1-2 nm, and γ_i is the interfacial energy which is accepted as half of the adhesion energy at D=0, given as γ_i=40-55 mJ/m^2 for fully hydrophobic surfaces [128]. Although there is not a theoretical model to express the hydration force, an exponential fit to the experimental data is a common way to describe the hydration effect of the solution.

3.4 Application of DLVO Theory to Collagen-Mica System

In our simplified model, we assume that the collagen molecule is a cylinder of radius R and length L and the mica surface is considered as a flat surface. With this assumption, we calculated the DLVO energy and the force between collagen molecules and the adhesion energy of collagen to mica at the contact distance. We also compared the calculated DLVO force with the hydration interaction between collagen molecules reported by our earlier study [122]. It should be noted that the electrostatic DL equations given by Eqn (3.12) and Eqn (3.14) is based on the continuous Poisson-Boltzmann (PB) theory which breaks down at very close distances. However, the DLVO theory is still very useful for estimating the force and the energy in terms of separation between surfaces as shown in Figure 3.6, 3.3, 3.4.

3.4.1 Debye length of the collagen buffer

Debye length, κ^{-1}, is the thickness of the electrostatic double layer formed around a charged surface in solution. It does not depend on any surface property such as charge density or potential, but only the type of electrolyte in solution such as monovalent, divalent, and concentration of each type and the temperature. The thermal energy at room temperature 25^0C (298 K), $kT = 1.38 \times 10^{-23} \times 298 = 411 \times 10^{-23}J$. The inverse of the Debye length, $\kappa(\lambda_D^{-1})$ is given by

$$\begin{aligned} \kappa &= \left(\sum_i \frac{c_i e^2 z_i^2 N_A}{\varepsilon_0 \varepsilon k T} \right)^{1/2} \\ &= \left(\frac{(1.6 \times 10^{-19})^2 \times 6.02 \times 10^{23}}{8.85 \times 10^{-12} \times 78.5 \times 411 \times 10^{-23}} \sum_i (c_i z_i^2) \right)^{1/2} \end{aligned} \tag{3.5}$$

where c_i is the ionic concentration of ion i in the bulk in the unit of mol/l (M), ε_0 and ε are the permittivity of free space and the material, respectively. N_A is Avogadro number and 'z' is the valency of each ion. For example, $z = +1$ for monovalent cations such as Na^+, $z = -1$ for monovalent anions such as Cl^-, and $z = +2$ for divalent cations such as Ca^{+2}. By taking into account each solution in the the collagen buffer, $\sum_i (c_i z_i^2) = 0.6$. Thus, the Debye length of our collagen solution is calculated as

$$\begin{aligned} \kappa &= 0.1799 \times 10^{10} m^{-1} \\ \kappa^{-1} &= \lambda_D = 5.55 \ \mathring{A}. \end{aligned} \tag{3.6}$$

Debye screening length is quite small in our system as compared to that of the pure water which is about $900nm$. That means that the electrostatic interaction between molecules can reach to the surfaces up to a half nm in length.

3.4.2 Surface potential of the collagen molecule

The electrostatic DL interaction energy described by Eqn (3.3) depends on the interaction constant of Z_{cc} and Z_{cm}. The interaction constant for symmetric systems such as collagen-collagen Z_{cc} not like collagen-mica, is defined by [115]

$$Z = 64\pi\varepsilon_0\varepsilon \left(\frac{kT}{e}\right)^2 tanh^2\left(\frac{ze\Psi_0}{4kT}\right) \ N \tag{3.7}$$

For a monovalent electrolyte such as KCl (z=1) at room temperature,

$$Z = 9.21 \times 10^{-11} tanh^2 \frac{\Psi_0}{103} \quad N \tag{3.8}$$

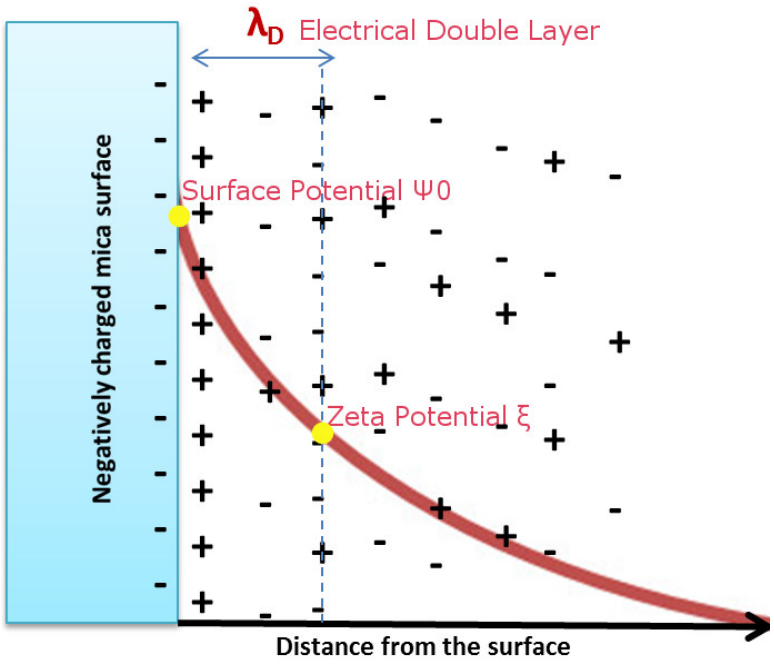

Figure 3.2: Electrostatic potential distribution of mica in electrolyte solution in terms of the distance from the surface.

where Ψ_0 is the surface potential in the unit of mV. Although the actual z is the mixture of monovalent and divalent ions, it is quite close to the situation of monovalent ions since KCl is the dominant electrolyte in the buffer solution. For low potentials (> 25 mV), the surface charge density becomes proportional to the surface potential Ψ_0. The correlation between the two is given by Graham equation [115]

$$\begin{aligned} \sigma &= \varepsilon_0 \varepsilon \kappa \Psi_0 \\ \Psi_0 &= \frac{q/A_0}{\varepsilon_0 \varepsilon \kappa} \end{aligned} \tag{3.9}$$

The surface charge density σ can be calculated by the net charge of the collagen molecule divided by its surface area, q/A_0. The net charge can be calculated

by counting acidic and basic amino acids on each alpha chain. By considering the triple helical structure of the collagen molecule, type-I collagen has the net charge of $37e^-$ with $9e^-$ on the $\alpha - 1$ chain and $19e^-$ on the $\alpha - 2$ chain while the type-III collagen has the net charge of $39e^-$ with $13e^-$ on each $\alpha - 1$ chain. We used Protein Knowledge Database, UniProtKB (http://www.uniprot.org/uniprot/) for charge calculations. By searching the specific α chain of the related source used in the experiment, that is rat tail tendon for the type-I source and Bos taurus (bovine skin) for type-III in our case, we obtained the amino acid sequence of each α chain. By using the specific sequence of that α chain and the amino acid calculator, $http://proteome.gs.washington.edu/cgi-bin/aa_calc.pl$, the number of each amino acid type was count as shown in Table 3.1. Taking into account the net charge on each molecule, the surface potential for the two types of collagen is calculated as

$$\begin{aligned} \Psi_0(I) &= \frac{1}{\varepsilon_0 \varepsilon \kappa} \frac{37e^-}{(2r(\pi L + \pi r))} = 1.67\ mV \\ \Psi_0(III) &= \frac{1}{\varepsilon_0 \varepsilon \kappa} \frac{39e^-}{(2r(\pi L + \pi r))} = 1.76\ mV \end{aligned} \tag{3.10}$$

The results are also consistent with previous experimental study of zeta potential for collagen molecule [3]. Note that, we assumed that both types have an identical molecule size. Therefore, the interaction constant Z_I or Z_{III} does not show much difference on the DL force between the two types.

Due to the screening effect of the solution, to measure the surface potential experimentally, Ψ_0, is in fact not possible, but Zeta potential, ξ. Particles in suspension carry an electrical charge. Their surfaces are surrounded by strongly bound counter-ions which is called stern layer. The increase on the distribution of counter-ions extends to the electrical double layer on which the experimental measurement of potential is taken place called zeta potential. The difference between the surface and

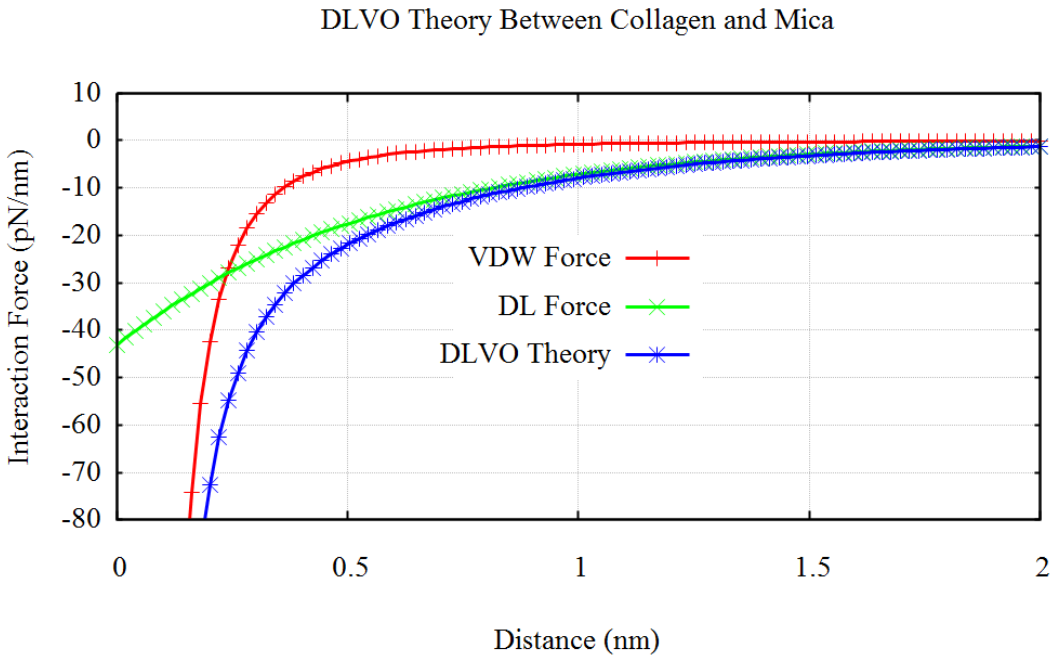

Figure 3.3: The net interaction forces between collagen and mica resulted in a monotonic attractive force with the contribution of the attractive VDW and electrostatic force. The pure attraction at long distance could be the explanation of adsorption on mica.

zeta potentials is shown in Figure 3.2. Zeta potential can be measured experimentally with electrophoresis that measures the ectrophoretic mobility of a particle as a function of zeta potential or streaming potential measurement at which the liquid is passed over the particles at different pressure trough the channel with charged walls [129]. In this study we used the zeta potential as the surface potential. Although it depends on the types of electrolyte and its concentration, the previous reports indicated that the measured zeta potential of the mica surface is about -100 mV [118, 129]. That corresponds the interaction constant of $5.18 * 10^{-11}$ according to Eqn (3.7), whereas it is calculated as $2.4 * 10^{-14}$ for collagen molecules. That brings a significant difference between the two terms in Eqn (3.3).

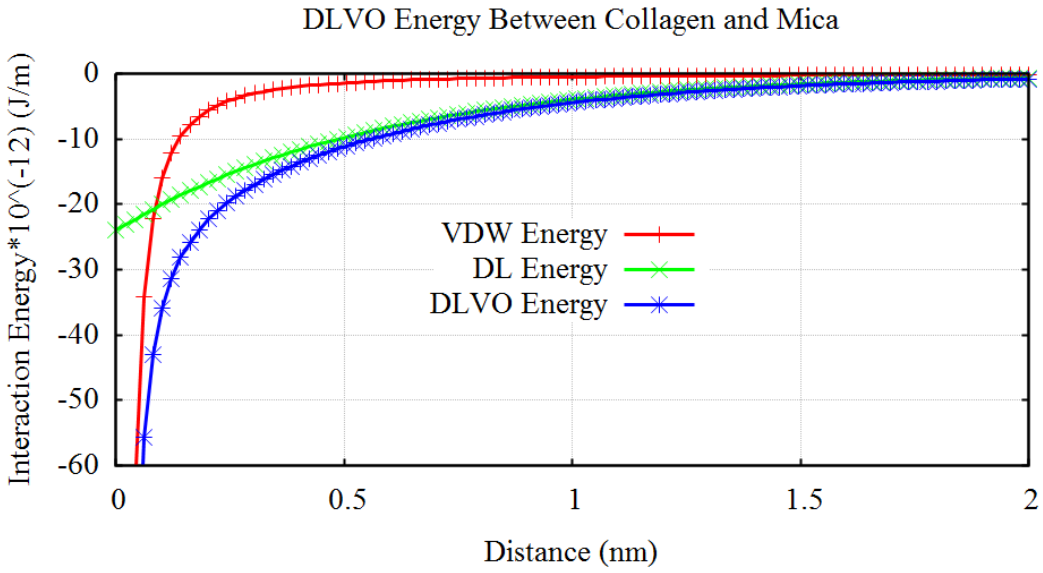

Figure 3.4: The DLVO energy between collagen and mica in terms of the separation between them.

3.5 DLVO Interaction Between Collagen and Mica at the Contact Distance

To determine the adhesion force, we calculated the net force between a collagen molecule and mica at the contact distance. The net interaction energy in the form of the VDW and the DL interaction can be calculated using the interaction energy given by Eqn (3.1) and Eqn (3.3) in the second terms. The adhesion force is

$$F = -\frac{\partial E(D_c, D_m)}{\partial D_m} \tag{3.11}$$

If we consider the contact distance as a hydration monolayer on the mica which is 3 $\mathring{A}$, DLVO pair interaction force between a collagen molecule and mica by taking the derivative of Eqn (3.1) and Eqn (3.3) is calculated as -40.55 pN/nm as following.

$$
\begin{aligned}
F_{cm}^{DLVO}(D_0) &= F_{cm}^{VDW}(D_0) + F_{cm}^{DL}(D_0) \\
&= \frac{-A}{8\sqrt{2}}\sqrt{R}D_0^{\frac{-5}{2}} - \kappa^{\frac{3}{2}} Z_{as}\sqrt{\frac{R}{2\pi}}e^{-\kappa D_0} \\
&= \frac{-10^{-20}}{8\sqrt{2}}\sqrt{\frac{1.5\times10^{-9}}{2}}(3\times10^{-10})^{-2.5} - (1.8\times10^{9})^{\frac{3}{2}} Z_{as}\sqrt{\frac{1.5\times10^{-9}}{4\pi}}e^{-1.8\times0.3} \\
&= (-15.42 - 25.13)\times10^{-3} \quad N/m \\
&= -40.55 \quad pN/nm
\end{aligned}
\tag{3.12}
$$

Note that we have used the surface potential of mica which was previously reported (-100 mV [118, 129]) in this calculation. Since the collagen molecule has much less potential compared to mica, the net surface potential of the interaction must be lower than this value used in Eqn (3.12). That means a lower DL force leading a lower DLVO interaction force. For the exact result, the net surface potential of the asymmetric system should be measured experimentally with electrophoresis or other techniques which we do not have.

The repulsive VDW force which means a negative Hamakar constant arises when the dielectric property of the intervening medium is in between the two of that of the interacting surfaces. That is not the case of our system, as the dielectric constant of the water is much higher that those of the interacting surfaces which are collagen and mica. Dielectric constant of mica is reported between (5.4 - 7.0) [115]. For some protein molecules, it is calculated by simulation between 15 and 40 [130] which is also much lower than that of water. So, the VDW force between a collagen and mica is an attractive force. The electrostatic DL force between negatively charged mica and positively charged collagen is also attractive. Therefore, the DLVO force

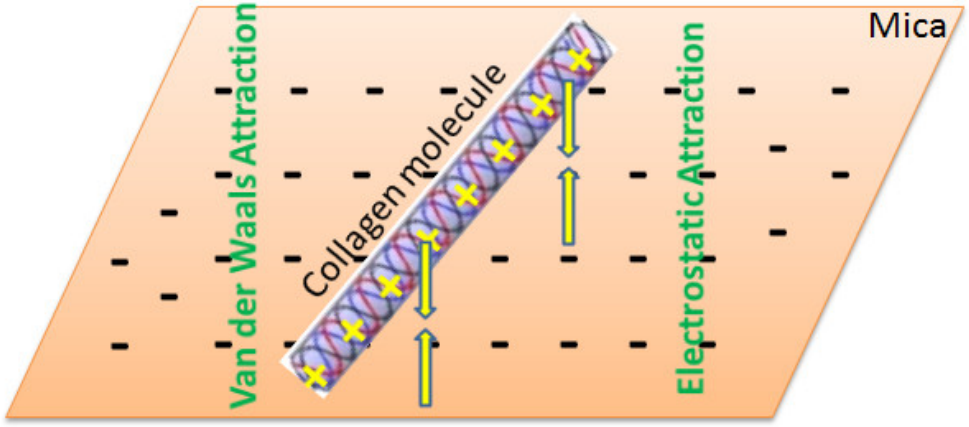

Figure 3.5: Illustration of the collagen-mica interaction near the surface indicating double attraction by the VDW and the DL force.

between collagen and mica is a pure attraction.

The adhesion energy of collagen and mica as a function of distance D according to DLVO theory

$$
\begin{aligned}
E_{cm}^{DLVO} &= E_{cm}^{VDW}(D) + E_{cm}^{DL}(D) \\
&= \frac{-A\sqrt{R}}{12\sqrt{2}} D^{\frac{-3}{2}} - \kappa^{\frac{1}{2}} Z_{as} \sqrt{\frac{R}{2\pi}} e^{-\kappa D} \\
&= \frac{-10^{-20}}{12\sqrt{2}} \sqrt{\frac{1.5\times10^{-9}}{2}} D^{-1.5} - (1.8\times10^{9})^{\frac{1}{2}} Z_{as} \sqrt{\frac{1.5\times10^{-9}}{4\pi}} e^{-\kappa D} \\
&= -0.509\times10^{-12}\times D_{nm}^{-3/2} - 0.464\times Z_{as}\times e^{-1.8\times D_{nm}} \quad J/m \\
&= (-3.098 - 13.97)\times10^{-12} \quad J/m \\
&= -17.07\times10^{-12} \quad J/m \\
&= 4.15\times10^{9} \quad kT/m
\end{aligned}
\tag{3.13}
$$

The resultant pure attraction at the contact distance calculated based on the DLVO theory means strong adhesion leading to a random distribution of fibrils ad-

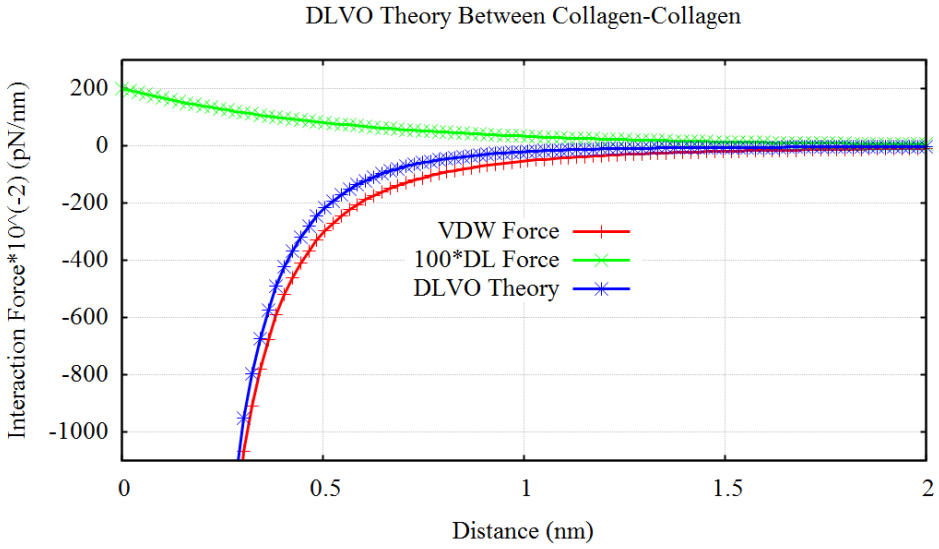

Figure 3.6: The interaction force as a combination of 'VDW+100*DL' between collagen molecules in terms of the surface separations. Even 100-fold increase on the repulsive DL force did not change the characteristic of the net force from a pure attraction showing the relative weakness of the electrostatic DL interaction.

sorbed onto the mica surface. On the other hand, the resultant fibrillar network of collagen exhibits highly organized self-assembled fibrils with a characteristic D-periodic structure. Therefore, the DLVO theory must not be the only force at the contact distance. The hydration force come into play at this point. In our previous study, [122, 131], the hydration force between collagen-collagen is reported as 100 pN/nm. This means that at the contact distance, hydration force is dominant force on the system as will be discussed more in the last section.

3.6 Collagen-Collagen Interaction Away from the Mica Surface

According to our model, we calculated the DLVO force between two parallel collagen molecules. The two main forces are illustrated in Figure 3.7. The symmetric

system exposes the repulsive electrostatic DL interaction and the attractive VDW interaction. At the molecular distance, an additional hydration force arising from the structural change of the solvent molecules is taken into account to explain the net interaction of the system [120, 121, 122]. By assuming the molecules as cylinders, the net DLVO interaction function in terms of the distance between them is

$$\begin{aligned} F_{cc}^{DLVO}(D) &= F_{cc}^{VDW}(D) + F_{cc}^{DL}(D) \\ &= \frac{-A}{16}\sqrt{R}D^{\frac{-5}{2}} + \frac{\kappa^{\frac{3}{2}}Z_{ss}}{2}\sqrt{\frac{R}{\pi}}e^{-\kappa D} \\ &= \frac{-10^{-20}}{16}\sqrt{\frac{1.5\times10^{-9}}{2}}(D_{nm}\times10^{-9})^{-2.5} + \frac{(1.8\times10^{9})^{\frac{3}{2}}Z_{ss}}{2}\sqrt{\frac{1.5\times10^{-9}}{2\pi}}e^{-1.8\times D_{nm}} \\ &= -540.4\times10^{-3}D_{nm}^{-2.5} + 14.44\times10^{-3}e^{-1.8\times D_{nm}} \\ &= (-54.04\times D_{nm}^{-2.5} + 1.44\times e^{-1.8\times D_{nm}})\times10^{-2} \;\; pN/nm \end{aligned} \tag{3.14}$$

In our calculation, we used the experimental Hamakar constant for the VDW force [114]. However, the electric DL force is based on the continuum mean field theory which means that the atomic structure is ignored. Although it fits well with the experimental results at long distances, at small separation such as below than a few water diameters, the DL theory breaks down and the net interaction force can not be described by DLVO theory only. The possible reasons and explanations are in Discussion.

3.6.1 Effect of the solution pH on the DL force

To characterize our system better, we examined the DLVO theory between collagen molecules depending on an experimental parameter, pH. Li measured the zeta potential of collagen molecules in solution in terms of solution pH [3] as tabulated

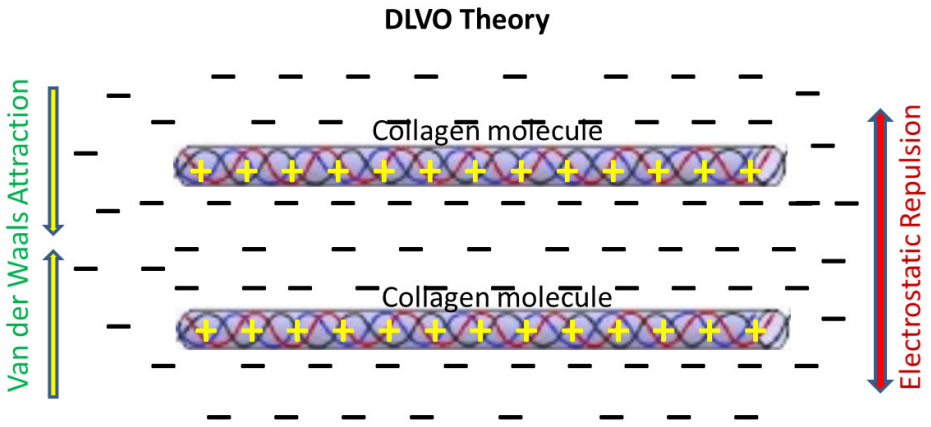

Figure 3.7: Illustration of collagen-collagen interaction away from the surface showing the repulsive Dl and the attractive VDW forces.

below in Table 3.1.

V_0=1.67 mV	pH≅7
V_0=-5 mV	pH≅8
V_0=-9 mV	pH≅10

Table 3.1: Measured zeta potential of soluble collagen as reported in Li's study [3].

The first row represents our experimental condition and the last two are taken from Li's study. Based on the experimental measurement and our condition, we calculated the DLVO force and plotted that depending on pH 3.8. It was reported that the presence of different electrolytes shifted the IEP of collagen [3]. The measurement was taken in the electrolyte solution consisting of 12 mM $NaCl$ and 10 mM Na_2HPO4. Although it does not exactly fit our experimental condition, it is still helpful to provide idea about how the surface potential might affect the electrostatic

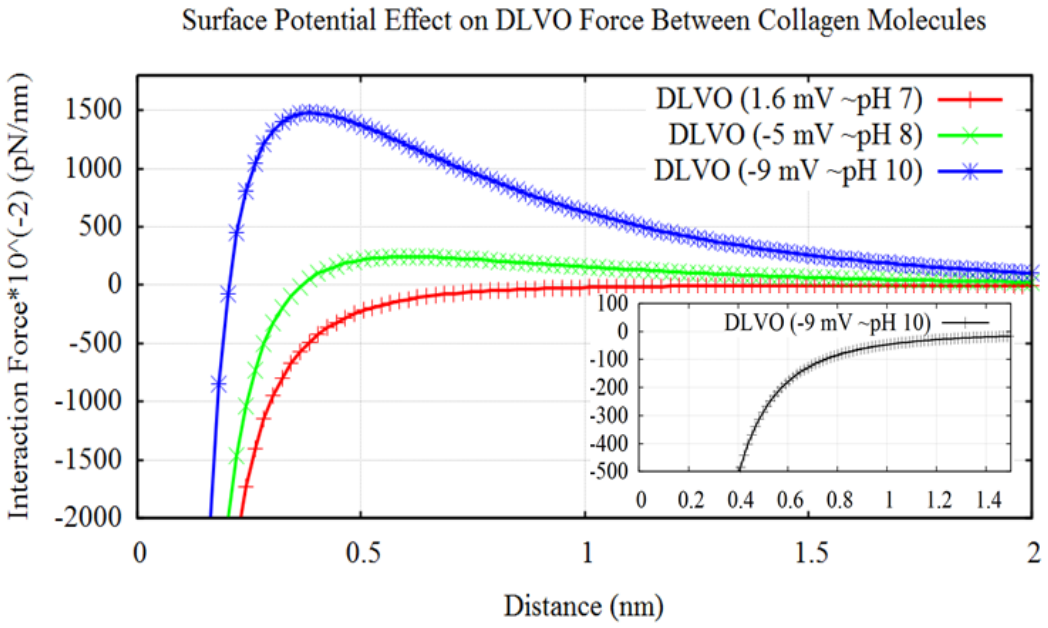

Figure 3.8: The influence of the surface potential of collagen on the interaction force. The interaction force is given as a combination of 'VDW+100*DL' as in Figure 3.6. The inset shows the DLVO force of the surface potential of 9 mV as the sum of 'VDW+DL'. The units of the inset are the same as the main graph. Zeta potential measurements are taken from an experimental study [3].

interaction between collagen molecules. Figure 3.8 exhibits a clear influence of pH on the DLVO force. However, we should remember that the plots represent the force as a combination of VDW and 100 fold DL force as in Figure 3.6. The inset shows that even for the highest surface potential of 9 mV, the real DLVO theory as a combination of 'VDW+DL' resulted in pure attraction at all separation.

3.6.2 Effect of [KCl] on the DL force

Among other electrolytes, KCl has double effects on the collagen-mica system. Mica surface has K layers which are partially taken out upon cleaving and that leaves the surface negatively charged. A previous study investigated the relative affinity of various monovalent cations such as K^+, Na^+ , Li^+ to mica and found that K^+ has a higher affinity [132] and it is a critical component for creating an ordered film [133]. Thus, K^+ has ion specific effect on the mica surface [134].

In the previous section, we mentioned that the electrolyte concentration strongly affects the electrostatic interaction because of the parameter κ. Any variance of the DL force between mica and collagen would not change the resulting picture except the magnitude of the interaction, since both of the DLVO forces are attractive, but that would make difference between the interaction of collagen-collagen since the DL force is repulsive in this case. To understand the effect of [KCl] on the electrostatic interaction between collagen molecules, we plotted the DL force with varying concentration of KCl according to Eqn (3.15) (Figure 3.9). Note that, that effect is caused only by electrostatic. The neutralization effect of [KCl] on the open K^+ pockets of cleaved mica surface is also taken account to interpret the resulting assembly network [133, 4].

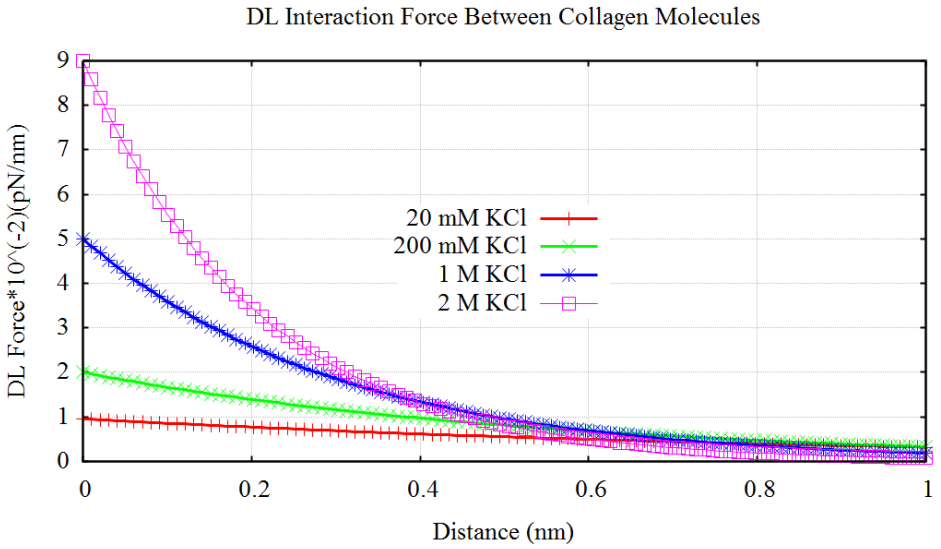

Figure 3.9: DL interaction force-distance curve between two collagen molecules showing how the long range electric DL force can be stronger depending on the concentration of KCl and might change the characteristic of the net DLVO force.

$$\begin{aligned} F_{cc}^{DL}(D) &= \frac{\kappa^{\frac{3}{2}} Z_{ss}}{2} \sqrt{\frac{R}{\pi}} e^{-\kappa D} \\ &= \kappa^{\frac{3}{2}} (2.62 \times 10^{-19}) e^{-\kappa D} \end{aligned} \tag{3.15}$$

As the concentration of KCl increases, the net DLVO force can be repulsive, attractive or some combination of the two depending on the strength of the electrostatic interaction. In our case, however, even a high concentration of KCl such as 2 M could not affect the resulting interaction much as shown in Figure 3.10 because of the relatively low magnitude of the electrostatic interaction compared to VDW.

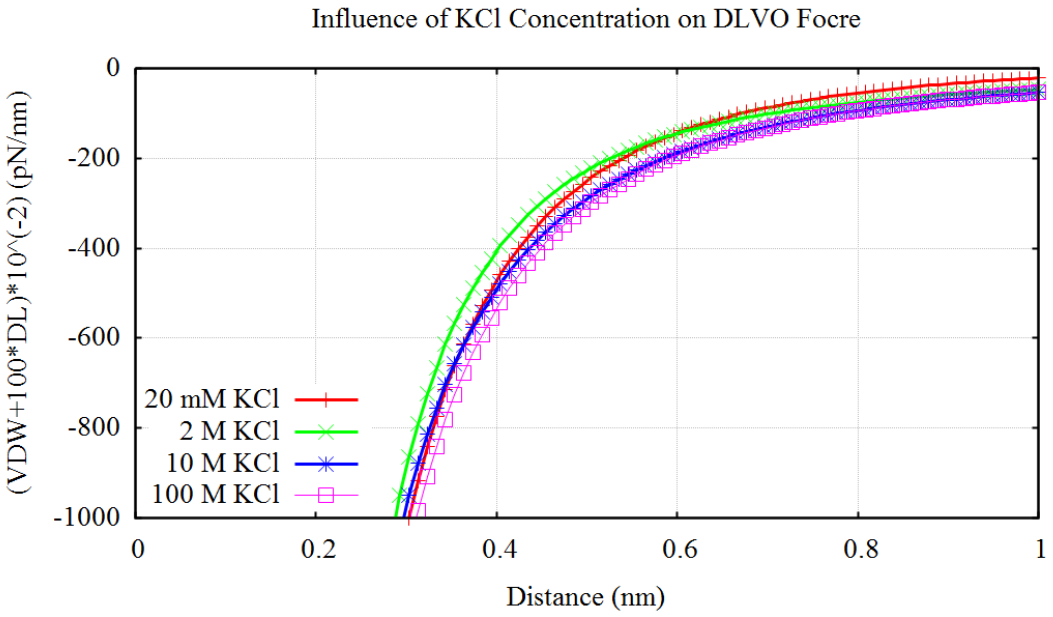

Figure 3.10: The effect of the KCl concentration on the DLVO force between collagen-collagen interaction. Although, a clear increase has been calculated with increasing KCl concentration shown in Figure 3.9, very small change on the DLVO force has been seen because of the relatively small magnitude of DL force between collagen molecules compared to VWD.

3.7 Discussion

In this section, we used the DLVO theory to understand the self-assembly of collagen molecule onto mica. In our model, we assumed that collagen molecule is a cylinder and mica is a flat surface and, we calculated the adhesion force and the energy of collagen to mica. We considered the influence of varying concentration of KCl and the surface potential of collagen on the DLVO force.

The DLVO theory is an approximate model as a combination of the attractive VDW and the repulsive DL forces between similar surfaces in liquid. It is the cornerstone of the understanding the interactions and characteristic of colloidal systems. In our case, the DLVO theory resulted in a pure attractive force at all distances. The long range attraction may promote the aggregation of molecules leading to self assembly. At short distance, however, the resulting pure attraction is a sign of the existence of a third interaction which would likely be repulsive based on the resulting highly organized fibrillar network of collagen molecules on mica as shown in Figure 6.3. Otherwise, the pure attraction, meaning a strong adhesion at the contact distance, would produce a randomly adsorbed irregular structure without any repeating pattern, in contrast to our collagen networks (Figure 6.3, Figure 7.2). The short range repulsive force is the hydration force. The hydration force between collagen-collagen molecule is reported as $100\ pN/nm$ [122]. The lubrication effect of hydration shells can counter the pure attractive DLVO force [122]. The dominant hydration force at the contact distance helps to arrange the molecules by sliding with each other to a characteristic D-periodic structure. With our simple assumptions, the DLVO theory provides a reasonable estimation of the energetics of the collagen self-assembly on mica.

We calculated the adhesion force and energy at the distance of 3 Å, which is

the thickness of one hydration shell, the diameter of a water molecule. When the hydration shell breaks and collagen approaches less than 3 Å to the mica surface, the DLVO theory predicts even stronger adhesion force. However, note that in very short distances DLVO theory breaks down in a number of ways. First, the steric repulsion starts to take effect, which prevents negative divergence of the DLVO attraction. Second, the DLVO theory breaks down in various aspects such as the continuum assumption of ionic distribution that underlies the electrostatic double layer theory becomes invalid.

4. SEQUENCE LEVEL ANALYSES OF THE INTERACTION FORCES INVOLVED IN THE SELF- AND CO-ASSEMBLY OF TYPE-I AND TYPE-III COLLAGEN

4.1 Introduction

We calculated the adhesion force and energy based on the DLVO theory in the previous section. Although the theory is useful to provide some estimation about the forces involved, the resultant attractive force showed that the classical DLVO theory does not fit the system at the contact distance. For the calculation of charge interaction, for instance, the net charge for the whole molecule does not implement the system, since it is a distribution of negative and positive charged side chains of residues. Similarly, hydrophobic interaction takes actually place between non-polar residues more locally, instead of whole net non-polar or polar characteristic of a molecule.

Information for molecular packing and higher level structure of a protein is actually carried by primary sequence of a polypeptide chain. However, due to the considerably higher number of residues of a polypeptide, approximately 1000 amino acid in one alpha chain, the success in a study of amino acid level molecular interaction requires a high level computer program that can recognize each amino acid and calculate corresponding interaction depending on user's demand. To achieve that, we used a scripting language, Python.

4.2 Python Analyses

Python is a high-level, interpreted, object-oriented programming language [135] used not only in commercial field, but also in scientific research [136]. It can be built

in the data types in different collections, such as strings, lists, and tuples. We used Python for three purposes in this research:

- For comparison the three main interaction forces, electrostatic, hydration, and polar interaction between the two types of collagen.
- For understanding the origin of the enhanced nucleation observed in Section 6, for the co-assembly of type-I and type-III collagen.
- For analyzing the distribution of the rigid amino acid, Proline for understanding the origin of flexibility.

4.2.1 Interaction forces between the collagen molecules in 1D: electrostatic, hydrophobic, and polar interactions

We investigated the interaction forces including electrostatic, hydrophobic, and polar hydration in one-dimension by using a scripting language, Python. To a first approximation, we consider collagen molecule as a linear molecule of only alpha-1 chain. Therefore, type-I molecule is considered as a homotrimer of alpha-1(I) and type-III molecule is that of alpha-1(III) chain. In our analysis, an alpha chain is arranged at specific staggered positions of 0D (D represents D-periodic space) which means that the molecules are perfectly aligned, 1D, 2D, 3D, and 4D with another alpha chain (Fig.4.1). The system gains score for some specific amino acid pairs in the two sequences located at a given positions for the degree of interaction forces. Note that we used only triple helical part of collagen molecule, which has 1014 and 1026 amino acids in alpha-1 chain of type-I and type-III collagen as polypeptides of a collagen molecule are not composed of G-X-Y motif in which G represents glycine and X and Y represent any other residues except glycine.

The program was written as follows: Two sequences are arrayed perfectly starting

from N-telopeptide end of the molecule (0D). A residue pair of negatively charged (aspartic acid-D, or glutamic acid-E) and positively charged (lysine-K, or arginine-R) side chain was counted as a score of one. Similarly, a pair of hydrophobic side chains (valine-V, methionine-M, isoleucine-I, leucine-L, phenylalanine-F) was given a score of one, since both have an attractive character. On the other hand, a pair of polar amino acids (serine-S, threonine-T, asparginine-N, glutamine-Q) was taken as a score of -1 due to its repulsive character. The rest of the pairs were counted as zero. The resultant score points the level of electrostatic, non-polar (hydrophobic) and polar hydration interactions between that two chains at a given binding position.

One important feature of our analysis is that we considered a range of ∓ 3 for charge interaction and ∓ 2 for hydrophobic and polar interaction as illustrated in Fig.4.2. This means that seven iterations for each amino acid and 1014×7 iterations for one type-I and 1026×7 for one type-III collagen molecule to evaluate the electrostatic interaction. Longer range of the electrostatic force compared to hydration force (hydrophobic/hydrophilic) is reflected by longer interaction range implemented to our program.

Our program continues with the arrangements of 1D, 2D, 3D, and 4D staggered positions, as illustrated in Fig.4.1. Collagen molecule possesses a length of $4.4\times$D where D is 67 nm repetitive banding space. Given the length of alpha-1 chain for type-I molecule, 1014 amino acid, D-periodic space corresponds to 234 ∓ 1 residues, consistent with Hulmes's study [112]. It is known that D-periodic staggered arrangement is more favorable than other random arrangements [112]. For 1D arrangement of the molecules, 234 residues are subtracted from the N-side of the whole chain and this updated range of the sequence is cycled for counting of the total interaction score, as shown in Appendix page from 115 to 123. Note that in the electrostatic interaction code in Appendix page 117, D1 represents the only interacting part of

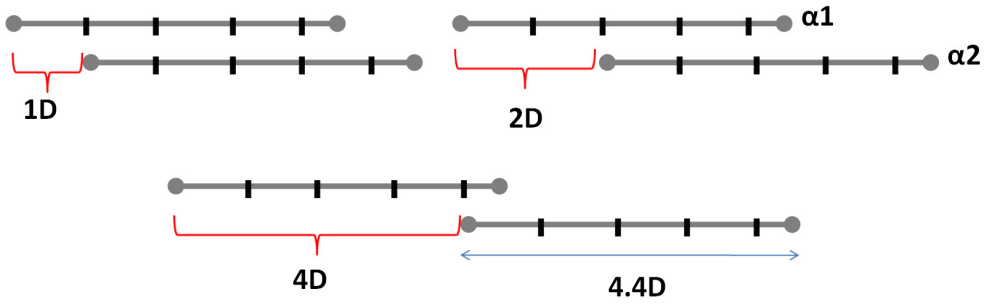

Figure 4.1: The part of our program which counts the electrostatic interaction between type-I molecules at 0D arrangement that means perfectly arrayed.

alpha-1(I) chain and D11 represents the corresponding range of the sequence of the other molecule which could be type-I or type-III collagen. The sequence of alpha-1(I) is given by 'aa1' and 'aa11'.

The program code that counts the hydrophobic interaction between type-I and type-III molecules is shown in Appendix corresponding the heterotypic interaction between the two types. The similar codes were written for type-I molecules, type-III molecules themselves for the homotypic assembly. The 'aa3' in the code represents the whole sequence of type-III collagen chain. Different ranges of alpha-1(III) chain were implemented for the interaction with the other molecule at 2D staggered position (Fig.4.1). Note that, although we limit the range of the second sequence, our program already imposes the range which will be set depending on the type of interaction which could allow +3 or +2 more iterations after the last residue of the first chain. In a similar manner, we build another set of code for the repulsive interaction between polar residues, at 0D, 1D, 2D, 3D, and 4D positions between type-I, type-III and hybrid molecules. For the resultant interaction force, the scores for each specific arrangement and for each interaction pair were calculated by adding the three main forces, the electrostatic, the hydrophobic and the polar hydration. Each and the

Interaction Scores						
		0D	1D	2D	3D	4D
Electrostatic	Type-I:I	125	76	50	27	5
	Type-III:III	129	70	46	28	4
	Type-I:III	79	71	55	25	2
Hydrophobic	Type-I:I	63	22	12	10	2
	Type-III:III	60	15	10	12	1
	Type-I:III	13	11	13	8	1
Polar	Type-I:I	-99	-34	-24	-13	-3
	Type-III:III	-106	-39	-17	-11	-3
	Type-I:III	-36	-27	-20	-12	-6
Total	Type-I:I	89	64	38	24	4
	Type-III:III	83	46	39	29	2
	Type-I:III	56	55	48	21	-3

Table 4.1: The scores calculated by our program for each and the total interaction between type-I, type-III, and type-I:type-III molecules.

net interaction scores were shown by histogram graph in Fig.4.3. For more detailed exhibition of interactions, Table 4.1 is added.

4.2.2 Distribution of proline and hydroxyproline

To understand the flexibility behavior of collagen molecules better, we investigated the distribution of Proline based motif G-P-P in both molecules. Here, G and P are glycine and proline, respectively. For this purpose, we first need to check

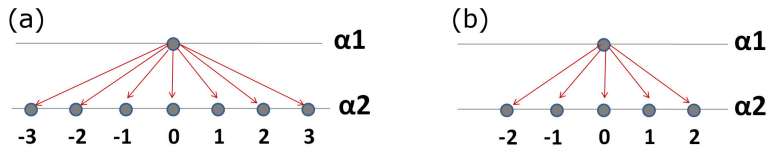

Figure 4.2: Illustration of number of amino acid for each residue considered for (a) electrostatic and (b) hydrophobic and polar interaction. $\alpha 1$ and $\alpha 2$ represent the same sequence for homotypic interaction and different sequences for heterotypic interactions.

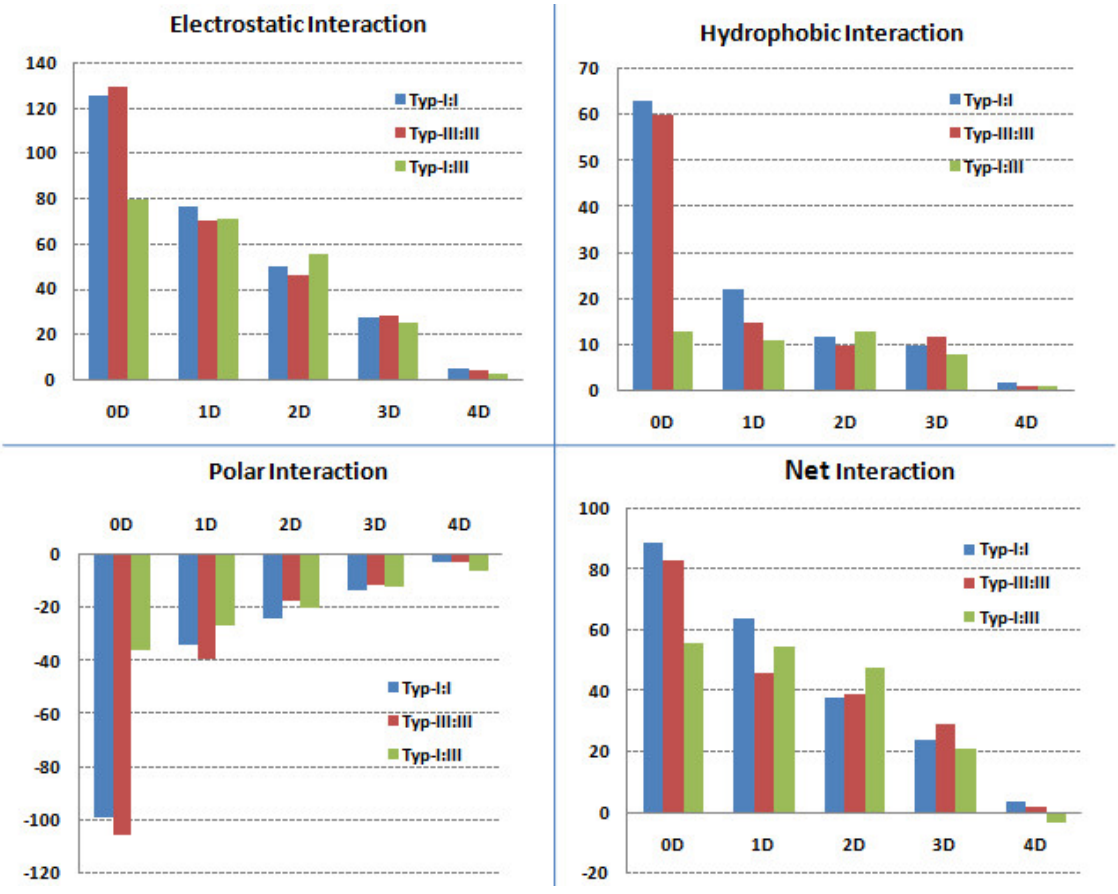

Figure 4.3: The histogram of interaction forces involved in self- and co-assembly of type-I and type-III collagen. a) The electrostatic, b) The hydrophobic, c) The polar, and d) The total interaction between like and unlike molecules.

```
>>> aa1I='GPMGPSGPRGLPGPPGAPGPQGFQGPPGEPGEPGASGPMGPRGPPGPPGKNGDDGEAGKPGRPGER
>>> print(aa1I.replace('M', 'X').replace('S', 'X').replace('R', 'X').replace
replace('A','X').replace('Q', 'X').replace('F', 'X').replace('N', 'X').repla
replace('E', 'X').replace('H', 'X').replace('I', 'X').replace('K', 'X').repl
GPXGPXGPXGXPGPPGXPGPXGXXGPPGXPGXPGXXGPXGPXGPPGPPGXXGXXGXXGXPGXPGXXGPPGPXGXXG
>>> aa1I='GPXGPXGPXGXPGPPGXPGPXGXXGPPGXPGXPGXXGPXGPXGPPGPPGXXGXXGXXGXPGXPGXX
>>> aa1I.replace('GXX','x').replace('GXP','b').replace('GPP','p').replace('G
'aaabpbaxpbbxaappxxxbbxpaxbxbxxxxxxaabbxbxabxbpxxxxxpaapbxxxaxxaxbpaxabxbxxb
>>> aa1I='aaabpbaxpbbxaappxxxbbxpaxbxbxxxxxxaabbxbxabxbpxxxxxpaapbxxxaxxaxbp
>>> len(aa1I)
338
>>> # 338*3 = 1014 as expected. Also, all aa counting was verfied, and doubl
>>> aa1III='GIAGYPGPAGPPGPPGPPGTSGHPGAPGAPGYQGPPGEPGQAGPAGPPGPPGAIGPSGKDGESG
>>>  print(aa1III.replace('M', 'X').replace('S', 'X').replace('R', 'X').repl
replace('A','X').replace('Q', 'X').replace('F', 'X').replace('N', 'X').repla
replace('E', 'X').replace('H', 'X').replace('I', 'X').replace('K', 'X').repl
```

Figure 4.4: The part of the script which replaces amino acids except glycine and proline with X, to check the consistency of G-P-X motif of alpha chain. Note that the figure is cropped from the main program so that the sequence of aa1I continues.

whether the alpha chains obey G-X-Y repetitive elements through the whole length. We kept glycine and proline's position the same and replaced the remaining amino acids (except glycine and proline) with X by using 'replace' function of python, as illustrated in Fig.4.4. Each sequence is divided to motifs of three amino acids G-P-X and its derivations. This part of the program is given in Fig.4.5. Note that the only small part of the sequence is exemplified in that figure (Fig.4.5).

After dividing the sequence to G-X-Y motifs, we named all possible configurations with small letters (e.g. GPP is p, GXX is x, GXP is b, ect.) by performing another 'replace' function. The related part of the script is shown in Fig.4.4 line 8. To check if replacement and division is performed correctly, the 'len' function of the program is used and 338 GXY motifs were found corresponding to the expected 1014 amino acids for alpha-1 chain of type-I molecule. Now we have more detailed information about the distribution of triplet motifs for each sequence. As GPP has the most stiff configuration, we plot the distribution of that to compare the two types in

```
>>> aa='GPXGPXGPXGXPGPPGXPGPXGXXGPP'
>>> [aa[i:i+3] for i in range(0, len(aa), 3)]
['GPX', 'GPX', 'GPX', 'GXP', 'GPP', 'GXP', 'GPX', 'GXX', 'GPP']
```

Figure 4.5: A sample code which splits the amino acid sequence into triplet elements. Note that the sequence used is just a small fraction of the actual amino acid line.

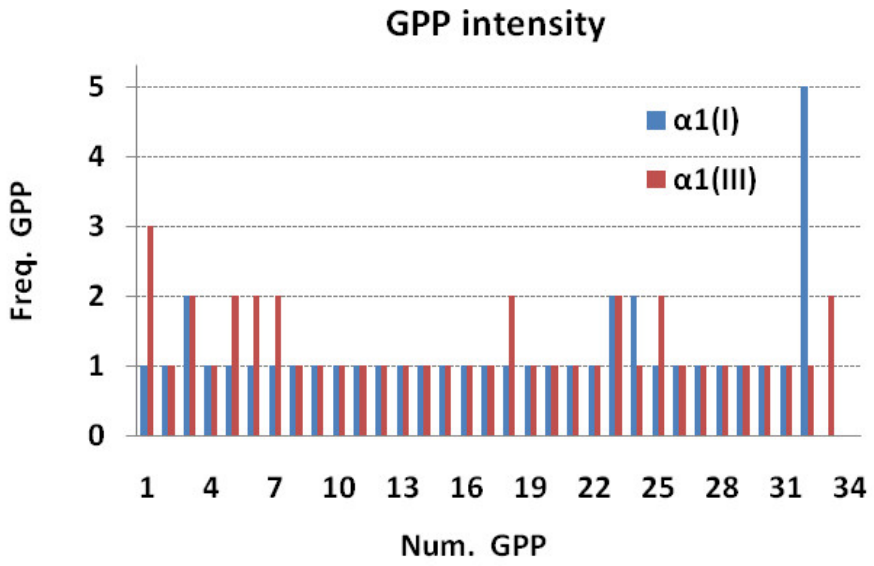

Figure 4.6: Histogram of GPP intensity of alpha1(I) and alpha1(III) chain. The vertical axis represents the frequency of GPP element and the horizontal axis shows the number of GPP through the whole sequence.

Fig.4.6. At the end, alpha-1 chain of type-I molecule has 39 elements, while type-III has 43 of that with more stable distribution. For a sophisticated understanding of the flexibility of each collagen molecules, different analyses and in depth knowledge about the subject is required.

4.3 Results

It is widely accepted that hydrophobic interactions are the dominant forces which build and stabilize the molecular architectures of proteins [137, 138]. In a theoretical work, only hydrophobic attraction between monomers was found to be sufficient to build compact copolymers [137]. With scoring system of only hydrophobic and polar residues, native structures of proteins were recognized with 85% accuracy [139]. Therefore, our hydrophobic interaction plot in Fig.4.3b has further importance. Interestingly, the hydrophobic interaction score of the co-assembly of type-I and type-III collagen (Fig.4.3b) remains approximately constant from 0D to 3D arrangement, even though there are 234 ∓ 1 amino acid difference between each interacting position. That means that 3D location has about 234×3 less amino acid than that of 0D binding location. That gives this force a wide range of interaction opportunities which might result in a dominant and stable factor during the co-assembly process.

The electrostatic interaction graph in Fig.4.3a could provide an estimation regarding to what level that could influence the resultant force and could be monitored by changing a solution pH. At 0D binding site, all the interaction types have maximum value as expected, since the sequences match perfectly leading to a higher number of charge interaction.

Our homotypic assembly experiment showed that type-I collagen nucleates and grows faster than type-III collagen. This phenomenon could be understood better with amino acid level force analysis. The total interaction score reflecting the net force between like molecules are stronger for type-I molecules for most cases, excluding 3D arrangement, which corresponds only 20% of the total binding possibility. That means a higher acceleration for type-I molecules leading to faster nucleation and growth as observed in our experiment (Fig.7.2).

In terms of heterotypic assembly, 4D arrangement is not favorable at all, partly due to nonequivalent length of the two molecular sequences. On the other hand, almost all of the remaining binding sites, particularly the first three arrangements, 0D, 1D, and 2D, have close to a stable level of demand for the assembly between the two types (Fig.4.3). At 2D, the heterotypic assembly even more favorable than the two homotypic assembly of the type-I and type-III collagen. That is actually quite interesting that the two sequences have a special design that is set for the co-assembly at this location. That resembles our synergistic enhancement of nucleation at the sample of mixture(3:1) shown in Fig.7.4.

5. EXPERIMENT

5.1 Materials and Methods

5.1.1 Materials

Two different types of collagen were used to conduct this experiment. Type-I collagen, acetic acid extracted from rat tail tendon, was purchased from BD Biosciences (Bedford, MA), in solubilized form of 3.54 mg/ml concentration. The collagen stock solution was prepared in the concentration of 1.65 mg/ml by diluting with 17.4 mM (0.1%, 0.5 M) acetic acid, and it was stored at 4^0C for use up to 3 months. Glacial acetic acid (500 ml, 17.4 M) was purchased from Biochemistry/Biophysics stockroom at Texas A & M University. 0.5 M (pH $\sim$2) diluted acetic acid was prepared with deionized water (DI). A sample solution of type-I collagen was prepared from this diluted stock solution with a buffer consisting of 30 mM Na_2HPO_4, 10 mM KH_2PO_4 and 200 mM KCl unless stated otherwise, at pH 7. Buffers were renewed once a month due to salt aggregations and dirts.

Type-III collagen, pepsin extracted from bovine skin, was purchased from Millipore Corporation (Temecula, CA) in lyophilized form of 10 mg. 1.25 mg type-III was measured and reconstituted to 1.25 mg/ml aliquots with 1 ml acetic acid of 0.5 M (at ph$\sim$2) by using a mini shaker at 4°C. For the first 30 min, the shaker was adjusted to the speed of 500 rpm. It was observed as homogeneous, but by setting the speed 400 rpm, the aliquot was kept in the shaker (at 4°C) about 2 h more to make sure that it was dissolved well. Dissolving may sometimes take longer time like overnight. The reconstituted 1.25 mg/ml type-III aliquot was divided into 10 aliquots of small volume and stored at -20°C up to one year from the date of receipt. The working type-III source was further diluted to 1 mg/ml by adding acetic acid

(0.5 M) and maintained at 4°C for short time using. With the same buffer indicated above, the sample solution of type-III collagen was prepared for deposition on mica. The rest of the type-III source was kept in -80°C for future using.

For AFM imaging substrate, muscovite mica disk (grade VI) were purchased from Ted Pella, Inc. (Redding, CA), and phlogopite mica sheets were ordered from Axim Mica (New Hyde Park, NY).

5.1.2 Sample preparation

Mica sheets were glued onto AFM metal disks and freshly cleaved by sticky tape ∼60 sec before each experiment. 50 μl of the sample solution was applied onto mica and deposited at room temperature for a given incubation time in a moisture chamber to minimize evaporation. Unabsorbed collagen was then rinsed away with 70 μl of DI (Deionized) water in multiple directions and was left to air-dry in room temperature for 15 min with a half-covered dish to protect the surface covered with assembled fibrils from unwanted substances/dirts. When the sample surface was dry, the AFM topography imaging was performed immediately, to minimize the contamination on the sample surface of the assembled collagen matrix. Same day scanning is highly recommended. If not, one should make sure that the sample is protected well by sealing the dish and by making the sample stable in dish by double side type.

5.1.3 Atomic force microscopy (AFM) imaging and image processing

Imaging experiments were carried out with different models of AFM at tapping mode. AFM CP-II instrument (Veeco, Camarillo, CA) was operated for Figure 2.3, Figure 6.1, Figure 6.2, Figure 6.3, Figure 8.4, Figure 8.5, Figure 8.7, Figure 8.11, Figure 8.10, Figure 8.12, Figure 8.13, Figure 8.14, Figure 8.15, Figure **??**, Figure

8.17, Figure 8.18, Figure 8.19, Figure 8.20, Figure 8.21, Figure 8.22, and Figure 8.23, AFM NanoScope IIIa (Multi Mode TM, Veeco) for Figure 7.1, Figure 7.2, Figure 7.8, Figure 8.2, Figure 8.3, and Figure **??** and Bruker Dimension Icon AFM was operated for Figure 5.2, Figure 6.7, Figure 7.4, Figure 7.7, and Figure 7.3, Figure 8.1, Figure 8.6, Figure 8.8, Figure 7.9 in the soft non-contact tapping mode (NCM) at room temperature in the laboratory environment. We used none-coating Si Force Modulation point probe from Nano Word with a force constant of 2.8 N/m, and dimension of 225 μ m (length) x 28 μ m (width) x 3 μ m (thickness), and resonance frequency of 75 kHz for Icon AFM scannings. FESP7 (Veeco Probes) silicon probe with a nominal force constant of 2.8 N/m was used. The samples were scanned with a speed of 0.5-2 Hz depending on the scan area. Di-SPMLab and Nanoscope SPM 4.42r8 software was used for image analysis and processing for AFM CPII and NanoScope IIIa, respectively. Line analysis was performed on height, diameter, and length of the collagen molecules and the fibrils.

All of experiments were conducted at room temperature and they were reproduced three times.

5.1.4 Data analysis

For qualitative data analysis of each sample of the homotypic and the heterotypic self-assembly, Image-J (Scientific image analysis software) were used (see Figure 5.1) [140]. The original AFM scan was first converted to an 8-bit type of image to set the threshold. Smoothen, sharpen, background subtraction, auto or local threshold, and binary are some of the image processes used to increase quality of the images depending on the roughness of the original scan. Measurement and particle analysis tool were used after image processing to analyse collagen scans.

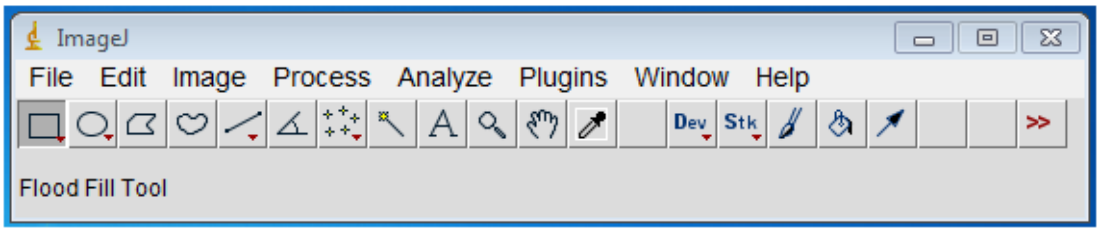

Figure 5.1: Image-J window when installed (Scientific image analysis software).

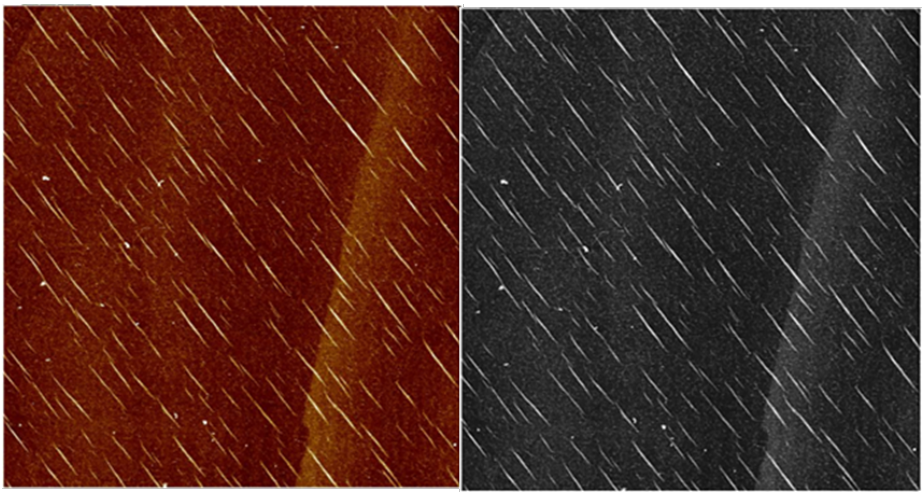

Figure 5.2: The original AFM image of mixture(3:1) sample opened with Image-J (left) and 8-bit type of image of the original scan to start the image processing with an adjusted threshold of the original AFM image (right).

5.2 Atomic Force Microscopy

Atomic force microscopy (AFM) or scanning force microscopy (SFM) was invented in 1986 by Binnig and Quate [141]. It is one of the highest resolution scanning probe microscopy. Working principle of AFM is based on the interaction force between the atoms of a tip and a sample surface. The sample surface is scanned with

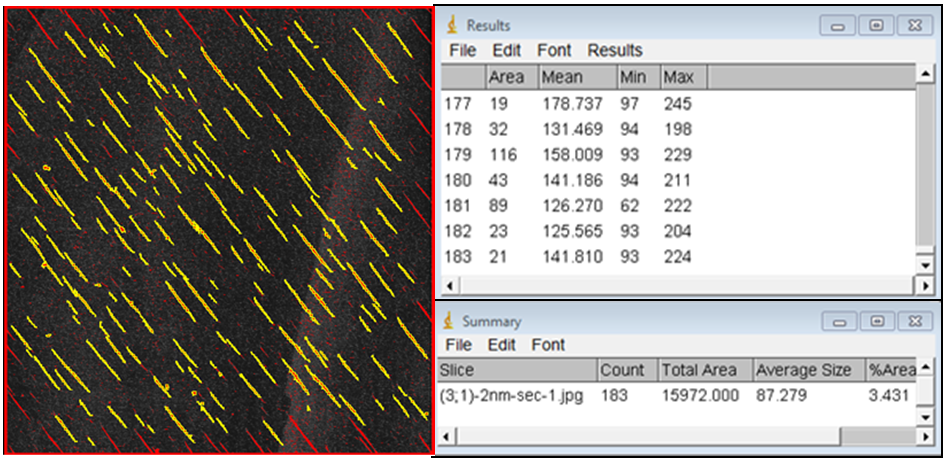

Figure 5.3: The final image after processing used for analysis (left). The result and the summary tables produced by Image-J after particle analysis tool applied (right).

an ultra small, sharp tip attached to a flexible cantilever with a low spring constant. As the tip approaches the surface, it starts to feel the interaction force between the tip and the sample. The force is kept the same throughout the experiment by piezo-electric scanner by changing the position of cantilever . As the sample is scanned, the change on the position of the cantilever is used as a feedback control. Depending on the magnitude of the force, the cantilever bends or contract. The deflection occurred on the cantilever is recorded by position sensitive photodetector exposed the reflected laser beam which is focused on the cantilever as demonstrated in Figure 5.4. Depending on the deflection, the force exerted by the tip is measured via Hooke's law as a function of distance between the tip and the surface. Image of the sample is created by horizontal and vertical movement of the piezo scanner [142, 143].

Hard sample surfaces can be imaged with AFM without damage, since the interactomic spring constant of the sample is on the order of 10 N/m. The spring constant of typical AFM cantilevers is in the range of 0.01-1 N/m meaning that the applied force on the cantilever is much lower than the force which would change the atomic

sites of the sample. On the other hand, there are challenges on imaging soft biological samples like proteins with AFM. They can be easily damaged by contact mode in which the tip touches the surface. The another imaging method is non-contact mode in which the tip oscillates on the sample surface and the changes on the amplitude of the oscillation is used to create the topography of the image. The forces involved in non-contact mode is on the scale of piconewton(pN), $10^{-12}N$, compared to $10^{-9}N$ in contact mode. Therefore, even the softest samples can be scanned without damage. However, the signal detection is another challenge due to very low magnitude of the force. More detailed discussion about imaging of biological samples with AFM is provided in Section 7.

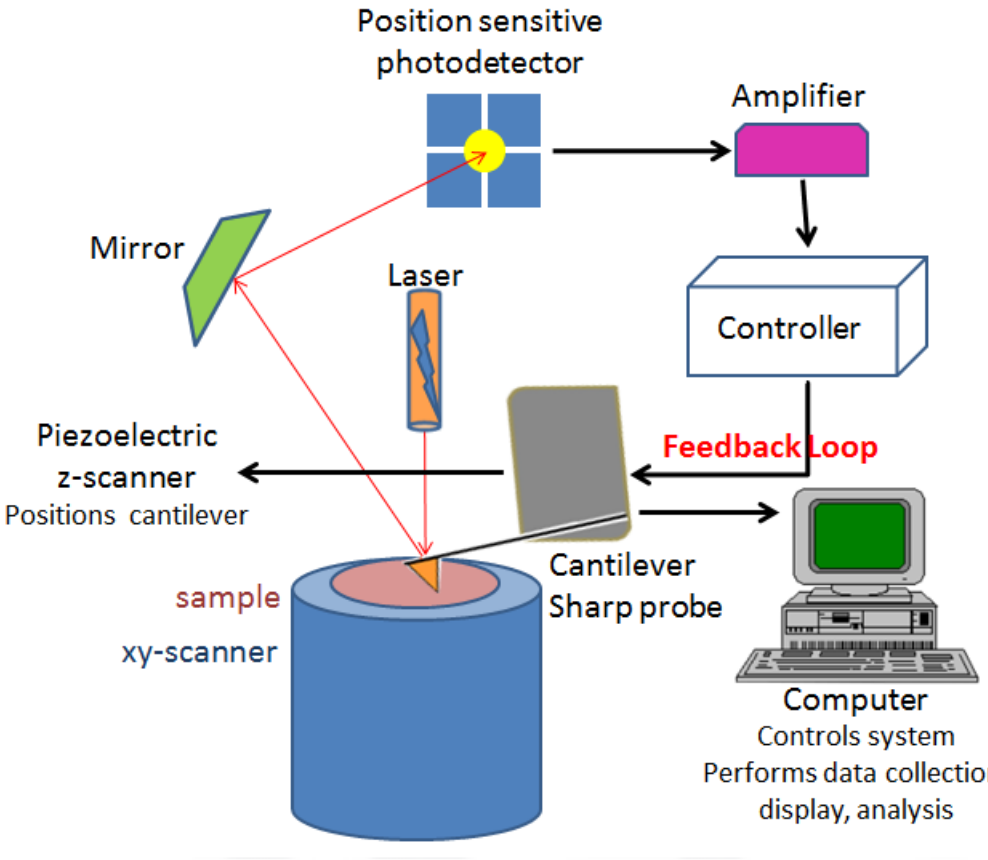

Figure 5.4: The general principle and components of AFM. The laser is focused on the cantilever and the changes in the angle of the reflected beam is detected by photosensitive detector.

6. SURFACE PATTERNING VIA SELF ASSEMBLY OF COLLAGEN

6.1 Epitaxially Guided Self-Assembly

Self-assembly ability of biomolecules on a solid substrate is a promising way of fabricating ordered structures at the nanometer level. Collagen type-I is used to coat non-biological materials [14, 144, 15, 145]. Self-assembly of type-I collagen has been investigated *in vitro* with varying micro environmental conditions such as temperature [146], pH [39, 4], ionic strength [133], and concentration [147, 4]. Another important factor which influences the assembly process *in vivo* is the existence of different types of collagen during the self-assembly. For typical connective tissues, such heterotypic fibrils co-assembles with two or more types of collagen. This is a new area to investigate the heterotypic assembly mechanism, with high resolution imaging technique, AFM [29] which is going to be addressed in the next section.

It was found that the buffer condition has a significant influence on the self-assembly mechanism [12, 39]. In this study, we investigated the influence of K^+ ion on the self-assembly process at the first half and after 2 h of the deposition on muscovite mica and phlogopite mica to understand the potassium ion effect on different substrates. The results showed that collagen self-assemblies to variety of morphologies depending on the substrate, the concentration of K^+ and the time of deposition.

6.2 Time and K^+ Ion Dependent Self-Assembly of Collagen

6.2.1 Assembly on muscovite mica

We have observed the growth steps of collagen fibrils as a function of time and KCl concentration in Figure 6.1. 5 $\mu g/ml$ concentration of type-I collagen with 100

mM KCl shows microfibrils aligned in three different directions separated by 60^0 at 30 min of deposition. However, two of them are predominate as indicated by the arrows in Figure 6.1. At 2 h, we have observed an image similar to that of 30 min incubation, but the direction of fibrils are reduced to two, with a dominant one and a higher fibril diameter as shown (Figure 6.1b). The two similar collagen matrices in the presence of 100 mM KCl (Figure 6.1a,b) point out that the molecules stick to mica strongly which inhibits mobility and reconstitution the morphology during the self-assembly mechanism. Strong adhesion is an obstacle to relaxed assembly.

When we increase the KCl concentration of the buffer solution from 100 mM to 200 mM, we have observed an interesting result. At 30 min of deposition, a unidirectional fibril network appeared with loose packed and native like organization of D-periodic structure of collagen (see Figure 6.1c). This structure organized to a more tightly packed, highly aligned and higher diameter of collagen fibrils at 2 h of self-assembly, covered almost the entire mica domain spanning more than hundreds of micrometers. The increase of the relative magnitude of collagen-collagen interaction is provided by the decrease of substrate-collagen interaction with lowered affinity of mica to collagen. With increased K^+ ion on the buffer solution, collagen molecules adsorb less and move with higher diffusivity. K^+ ion occupancy of muscovite mica surface were found to vary from more than 50% to near 100% as the concentration of KCl increases from 10 to 500 mM [148]. This means that in all of our experiments, unoccupied K^+ pockets present on the mica surface (Figure 6.5) leaving the surface negatively charged, which is a prerequisite of the adsorption stage of the assembly process.

6.2.2 Assembly on phlogopite mica

To understand the effect of substrate on the self-assembly process, we have investigated the assembly on a different substrate, phlogopite mica. At 30 min of deposition, 5 $\mu g/ml$ collagen with 100 mM KCl, three different directions of alignment are seen separated by 120^0 as shown in Figure 6.2a. Less fibril density with higher diameter and longer fibril length were observed compared to the assembly on muscovite mica under the same experimental condition (see Figure 6.1a). In time, fibrils grow further and triaxial structure of the collagen matrix become more apparent (see Figure 6.2b). The remarkable difference between the two sets of experiments (see Figure 6.1a and Figure 6.2a), is that the growth rate of collagen fibrils, in another saying the assembly kinetics of collagen molecules, is faster on phlogopite mica than that on muscovite. This result is in agreement with finding that phlogopite mica has lower affinity to collagen than that of muscovite mica [116]. Lower affinity of phlogopite promotes the growing kinetics leading longer and higher fibrils.

The higher concentration of KCl, 200 mM, reveals the three directions of collagen fibrils at 30 min of deposition with even higher fibril diameter and longer fibril length than the stage of 2 h deposition at the condition of 100 mM KCl (Figure 6.2b versus Figure 6.2c). After 2 h incubation, a triangular pattern of fibrils is observed via self-assembly ability of collagen molecules which is going to be utilized to investigate and characterize the future heterotypic self-assembly mechanism in the next section. By monitoring K^+ ion effect on the assembly and manipulating the fibril formation mechanism, we resulted in two different, ultrathin, nanoscopically patterned templates for our next study of the heterotypic self-assembly mechanism of type-I and type-III collagen.

The statistical analysis which were performed with Image-J over 25 data points

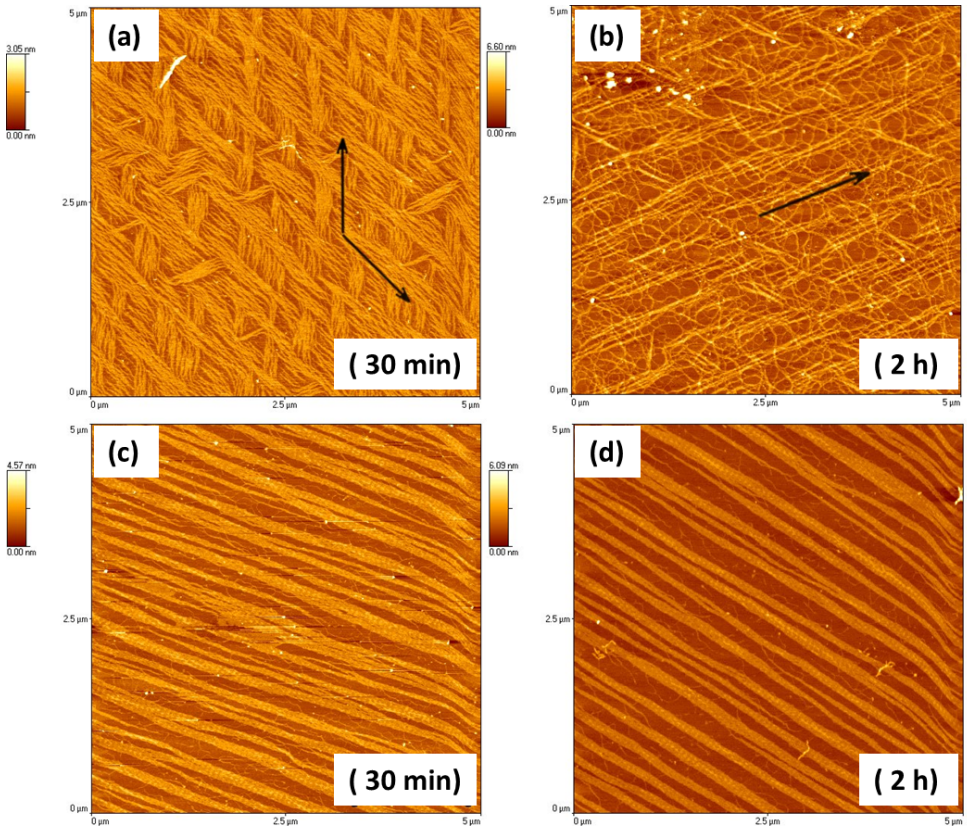

Figure 6.1: Effect of K^+ ion on the assembly mechanism of type-I collagen on muscovite mica surface: All images are with 5 $\mu g/ml$ collagen in a buffer solution containing of 30 mM Na_2HPO_4, 10 mM KH_2PO_4 and (a, b) 100 mM KCl, (c, d) 200 mM KCl at pH 7. (a, c) Assembly morphology of 30 min, and (b, d) 2 h of the incubation.

of the two samples of Figure 6.1a, and Figure 6.2a shows the effect of substrate on the assembly of collagen. The average thickness of collagen fibril was measured 9 ± 2 nm on muscovite mica, while it is 23 ± 5 nm on phlogopite mica under the same experimental condition over the chosen thinnest fibrils on the substrates.

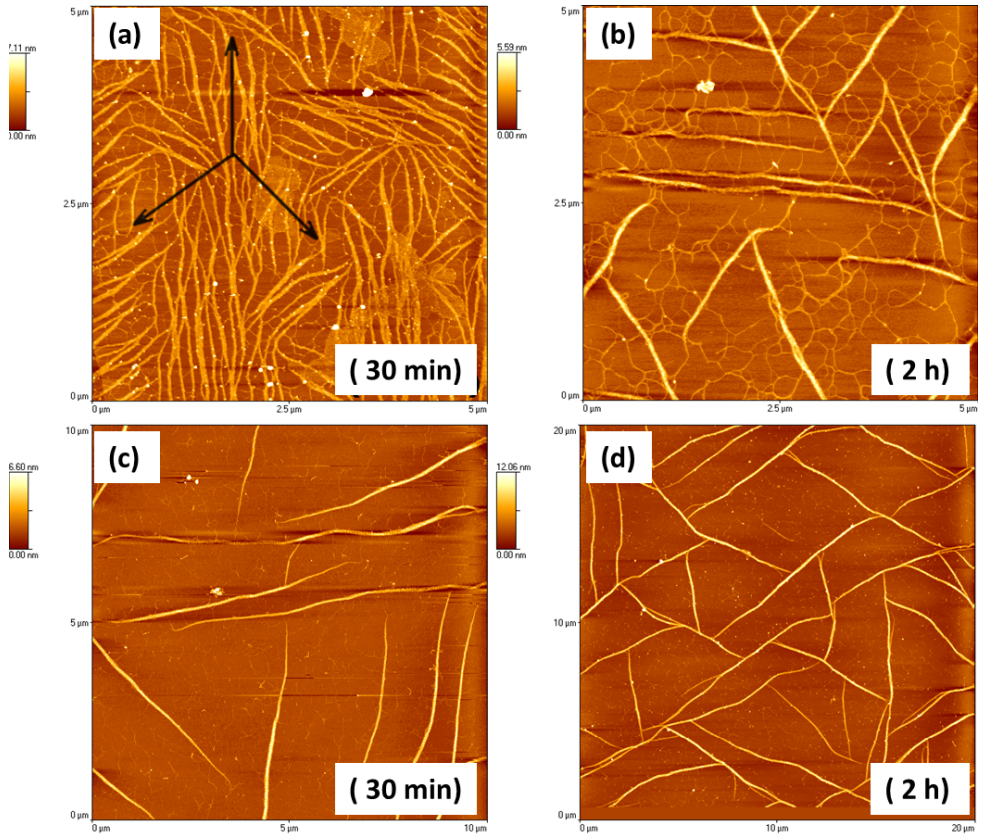

Figure 6.2: Effect of K^+ ion on on the assembly of type-I collagen on phlogopite mica: All images are with 5 $\mu g/ml$ collagen in a buffer solution containing of 30 mM Na_2HPO_4, 10 mM KH_2PO_4 and (a, b) 100 mM KCl, (c, d) 200 mM KCl at pH 7. (a, c) Assembly morphology at 30 min, (b, d) 2 h incubation time.

6.3 Structure of Muscovite and Phlogopite Mica

Micas, specifically the muscovite mica, are the most widely used substrate for AFM due to their perfect cleavage along the (001) plane, and they have highly charged and chemically rich surfaces [149]. Atomic structure of the tetrahedral sheet of dioctahedral muscovite mica and trioctahedral phlogopite mica are modelled in our previous study [4]. Surface topographies of both substrates were provided with AFM indicating a tilted hexagonal symmetry on muscovite and close to a perfect hexagonal symmetry on phlogopite mica [150]. The distortion of the lattice on muscovite [151, 150, 152, 153] is apparent as the atoms lack vertical alignment as seen in Figure 6.5. Phlogopite mica, on the other hand, has a more symmetric structure with more vertically aligned atoms. Another important difference between the two types of mica is the orientation of the OH group in the octahedral sheet [4]. The O-H...K^+ distance is also shorter in phlogopite, 3.3 $\mathring{A}$, while it is 3.9 $\mathring{A}$ in muscovite mica. With the H atom in the hydroxyl group having a partial positive charge, K^+ ion binds less strongly to phlogopite [116], which is consistent with the weaker binding and the higher thickness of collagen fibrils observed in our records (see Figure 6.1, Figure 6.2).

We used the two types of substrates muscovite and phlogopite mica in this study. AFM topography image of muscovite mica showed broken hexagonal surface symmetry and close to a perfect hexagonal symmetry on phlogopite mica [150]. Much larger degree of surface relaxation on muscovite upon removing of the K interlayer with cleavage created a negatively charged arrays on the surface [150], and it is suggested that the unique direction of the alignment of collagen fibrils in Figure 6.3a produced by oxygen atoms on muscovite surface [154]. We have also reported in the previous study that the hexagonal surface symmetry of phlogopite mica leads to

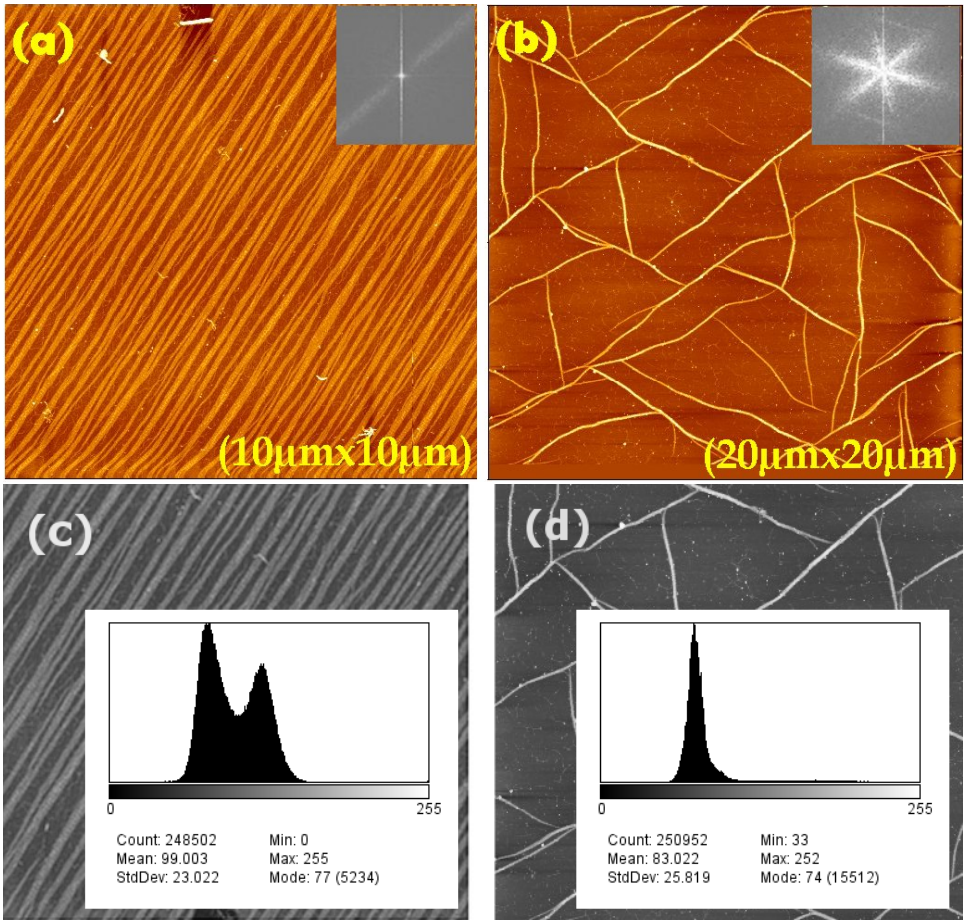

Figure 6.3: Collagen matrices fabricated by the self-assembly of 5 $\mu g/ml$ type-I collagen at 1 h deposition on (a) muscovite and (b) phlogopite mica in a buffer solution consisting of 30 mM Na_2HPO_4, 10 mM KH_2PO_4, and 200 mM KCl at physiological pH (pH 7). Under the appropriate condition, collagen molecules result in triaxial pattern on phlogopite and highly unidirectional alignment on muscovite mica pointing out the surface topography of the underlying lattice of the substrates. Color scale corresponds to a vertical range of (a) 5.33 nm and (b) 12.06 nm. The insets are Fast Fourier Transform (FFT) data of the images. (c-d) Histogram analysis of image (a) and (b), respectively, on the gray scale.

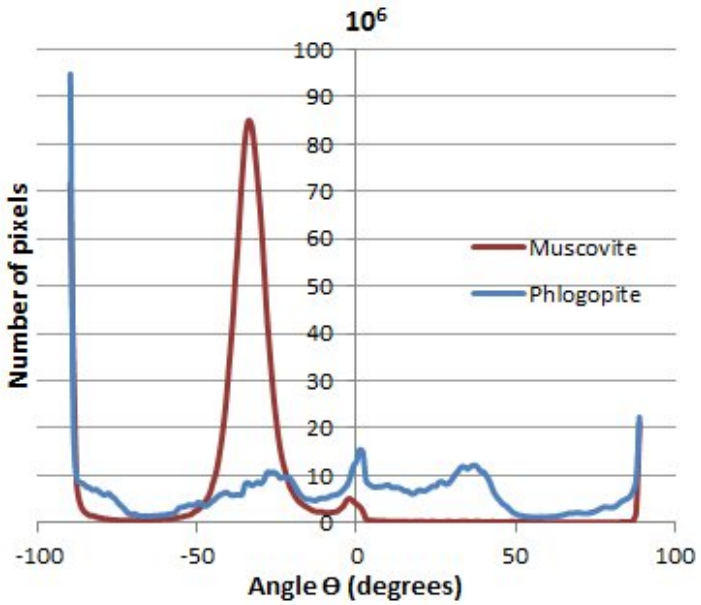

Figure 6.4: Orientational distribution of collagen network of Figure 6.3 showing a dominant unidirectional alignment at -34^0 for muscovite and three peaks at $-28^0, 1^0$ and -33^0 for phlogopite mica.

formation of a triangular collagen network at three growth directions separated by 60^0 from each other [5]. Thus, by using the effect of the lattice of the underlying substrate and K^+ ion on the self-assembly process, we produced a unidirectional and triangular network of collagen fibrils on muscovite and phlogopite mica, respectively, as seen in Figure 6.3 including insets showing Fast Fourier Transform (FFT). Figure 6.4 shows the orientational distribution of both images indicating one dominant direction on muscovite mica while three direction with an almost equal mode on phlogopite mica.

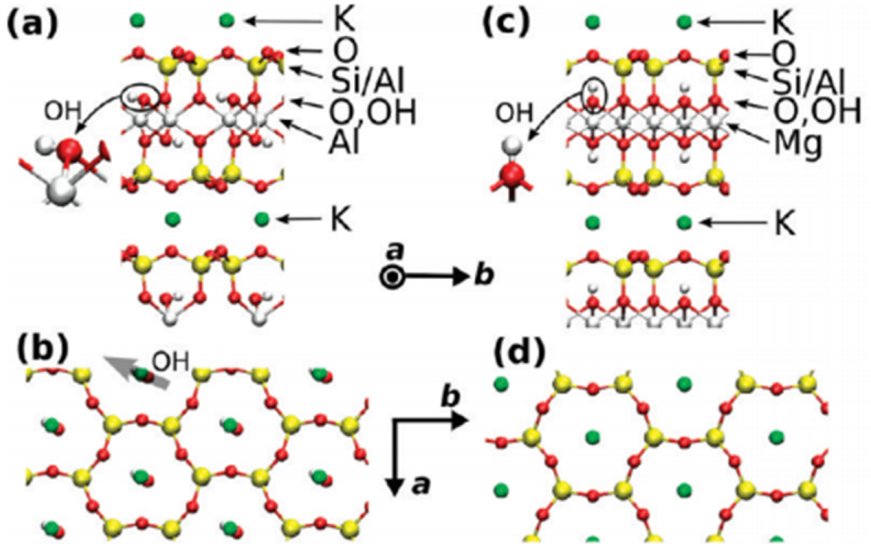

Figure 6.5: Schematic representation of muscovite (a, b) and phlogopite mica atomic structure (c, d). Muscovite contains aluminium in the center layer, while phlogopite has magnesium. The insets show different orientation of the OH groups in the two lattices. Proximity and position of OH group to K^+ atom in phlogopite reduces the affinity of collagen. Atoms are vertically aligned in phlogopite compared to muscovite mica. (a, c) View from the a axis of the unit cell. (b, d) View from above the cleavage plane (ab plane. Only top layer including K, O, Si/Al are shown for clarity. In (b), the OH group is also shown to indicate its direction of tilt (transparent grey arrow) [4].

6.4 Model Systems to Investigate the Homotypic/Heterotypic Assembly Process

When collagen molecules self-assemble on a solid surface, their growth direction is controlled by the lattice structure of the underlying substrate (Figure 6.6. This so-called orientational linear epitaxy (OLE) observed in many biological and non-biological systems [4, 155, 156, 157, 158] is studied with a new developed computational and theoretical model provided in our previous study as shown in Figure 6.7 [5]. In OLE model, when molecules deposits on the substrate, they are absorbed, diffuse on the surface and nucleate into fibrils. The growth direction is determined in the nucleation step. After they start growing linearly, when they encounter the other fibril, they stop.

In our model of OLE [5], filaments nucleate with rate n (per unit time in a square substrate of width w). After nucleation, they grow with rate g which is a system dependent parameter. The OLE process can be divided conceptually into three stages: (i) early nucleation where filaments grow on mostly empty substrate, (ii) encounters among the early-formed filaments, and (iii) self-similar network formation. Stage (i) lasts longer for smaller n (sparser filaments) and smaller g (slower elongation). In stage (ii), filaments are still sparsely distributed and growth terminates mostly by random encounters. In stage (iii), the substrate is divided into polygons possessing a given orientational symmetry, which are divided by new filaments into progressively smaller ones in a roughly self-similar manner.

We use a mean-field theory (MFT) for stage (i) since filaments grow independently [5]. Let L be the filament length (number of subunits). The master equation for its

distribution $P_L(t)$ at time t is

$$\begin{aligned} \dot{P}_1 &= n - gP_1 \\ \dot{P}_1 &= g(P_{L-1} - P_L), (L > 1) \end{aligned} \tag{6.1}$$

Here, n describes the increase in P_1 by nucleation. The gain (gP_{L-1}) and loss ($-P_L$) terms are due to subunit addition.

To consider encounters among filaments in stage (ii), we add second-order interaction terms to Eqn 6.1. The solution to Eqn. 6.1 is given as an asymptotic exponential function. After the MFT-like growth of initially nucleated filaments, shorter filaments start to increase in number as their growth becomes limited. Similar to Eqn 6.1, P_L for long filaments is exponential, e^{-kL} for stage (ii). Later on, P_L becomes a power law as shorter filaments progressively fill smaller areas with similar geometric features determined by the orientational symmetry of the network ($P_L \sim L^{-b}$).

Our model of OLE provides a general framework for understanding sterically limited filament assembly on surfaces. By utilizing the underlying substrate effect, we have founded that muscovite and phlogopite mica create different pattern structures under an appropriate conditions [4]. Thus, we fabricated two templates patterned by self-assembly of collagen fibrils (see Figure 6.3). These triangular and unidirectional patterned surfaces will be used as templates for our next part of the project on the homotypic and the heterotypic self-assembly of type-I and type-III collagen.

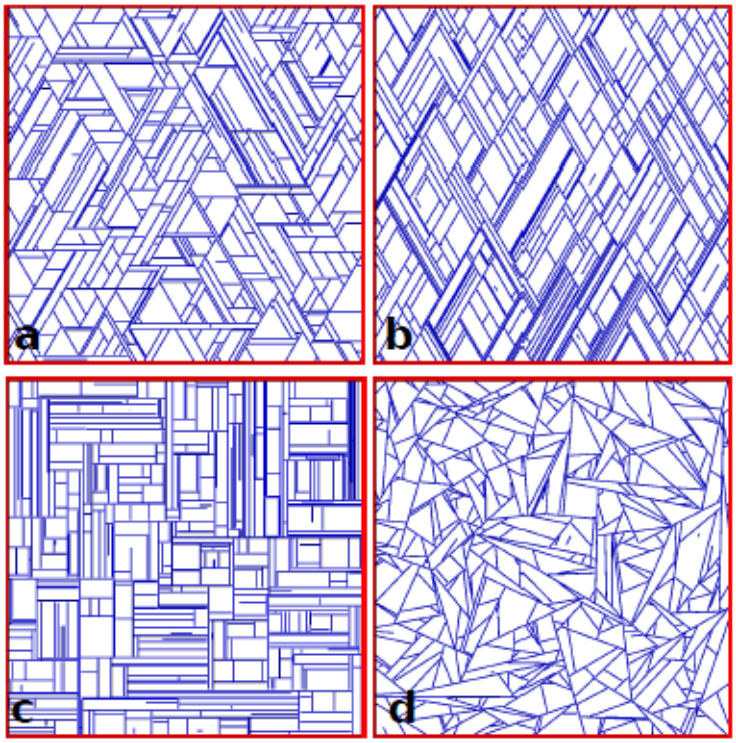

Figure 6.6: Stochastic simulation of four types of OLE networks that have been experimentally observed: **a.** Triaxial [14,16,26], **b.** biaxial [7,9], **c.**regtangular [1,2,11], and **d.** random [21-24, 8]. **a,b** form on hexagonal lattices, notably on mica. **c** forms on cubic lattices such as KCl. **d** forms when the orientational bias not strong.

6.5 Discussion

Mica lattices have layers of potassium between silicate sheets separating with a distance of 9.98 $\mathring{A}$ for muscovite and 10.24 $\mathring{A}$ for phlogopite mica. These layers become the cleavage plane [159] and provide an atomically clean surface after each cleavage. Cleaving takes about the half of the potassium out and leaving the surface a negatively charged with empty K^+ binding pockets. On the other hand, collagen is positively charged at neutral pH due to its high isoelectric point IEP of 9.3. Therefore, the amount of K^+ ion in the buffer solution is important for the assembly process. If there exist insufficient amount of potassium ion in the buffer,

positively charged collagen molecules will adsorb to the partially negatively charged mica surface strongly and will diffuse less, as the surface K^+ occupancy on muscovite mica reach to 100% at the concentration of 500 mM KCl [148]. However, a sufficient amount of potassium will fill the empty pockets on the surface decreasing the binding affinity of collagen to mica. That means a higher freedom given to collagen molecules promoting its mobility on the surface. This increases the possibility to orient molecules through the underlying surface lattice [4]. We showed that the insufficient K^+ ion in the buffer solution reduces the ability of movement of collagen molecules with a higher collagen-substrate interaction and affects the network morphology during the fibril formation process.

We have found that to obtain formed network of collagen fibrils, the surface adsorption should not be too strong as it inhibits fibril formation by constraining the mobility of collagen molecules. This prevents them to aggregate and to form elongated fibrils as seen in Figure 6.1, and Figure 6.2. At higher concentration of K^+ ion, the assembly could not initiate either, as the adsorption could reduce too much and fibrils can not form on the substrate, but just globular forms of the molecules on phlogopite [4].

The function of potassium ion was tested with other alkali cations and found that 10-fold more sodium ion Na^+ is required to provide effect comparable to that of potassium [133]. It is also observed that Cl^- ion does not have a significant effect on the binding affinity during the assembly [133]. These findings indicates that K^+ ion binds more tightly to the mica surface and the function of potassium is not only limited to a neutralization level. The high potassium selectivity of mica [160] may play a greater role on the assembly mechanism, since K^+ promotes the surface assembly more strongly than other alkali ions do [134, 133].

Another possible effect of increased concentration of KCl could be on the elec-

trostatic interaction between molecules. Decreasing Debye screening length with increasing concentration of KCl may assist with the bundling of collagen molecules in Figure 6.1 and Figure 6.2. However, Debye length varies in the range of between 7.9 $\mathring{A}$ to 5.5 $\mathring{A}$, with other electrolyte in the buffer, when the concentration of KCl increase from 50 mM to 200 mM. Therefore, the effect of this fairly short change of KCl on the electrostatic interaction is unlikely to be significant.

Interaction of collagen with mica surface will be mediated by van der walls forces across the entire molecule. However, electrostatic interaction between negatively charged mica and positively charged amino acid side chains on the collagen has a more local effect. More importantly, the hydration shells formed around these charged groups [161, 160, 122] has a lubricating effect which will promote surface diffusion as in the case of high [KCl] in Figure 6.1 and Figure 6.2. Despite these possible approaches to explain the mechanism underneath, it is still unclear how mica guides the growth direction of the large and flexible collagen molecule. In reality, it is likely that the the growth direction is determined by interplay between multiple factors, including surface topography and electrostatic interactions.

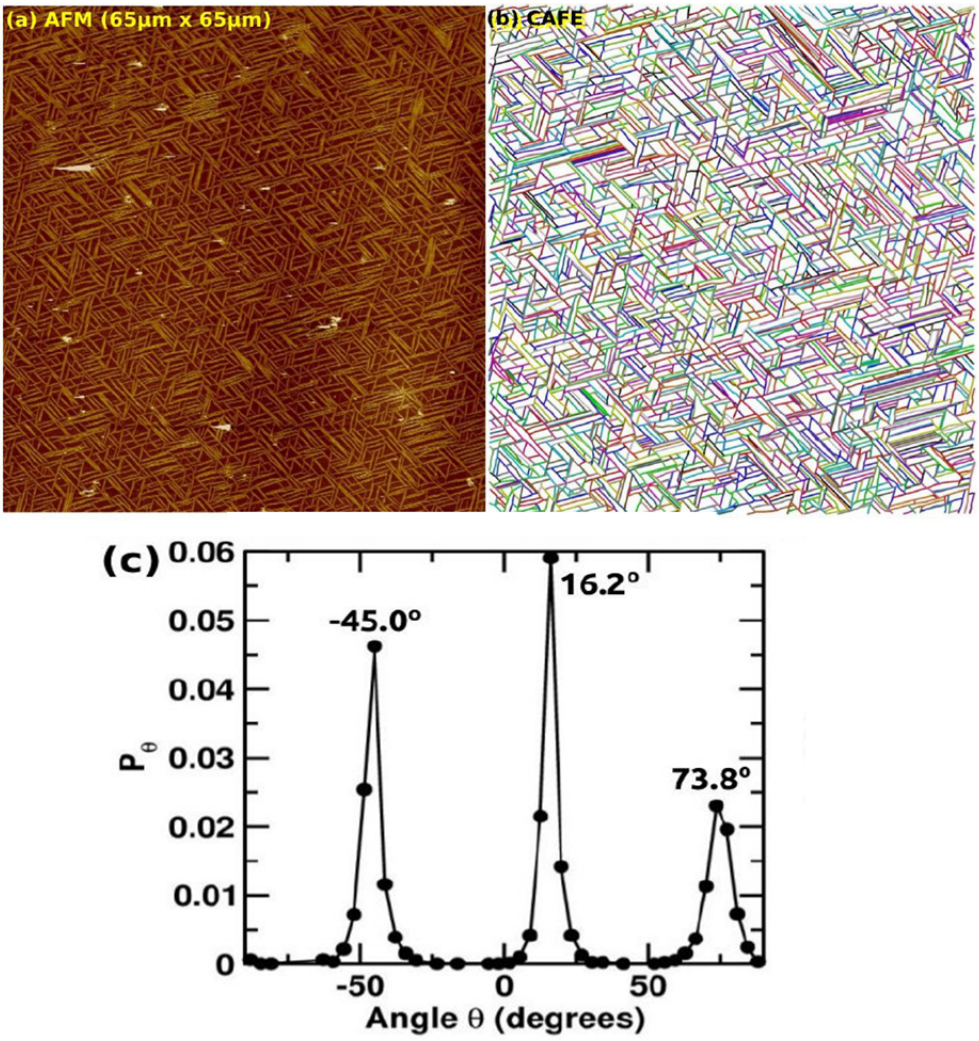

Figure 6.7: Analysis of a triaxial collagen network. (a) AFM scan of concentration of 5 $\mu g/ml$ after 5 h deposition on phlogopite mica. (b) Corresponding in silico network extracted via CAFE (Computer-Aided Feature Extraction program). Filaments are individually recognized and coloured randomly. (c) Filament angle distribution. Angle θ is measured relative to the horizontal direction in (a) [5].

7. CO-ASSEMBLY OF TYPE-I AND TYPE-III COLLAGEN

7.1 Introduction

Co-assembly of proteins is important in both biomedical and biomaterial applications. Tissues have unique ECM composition and morphology. The ECM is mostly composed of fibrillar proteins, collagen with its various types, to give structural strength and integrity to tissues and to support resident cells. With its diverse nature and composition, ECM can serve many functions such as cellular communication, cell growth, migration, and differentiation [162]. However, there are only limited number of studies investigating the heterogeneity of ECM on a solid surface, which is not only of scientific importance, but also is implicated in interactions between medical implants and biological tissues. Biochemical and morphological properties of adsorbed matrix of collagen type-I, type-III, and fibronectin onto titanium surface with very high concentration (500 $\mu g/ml$) were investigated [21]. Structural and rheological properties of collagen type-I and type-V composition were studied and found that type-V collagen lowers the stiffness of reconstituted heterotypic network [29]. Co-assembly of type-I collagen with decorin which is a connective tissue component binding to type-I was studied, and an increase on the tensile stress of hybrid fibril was evaluated upon incorporation of decorin [163]. Likewise, collagen type-I and type-III molecules present in many tissues in a cooperation. To understand co-assembly of the two types may help to interpret the communication between cells and ECM. As a first step for understanding this, we investigated the heterotypic self-assembly of type-I and type-III collagen of low concentration (most 5 $\mu g/ml$) on mica surfaces by utilizing AFM.

7.2 Monomer Analysis

To characterize the monomer molecules of the two types, we used a concentration of 0.3 $\mu g/ml$, well below the critical concentration for collagen fibrillogenesis in bulk solution (4.73 $\mu g/ml$ at 29 ^0C) [108]. At 85 s, randomly adsorbed molecules of both types are observed on the surface. They are approximately 200-350 nm in length, corresponding to the length of a single collagen molecule [85, 164]. The mean length of type-III was measured as 247.4 nm, while it is 203.7 nm for type-I in a good proximity with the end-to-end distance 220 nm for type-I and 259 nm for type-III reported by Silver and Birk [165]. The mean length was measured with N=13 molecules for type-III and with N=12 molecules for type-I analysis from two images. The results verified that the length of triple helix is slightly longer for type-III than that of type-I [100, 101]. That actually raises a question. Type-I source from BD Bioscience is acid extracted collagen, so we expect to have a monomer triple helix with telopeptide ends which means the length of 1056 amino acids for alpha-I chain according to Table 7.1. On the other hand, type-III molecule from Milipore undergoes milk pepsin treatment during the extraction process meaning broken telopeptides from the helical part which corresponds to 1026 amino acids. That contradiction could be either related to the heterotypic triple helical structure of type-I molecule versus homotypic triple helix of type-III or pepsin extraction does not completely remove telopeptides as provided before [166, 167]. The second contradiction is that the monomer molecules of type-I show rod-like structure, whereas type-III molecules are more flexible with its frequent bends and sharp kinks in Figure 7.1 [168]. This either contradicts with the study of Paterlini [169] and the diagram suggested by Silver [168] offering that the source of flexibility is lack of proline and hydroxiproline, because type-III has them more than type-I, 744 versus 667, or homo/hetero-trimer

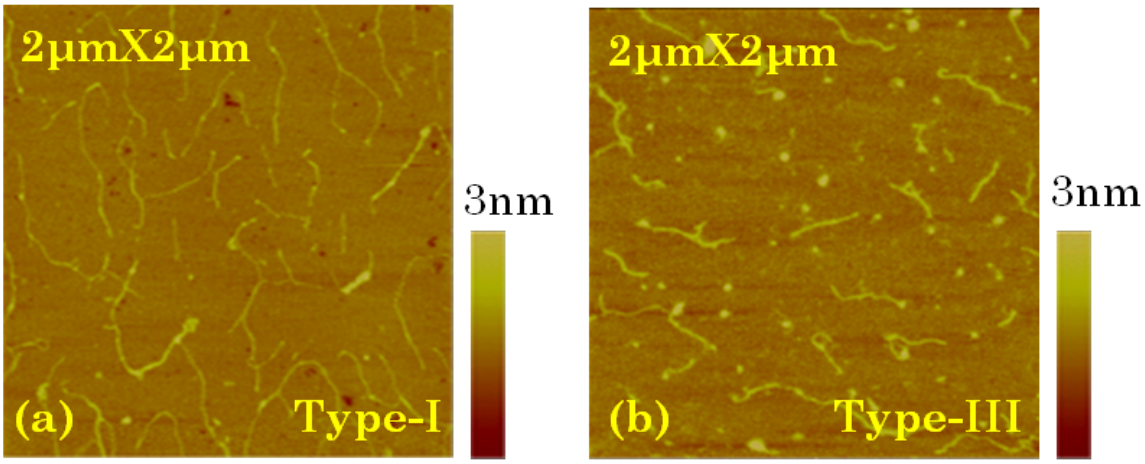

Figure 7.1: AFM topography images of monomer molecules at the concentration of 0.3 $\mu g/ml$ type-I and type-III collagen at 85 s of the deposition on muscovite mica. The images exhibit a color scale corresponding to a vertical range of 3 nm.

structure of the monomer molecules play a role on the flexibility. Moreover, type-III was observed to be less diffusive and have more beaded structure as reported before [170] mostly due to its higher surface charge and higher number of hydrophilic side groups.

7.3 Primary Structure of Type-I and Type-III Collagen

To understand the driving interaction force of the heterotypic assembly mechanism, we first investigated the hydrophobicity of both types to compare its contribution to the net force as hydrophobic force. To do that, we calculated the number of hydrophobic amino acid on each triple helix by using Protein Knowledge Database, UniProtKB (http://www.uniprot.org/uniprot/). By searching the specific alpha chain of the related source used in the experiment, that is rat tail tendon for the type-I source and Bos taurus (Bovine) for type-III in our case, we obtained the amino acid sequence of each alpha chain. By using the specific sequence and the program of

the amino acid calculator, $http://proteome.gs.washington.edu/cgi-bin/aa_calc.pl$, the number of each amino acid was counted. Therefore, the number of highly hydrophobic amino acids of type-I triple helix is 230 ($2\alpha_I(1)+\alpha_I(2)$), while it is 147 for type-III triple helix ($3\alpha_{III}(1)$). Possible effects of this significant difference will be discussed below. Similarly, we calculated the net charge of the two types and found that the number of negatively charged amino acids on type-I triple helix is 37, and 39 in type-III. Therefore, type-III collagen is more charged and has more hydrophilic structure than type-I triple helix does. Table 7.1 shows the details of each alpha chains of proteins.

7.4 Homotypic Self-Assembly

7.4.1 Homotypic assembly on muscovite mica

Self-assembly of collagen type-I has been investigated for decades [37, 133, 154, 39], but very little is known about the self-assembly of type-III. After observing the difference between the two types at the monomer level, we investigated homotypic assembly of both types at the nucleation level. To capture the nucleation events of type-I, we started with concentration of 2 $\mu g/ml$ and searched different incubation times to catch of fibril nucleation point. We found that straight collagen fibrils corresponding to the nucleation events appeared for type-I after 2 min (see Figure 7.2a). However, in the case of type-III with 2 min incubation, we observed that the substrate was fully covered by the collagen molecules without any nucleation sign yet. When we increased the concentration to 4 $\mu g/ml$, the formed fibrils became more abundant and aligned unidirectionally on the muscovite mica, while there was still not much change on the type-III assembly. At the concentration of 5 $\mu g/ml$, type-III molecules just resulted in small fibril formation, whereas small fibrils seen

Gene	COL1A1	COL1A2	COL3A1
Uniport ID	PO2454	PO2466	PO4258
Triple helix	1014	1023	1026
Telopeptides	16(C) + 26(N)	-	14(C) + 9(N)
Non-polar a.a.	63+(12)	104	49+(15)
Polar a.a.	92+(30)	128	117+(9)
Acidic a.a.	-78+(-10)	-66	-73+(-9)
Basic a.a.	87+(6)	85	86+(3)

Source	Type-I Rat tail	Type-III Bovine skin
Net charge	-37+(-4)	-39+(-6)
Nonpolar a.a.	230+(12)	147+(15)
Polar a.a.	312+(30)	351+(9)

Table 7.1: The top table shows the characteristic properties of type-I and type-III collagen in terms of side-chains specific to each amino acid. Type-I collagen is a heterotrimer consisting of two $\alpha 1(I)$ (COL1A1) chains and one $\alpha 2(I)$ (COL1A2) chain, whereas type-III collagen is a homotrimer of $\alpha 1(III)$ (COL3A1) chain. The numbers in parenthesis represents the number of amino acids in telopeptides. a.a stands for amino acid. The bottom table shows the net molecular properties of each type of collagen. For the number of hydrophobic amino acid, we considered Val, Leu, Ile, Met, Phe, Trp, Cys [6]. For polar amino acids, we considered Gln, Asn, His, Ser, Thr, and Tyr.

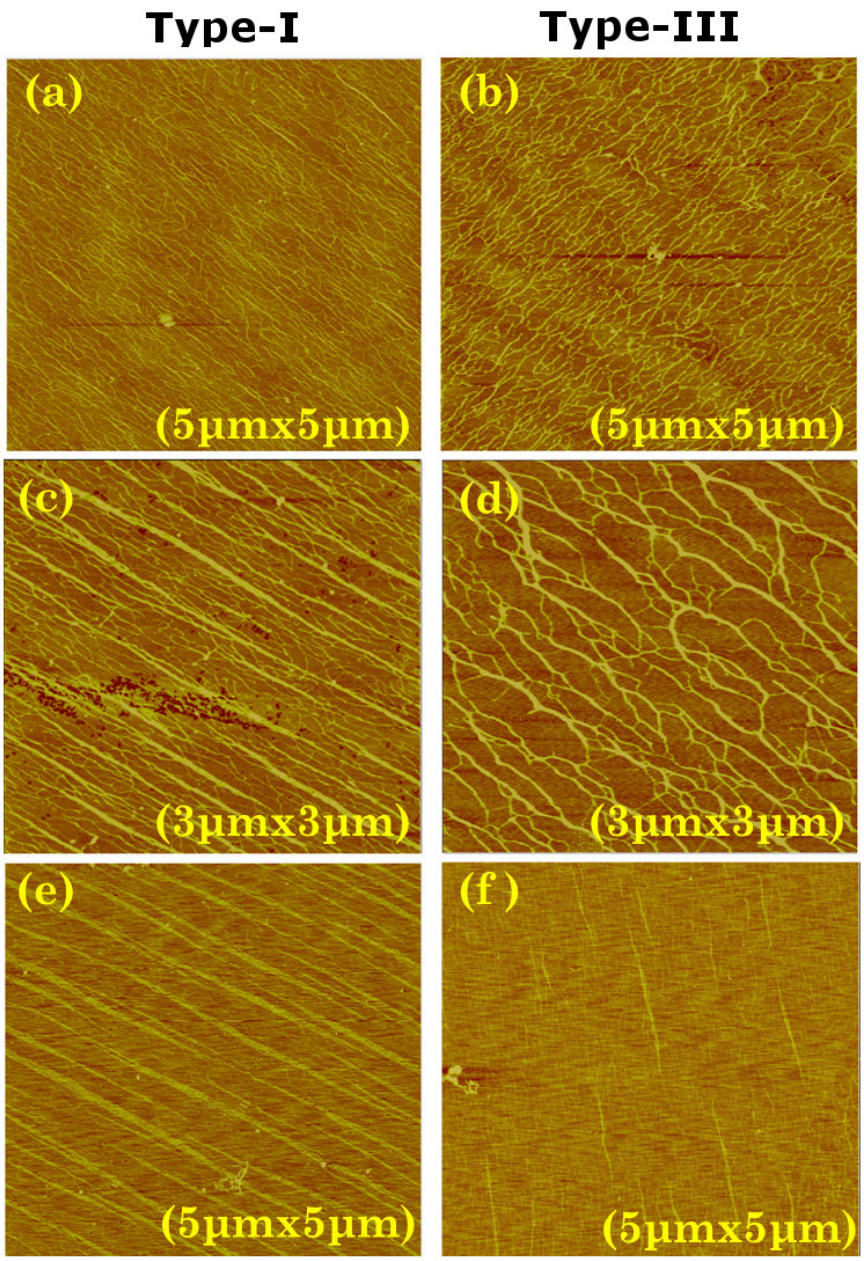

Figure 7.2: Concentration dependent homotypic self-assembly of type-I (a,c,e) and type-III (b,d,f) collagen at 2 min of the deposition. (a-b) 2 $\mu g/ml$, (c-d) 4 $\mu g/ml$, (e,f) 5 $\mu g/ml$ concentration of collagen in the buffer solution consisting of 30 mM Na_2HPO_4, 10 mM KH_2PO_4, and 200 mM KCl at physiological pH (pH 7). The images exhibit a color scale corresponding to a vertical range of (a,b,c,d) 2 nm and (e,f) 5 nm.

in Figure 7.2a became thicker and longer in the case of type-I, Figure 7.2e,f. The minimum concentration of type-III nucleation was found as 5 $\mu g/ml$, whereas the fibril formation has already started at 2 $\mu g/ml$ at 2 min deposition.

Collagen self assembly onto mica is mediated by adsorption to mica [4]. The adsorption must be strong enough to hold molecules to initiate accumulation and not too strong, to allow rotation and mobility to molecules leading fibril nucleation. In homotypic assembly shown in Figure 7.2, this stage is overcome by the increase of the concentration leading to a relatively stronger and dominant collagen-collagen interaction compared to collagen-substrate interaction.

The observation of fibril formation of both collagen molecules shows that type-III collagen has a longer lag phase than type-I does. This results contradict with the previous observation of homotypic self-assembly of type-III performed by turbidity-time assay [78, 171, 73]. They reported that type-III has a shorter lag phase and nucleates faster than type-I. The reason for this results could be the interaction between collagen molecules and mica surface which does not exist in the turbidity-time experiment performed in solution. The electrostatic interaction between negatively charged mica and positively charged collagen molecules is a little higher for type-III than that for type-I molecules, since it has a little more negative charge. However, more significant effect could be from the more hydrophilic structure of type-III. The interaction between hydrophilic mica and hydrophobic type-I molecules could be a stronger attraction like the attractive interaction measured from a variety of hydrophobic-hydrophilic systems [172, 173, 174]. The self-assembly of collagen on mica initiates with adsorption of molecules to mica [4]. The adsorption should be both strong enough to hold molecules to some level to allow accumulation and nucleation and not much strong, at the same time, to allow rotation and mobility to molecules leading to nucleate into fibrils. From our observation, this adsorption stage

could be overcame by increase of the concentration meaning that a stronger and dominant collagen-collagen interaction compared to collagen-substrate interaction or by increase of the concentration of KCl which reduces affinity of mica to collagen. Moreover, the attractive hydrophobic interaction between collagen molecules becomes weaker in the case of type-III due to the less number of hydrophobic amino acid on its surface. A similar result for the heterotypic assembly of type-I and type-III collagen is reported by Bierbaum on a titanium substrate supporting the longer lag phase of type-III observed in our experiment [21].

7.4.2 Homotypic assembly on phlogopite mica

Self-assembly of collagen *in vitro* is a time dependent process. In this study, we used AFM to capture nucleation event of both types and performed a set of concentration dependent homotypic assembly experiment on muscovite mica. Eventually, we observed in the previous section that the lag phase of type-III is longer than that of type-I. To investigate the next step, the growth phase and to compare the relative growth rate of the two types, we prepared the samples of 5 $\mu g/ml$ collagen deposited for 1 h on phlogopite mica. The reason to choose phlogopite mica this time is that more growth directions of collagen fibrils on phlogopite mica as shown before (see Figure 6.3) provide opportunity to distinguish the fibrils better in three directions than one as produced on muscovite mica. The resulting network of longer fibrils on the sample of type-I exhibits that the growth rate of type-I collagen is faster than that of type-III which is consistent with a recent work of fibrillogenesis of 250 $\mu g/ml$ protein in solution [21, 78]. The surface area of type-I assembly of 5 $\mu g/ml$ collagen sample shown in Figure 7.3a calculated by Image-J is 67,518 μm^2 and it is 36,573 μm^2 for the sample of type-III shown in Figure 7.3c. Snapshots of the

intermediate steps of image analysis is shown in Figure 7.9. The possible reasons to the 2-fold less surface area could be several. First of all, the longer phase of type-III might retard the assembly process. Therefore, even tough they could have the same assembly kinetics, type-III could result in a smaller length of fibril upon the same amount of deposition time. Second, phlogopite mica could have a lover affinity to type-III than that to type-I. That could reduce the amount of molecule adsorbed to the substrate. The necessity of a sensitive amount of adsorption to initiate the self-assembly mechanism could not be provided for the case of lower affinity. In this case, monitoring the assembly mechanism in lower [KCl] could be a solution. That would increase the number of empty K^+ pockets on the substrate and then enhance the electrostatic attraction between collagen and mica. Monitoring the assembly at lower pH could also increase the affinity. By checking these situations, whether the affinity has an influence on the growth rate could be understood. The third possible reason is a lower magnitude of hydrophobic attraction between molecules of type-III which slows down the kinetics of assembly.

Another striking difference between the two types of homotypic self assembly is not only the growth kinetics, but also fibril morphology of the resulting network. A small area scan of both samples show that the each type self assemblies to a different type of fibril structure. Type-I molecules form fibrils assembled into D-periodic structure of 67 nm banding repeat with a high packing ratio as it is *in vivo*. Formation of D-period indicates that collagen molecules in the fibril are ordered in a native-like manner [85]. However, self-assembly of type-III did not show D-periodic structure, but loose and more flexible fibril formation on this phlogopite mica.

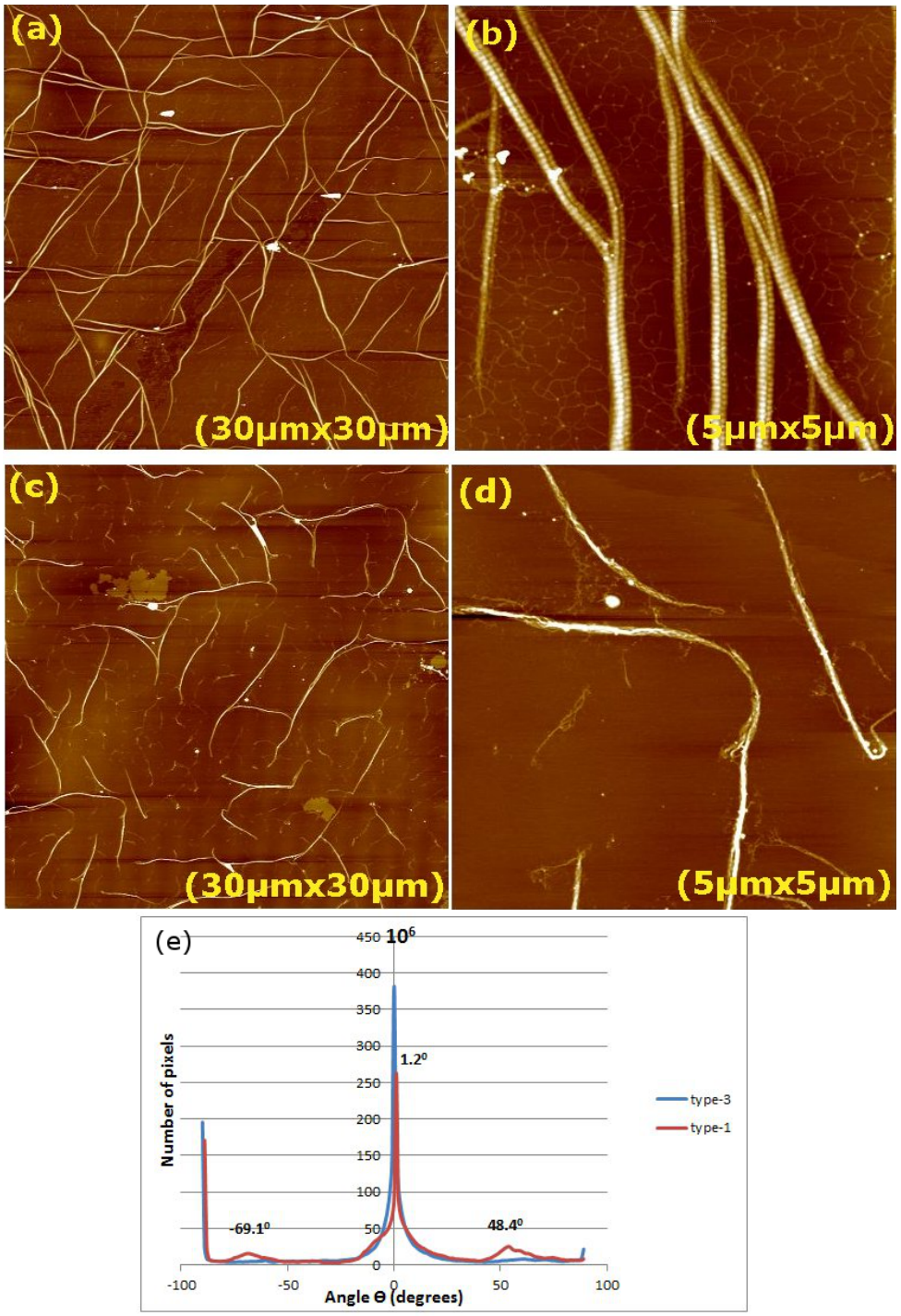

Figure 7.3: AFM topography images of homotypic self-assembly of type-I and type-III collagen at the concentration of 5 $\mu g/ml$ at 1 h deposition on phlogopite mica. The images exhibit a color scale corresponding to a vertical range of (a,b) 7 nm and (c,d) 4 nm. The surface area of the fibrils are (a) 67.52 μm^2 and (c) 36.57 μm^2 measured by image-J. e) The orientational distribution of fibrils on panel (a) and panel (c).

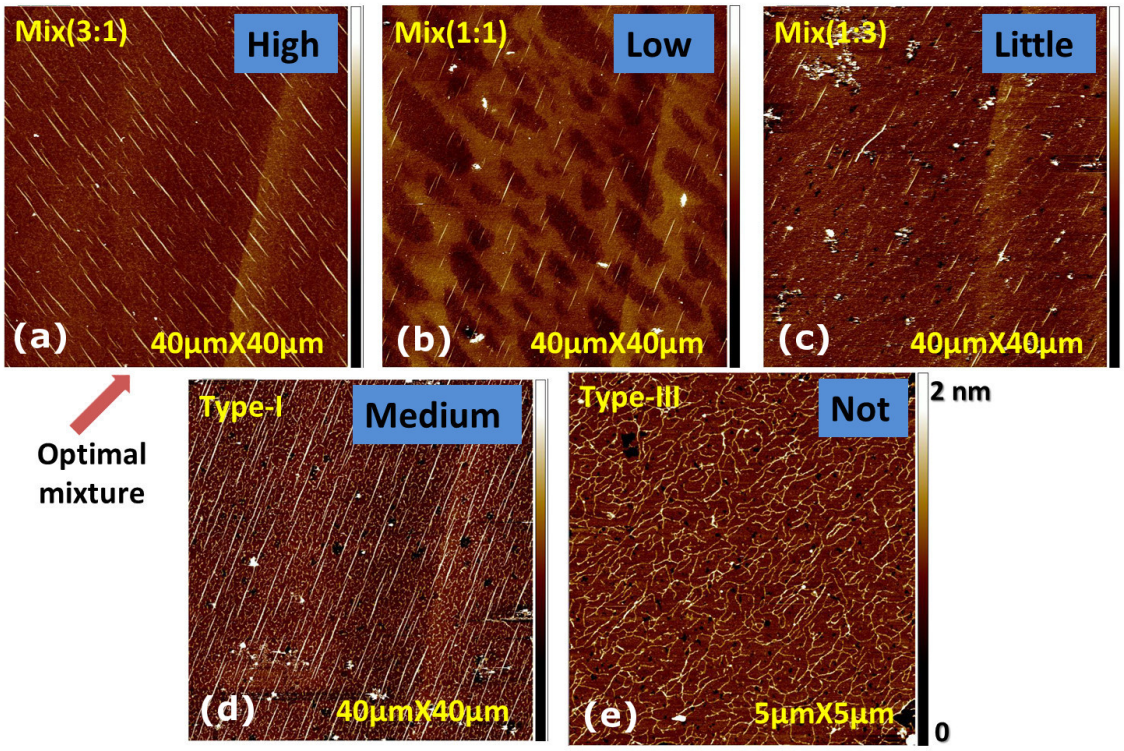

Figure 7.4: Effect of type-III on the self-assembly of type-I. All images are with 0.5 $\mu g/ml$ final concentration and 30 min deposition. The small area scan in the case of type-III shows low level of assembly with very low z-scale of the sample covered by type-III monomers in panel (e). All images have a color scale corresponding to a vertical range of 2 nm after flattening.

7.5 Heterotypic Self-Assembly

7.5.1 Heterotypic assembly on muscovite mica

The number of studies regarding the co-assembly of type-I and type-III collagen *in vitro* is limited [21], and assembly process are generally monitored with turbidimetry assay [78, 79, 175, 22]. This method gives indirect results about the process as the measurement is technically based on the light passing through solution. It has also limitations in catching small fibrils. In this study, we used AFM to observe fibrils

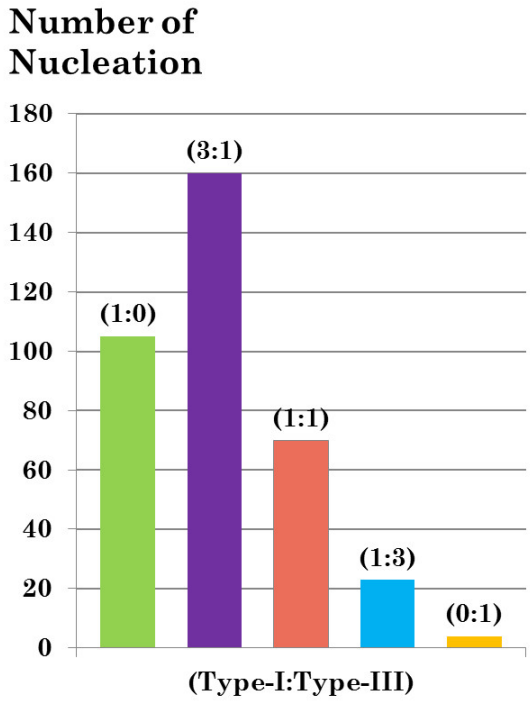

Figure 7.5: The number of fibrils formed on the sample sets of heterotypic assembly of 0.5 $\mu g/ml$ collagen, shown in Figure 7.4. Enhanced nucleation was observed for the mixture(3:1) sample (Type-I:Type-III=3:1), shown in Figure 7.4a.

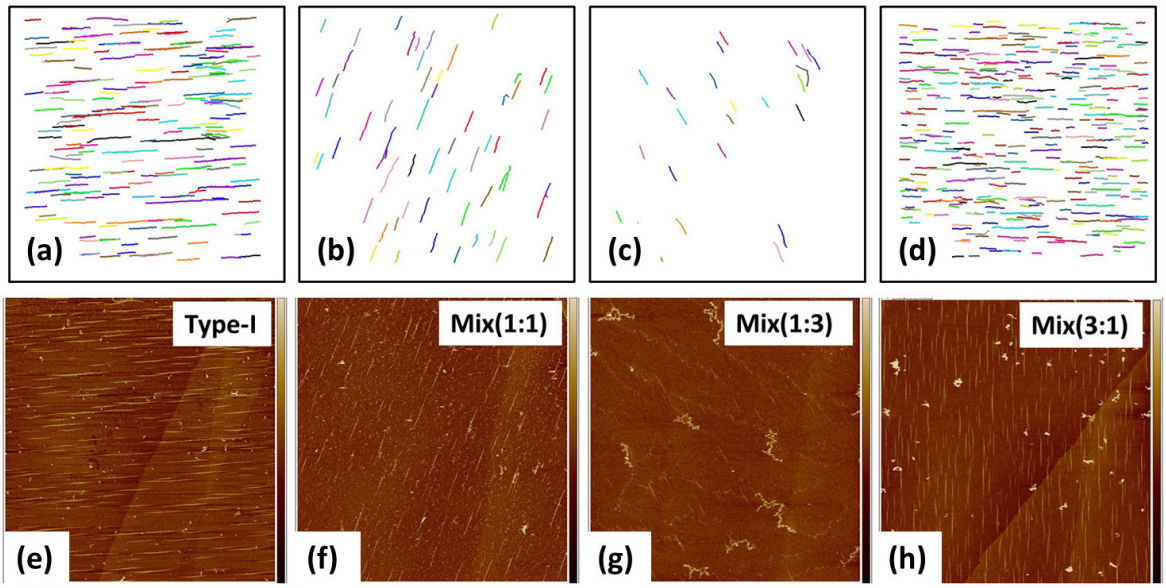

Figure 7.6: Nucleation analysis for co-assembly of type-(I+III). (a,b,c,d) Corresponding in silico network extracted via CAFE for topography image of (e,f,g,h) type-I, mixture(1:1), mixture(1:3) and mixture(3:1) respectively. All images are with 0.5 $\mu g/ml$ final concentration and 30 min deposition. The color scale is 3 nm for (e) and 4 nm for (f,g,h).

at very low concentration and nano scale. To investigate the influence of type-III on the early stage of the co-assembly process, we performed a set of experiments with varying ratio of type-III to type-I at the final concentration of 0.5 $\mu g/ml$ shown in Figure 7.4. At 30 min incubation, we showed that the mixture(3:1) sample (Type-I:Type-III=3:1) resulted in an enhanced number of fibril formed even more than the homotypic type-I sample. The resulting number of fibrils are shown in Figure 7.5. The ratio of 25% type-III to type-I, which represents the mixture(3:1) sample, is significant because the type-I rich heterotypic fibrils in skin contain about 20% type-III collagen by mass [28]. We would result in even higher nucleation, if we would go further down to 20% type-III. Due to the experimental difficulties, our set consisted of three different hybrid ratios separated equally from the next as 0, 25, 50, 75 and 100% content of type-III collagen to type-I.

Resulting enhanced nucleation observed in Figure 7.4 shows that in the presence of the two types of collagen, the heterotypic assembly is more favourable than homotypic fibril formation as suggested by Fleischmajer [98]. When we compared type-I and mixture(3:1) samples, we observed that the existence of type-III increased the lag phase of type-I, in another saying decreases the rate of nucleation about 2 fold which is lower than the reported value 5 fold decrease obtained by SDS-PAGE (sodium dodecyl sulfate polyacrylamide gel electrophoresis) technique [79]. The reasons of the difference could be several. The different experimental technique could be the first reason. Covering proteins by SDS (sodium dodecyl sulfate) denatures them and they lost their secondary or tertiary structure. Very low concentration we used, 0.5 $\mu g/ml$, compared to 100 $\mu g/ml$ used [79], or the affinity of mica to collagen which is not the case for electrophoresis, should be among possible reasons.

Another striking effect of type-III on the morphology and kinetics of type-I assembly is decrease on the length distribution of fibrils. Figure 7.6 shows another

set of co-assembly of type-(I+III) experiment with corresponding the new developed image analysis program [5], CAFE network. Image analysis performed by image-J and verified by CAFE. The length distribution of fibrils is measured as 4.3, 2.83, 3.62, and 2.94 μm for type-I, mixture(3:1), mixture(1:1), and mixture(1:3) samples, respectively. The number of nucleation is counted as 209, 364, 61, and 27 for type-I, mixture(3:1), mixture(1:1), and mixture(1:3) samples, respectively, while no fibril is formed on type-III sample. The results suggest that type-III collagen decreases the rate of propagation of fibrillogenesis, although further experiments with higher concentration should be performed to verify this hypothesis. Our results do not give information about how much time the mixture(3:1) sample required for its lag phase. The time left for fibril growth after the lag phase would give more specific knowledge about the relative rate of propagation.

7.5.2 Heterotypic assembly on phlogopite mica

To investigate the influence of type-III on the growing stage of the co-assembly process, we incubated 5 $\mu g/ml$ final concentration of type-I, type-(I+III) meaning that 50% by each, and type-III collagen for 1 h on phlogopite mica, which is a generous gift from Frank Balzer at the university of Southern Denmark. In addition to the enhanced nucleation effect of type-III on the self-assembly of type-I, we observed one more interesting result showing the regulatory effect of type-III on the co-assembly process . The addition of type-III leads to formation of more parallel and organized fibrils with smaller length as seen in Figure 7.4. We have analysed the number of fibril on each sample and the result is consistent with the enhanced nucleation effect of type-III that we observed on the nucleation phase (see Figure 7.4. The number of fibrils is count 103, 1044, and 590 by image analysis software CAFE on the sample

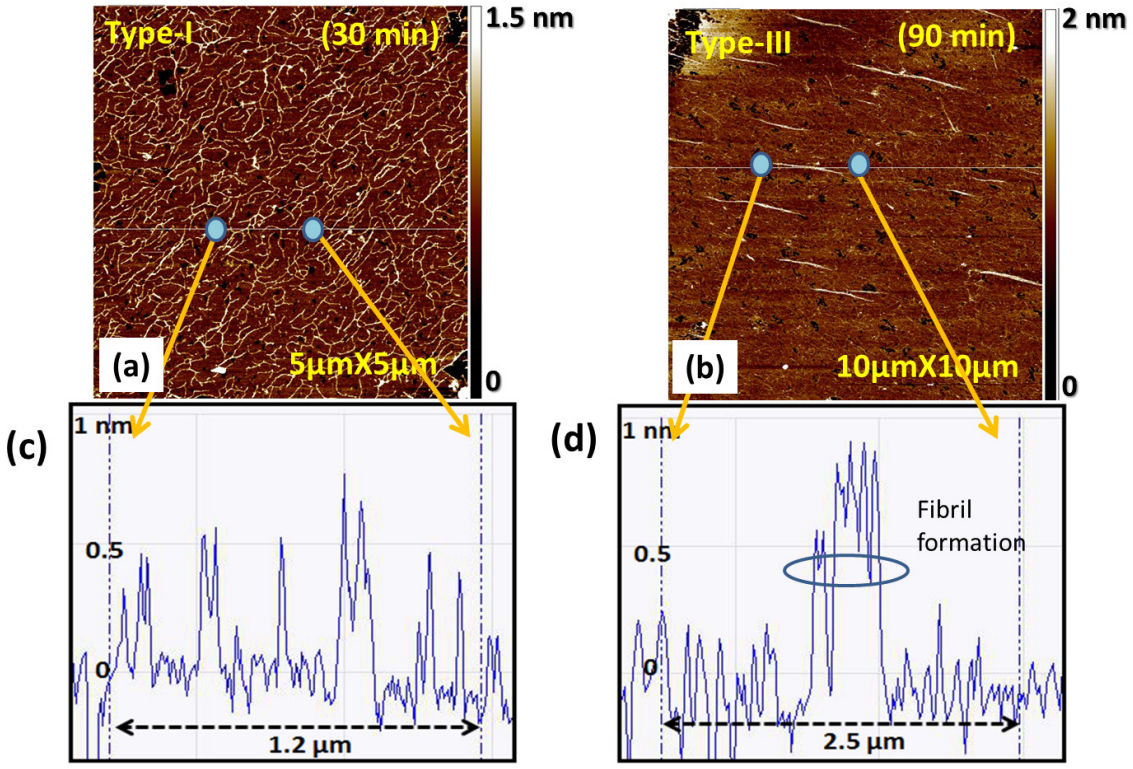

Figure 7.7: AFM topography images of type-III collagen at 0.5 $\mu g/ml$ at (a) 30 min and (b) 90 min of the deposition on muscovite mica. The images exhibit a color scale corresponding to a vertical range of (a)1.5 and (b) 2 nm. (c-d) The line section of the image (a) and (b), respectively.

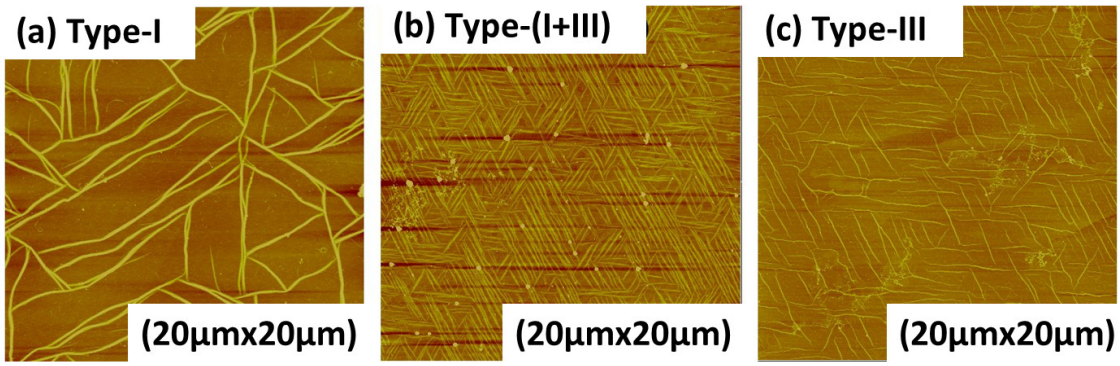

Figure 7.8: AFM topography of the homotypic self-assembly of type-I and type-III collagen at the concentration of 5 $\mu g/ml$ at 1 h deposition on phlogopite mica. The resulting network of collagen fibrils revealed a regulatory effect of type-III collagen on the fibril length distribution of the heterotypic self-assembly network. The images exhibit a color scale corresponding to a vertical range of (a,c) 10 nm and (b) 15 nm.

of type-I, type-(I+III) and type-III, respectively, shown in Figure 7.8. This result might explain the function of type-III in wound healing process to recover damaged tissues faster and in embryonic tissues to promote cell growth and DNA synthesis. Suppression of type-III collagen suppressed the growth of cells, while it was not observed on suppression on type-I. It was suggested that type-III has important role in the early stage of growth stimulation of human osteoblastic cells [71]. The result is also consistent with the reported smaller and uniform fibril distribution in human, bovine and rabbit cornea [176, 177].

Notbohm's study regarding the heterotypic self-assembly of type-I and type-III collagen by turbudity-time assay [175] found that type-III reduces the absorbance, in other words the fibril formation. They studied co-assembly till 30% of type-III to type-I ratio and determined with electron microscopy that the average fibril diameter is inversely and non-linearly proportional to the content of type-III. The acid soluble collagen was found to be affected by type-III content more with stronger decrease in

absorbance maxima than the pepsin extracted protein which has only the triple helix part. The pepsin soluble fibrils appeared to have a higher thickness. The inhibitor function of type-III was suggested to be due to the decreased hydrophobic interaction of type-I fibrils due to type-III molecules on the surface.

7.6 Discussion

The interaction between hydrophobic and hydrophilic surfaces has been investigated for a variety of systems since the last a few decades and the results are controversial. Interaction mechanism of a model asymmetric system of hydrophobic polystyrene (PS) and hydrophilic mica was investigated with Scanning Force Microscopy (SFA) in 5 different electrolytes at the concentration of 0.001M and 1M. Measured range of repulsion was decreased as the concentration of electrolyte increased in NaCl, CaCl2 and NaOH, but did not show a significant difference in HCl and CH3COOH because of the ion specific effect of formation and stability of air bubbles on PS surfaces [117]. Another pure repulsion on the asymmetric system of PS [(C8H8)n] coated cantilever and a clean glass surface which is hydrophilic was reported by Thormann and DLVO-like interaction was observed in water. On the other hand, there are also studies reporting an attractive net force between symmetric surfaces. Papastavrou [178] reported a pure attraction between chemically modified gold-coated surface terminated with COOH and CH3 in water by SFM and that decreased with increasing ethanol content in water. An attractive interaction of an asymmetric system of silica cantilever and coated glass ($\theta = 113$) is also reported by Lee [173]. The interaction range and magnitude was effected by degassing, surface character, types and concentration of the electrolytes affecting the stability and the formation of bubbles. In high electrolytes, we expect to have a net attractive force

due to the screening effect according to DLVO, but this did not happen in the system of hydrophilic mica and hydrophobic PS surfaces [117]. Therefore, previous reports about the interaction of hydrophilic-hydrophobic surfaces is mostly on macro scale unlike our nano scale system, and still open questions exist. The results shows that the net interaction force is system specific and highly depends on the characteristics of the each system.

Previous observations about the asymmetric system of type-I and type-III collagen assembly indicated that type-III was found mainly on the surface of fibrils [78, 70, 179, 180, 181]. By using the suggestion that the type-III collagen regulates the fibril diameter by coating the surface of type-I fibril, the enhanced nucleation might be explained. Type-III coating on type-I fibrils makes the surface more hydrophilic. Type-I has a higher hydrophobic surface with more hydrophobic amino acids as shown in Figure 7.1 compared to type-III. The addition of type-III may reduce the hydrophobic attraction between type-I molecules and increase the repulsive hydrophilic forces between type-III coated heterotypic fibrils. That may lead a longer lag phase and then lower reaction barrier for fibril formation and cause an enhanced number of fibril.

	A		B		C		D	
	Type-I(*)	Type-III(*)	Type-I(*)	Type-III	Type-I	Type-III(*)	Type-I	Type-III
Net charge	-41	-45	-41	-39	-37	-45	-37	-39
Nonpolar a.a.	242	162	242	147	230	162	230	147
Polar a.a.	363	393	363	381	331	393	331	381

Table 7.2: Possible scenarios in terms of the presence of telopeptides in the collagen molecule of type-I and type-III. Asterisk (*) represents the existence of telopeptide ends in the monomer molecule.

We have categorized different possible scenarios in Table 7.2, depending on the presence of telopeptide ends on the monomer molecule. Scenario A represents the case that both types have telopeptide ends in their monomer structure. In this case, type-III molecule has more negative charge than type-I. That causes a stronger electrostatic repulsion between type-III molecules. The number of hydrophobic amino acid is much higher in type-I meaning that hydrophobic attraction between molecules acts stronger than that of type-III. Moreover, hydrophilic side chains enhance the repulsive interaction between type-III molecules. This situation explains the longer lag phase of type-III collagen and smaller fibrillar diameter. Type-I molecules, on the other hand, nucleates in a shorter time with the support of strong hydrophobic attraction in addition to weaker repulsive DL force.

Scenario D represents the case that telopeptide ends were cut down during the collagen extraction process and both monomer molecules have the triple helical structure left only. Type-III molecule is more negatively charged again, but the difference is lower than scenario A. In all cases, except scenario B, surface charge is higher for type-III molecules than type-I. Therefore, the the electrostatic repulsion between molecules will be stronger for type-III. Hydrophilic interaction is also stronger for type-III molecules in all cases. Therefore, they expose a stronger repulsive force during the self-assembly. That could be one of the reasons of longer lag phase. However, hydrophobic interactions which are attractive powerfully act on type-I molecules leading a stronger driving force for the assembly as supporting the shorter lag phase than type-III.

The higher surface charge of type-I in scenario B is expected to enhance the repulsive electrostatic interaction. The effect of two electrons on the surface potential will be as small as in Eqn 3.10. That small difference on the potential will not bring a significant difference on the electrostatic interaction constant Z, Eqn 3.8. Therefore,

even for scenario B, the net system will not become repulsive. In all cases in Table 7.2, the net interaction will be always attractive that supports the self-assembly tendency of collagen.

The extraction process of our collagen sources includes acetic acid digestion for type-I and pepsin digestion for type-III. This suggests that type-I molecules in our source most likely have telopeptide ends. Type-III molecules, on the other hand, might not have telopeptides due to pepsin digestion during the collagen extraction [175, 171, 182]. Although the enzyme method such as pepsin extraction is believed to destroy telopeptides, evidences have been provided that pepsin digestion of collagen does not completely remove telopeptides [166, 167]. In the possibilities that we have categorized in Table 7.2, scenario B is a less likely case. Possibility of cases C and/or D is quite low, because acetic acid extraction is known to leave telopeptides. The question is mostly on if pepsin digestion breaks down all telopeptides which is represented by scenario B, or leave some amino acids that is A. Therefore, scenario A is the most favourable case in terms of electrostatic force since that has the higher difference on the repulsive DL force between the two types. The reality will be probably in between the two cases with and without telopeptides in the mixture of stated possibilities.

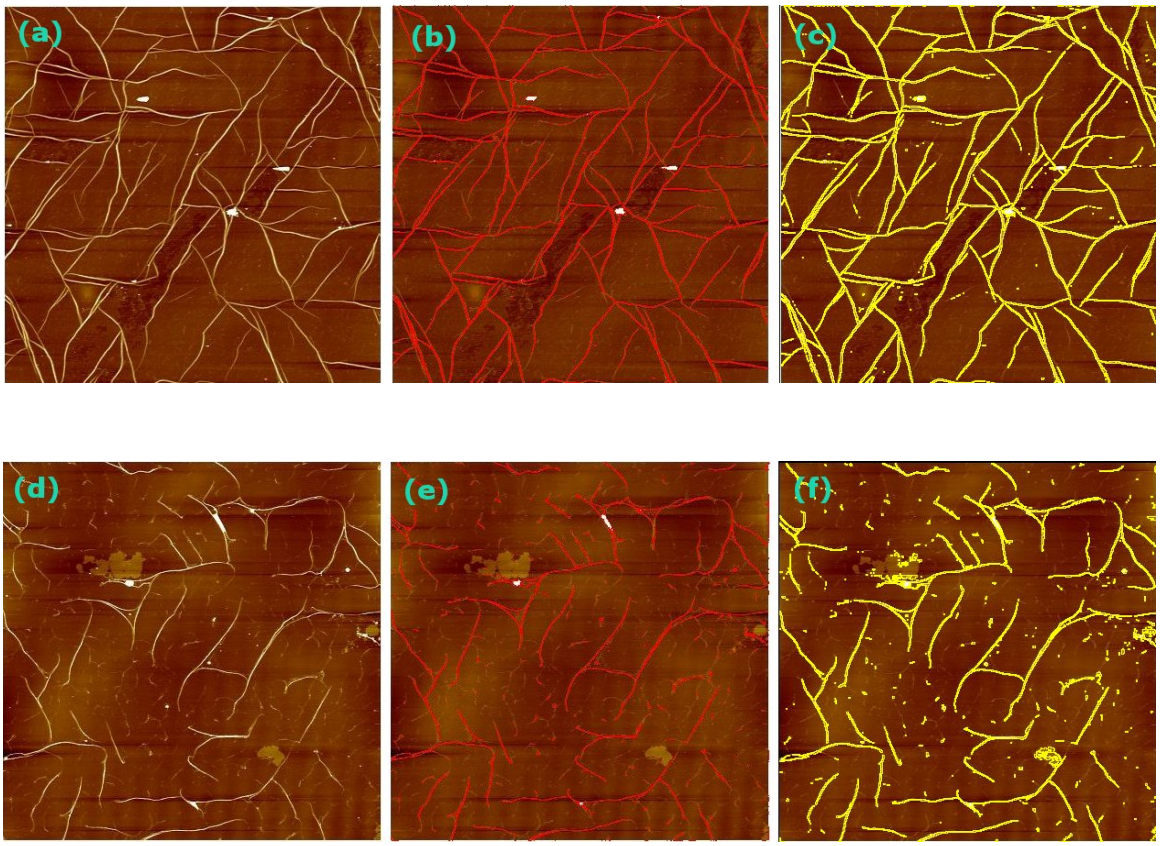

Figure 7.9: Snapshots of the intermediate steps of image analysis program Image-J applied to Figure 7.3. (a,d) The original AFM scan. (b,e) Filtered image (colored red) of the original by color thresholding tool. (c,f) The final version of the selected fibrils (by yellow) to measure the surface area of each type.

8. ADDITIONAL DATA AND PRACTICAL CONSIDERATIONS

8.1 Obstacles in AFM Study of Biological Samples

Investigation of biomolecules with a scanning force microscopy has various types of difficulties based on different sources. They can be divided into three categorises according to their source such as AFM based obstacles, substrate related defects, and buffer solution and protein related difficulties. In this section, we discuss practical issues encountered during the investigation of collagen self-assembly, and suggest possible remedies. The sample solution of the images provided in this section were prepared in a buffer solution consisting of 30 mM Na_2HPO_4, 10 mM KH_2PO_4 at pH 7. In addition to those, varying amount of KCl and glycine will be mentioned in case they are involved.

8.1.1 AFM related artifacts

While AFM has been increasingly used in study of bio-nanotechnology with its high spatial resolution, artificial "ghost" images can occur [183, 184]. These artifacts emerge more, when the size of the features of the imaged object is on the same order of the radius of curvature of the AFM tip. One of the common artifacts is "Double tip effect". It is caused by a broken or contaminated tip. The sample surface is scanned by both the tip and the contamination.

Figure 8.1 is obtained by 5 $\mu g/ml$ concentration of type-I collagen deposited for 1 h on phlogopite mica in presence of 200 M KCl. The double tip effect is observed on collagen fibrils as a result of a dirty or broken tip. In the figure, each collagen fibril has a 'twin' next to itself caused by double tip.

Background noise is another obstacle in AFM imaging of biomolecules, as ex-

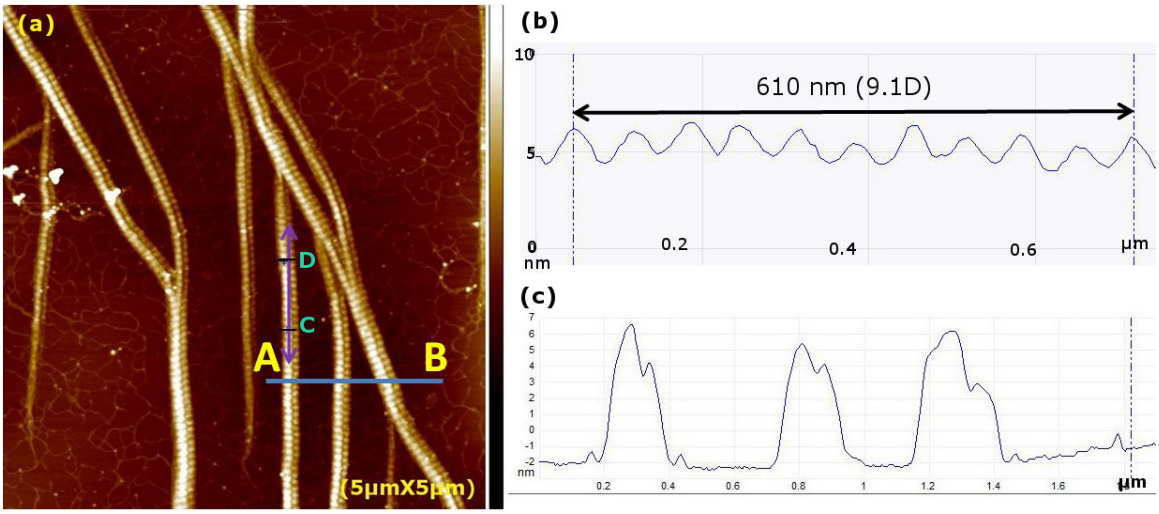

Figure 8.1: Double tip effect. a) AFM image of type-I collagen fibrils. The color scale corresponds to 15 nm. Bruker Dimension Icon AFM was operated. b) Line section between the point C and D verifying characteristic D-period of a collagen fibril. c) Profile plot from the point A to the point B shown on the image exhibits double tip effect on the recorded topography data.

emplified in Figure 8.2. While this does not cause a significant damage on hard samples, it may damage softer biological samples. In Figure 8.2a, background noise reduces the image quality and complicates image analysis. To eliminate noise, we have set a suspension system under the AFM table and obtained the later scans in higher quality. Figure 8.2b shows another defect on the overall surface. Because of the drifts covered the whole image, the fibrils looks swollen and to distinguish the fibrils is more difficult. A possible source of the drifts is a contaminated tip. A small debris could be attached to the AFM probe, and that causes drifts on the image. By exchanging the AFM probe we eliminated the problem.

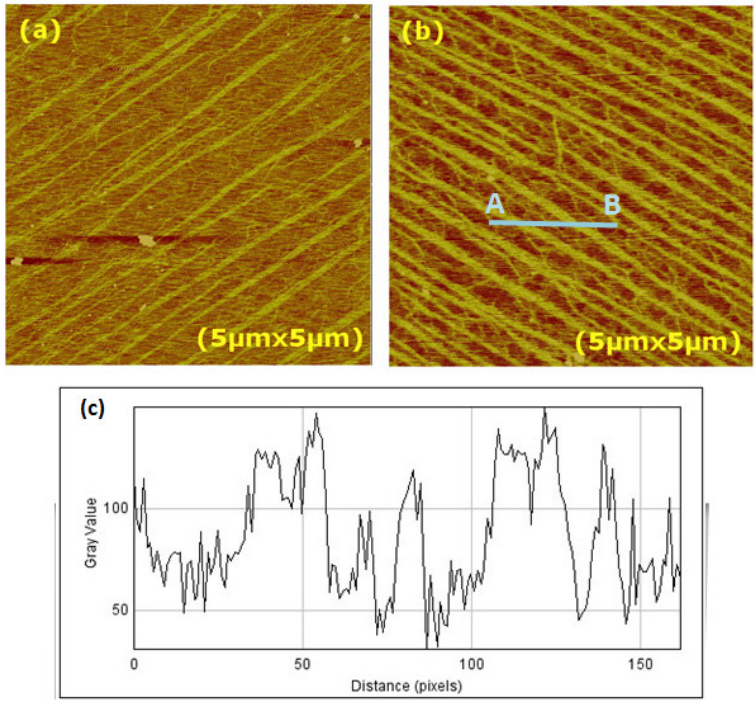

Figure 8.2: Noise effect on topography signal. 5 $\mu g/ml$ concentration of type-III collagen was deposited for 30 min on muscovite mica in the presence of 200 mM KCl. a,b) AFM image. Z-scale is 6 nm for both images. AFM Nanoscope IIIa was performed. c) Plot profile for the line shown in panel b. The x-axis represents distance along the line and the y-axis is the vertically averaged pixel intensity.

8.1.2 Buffer solution or protein related defects

AFM study of biomolecules could fail due to the defects occurs during the preparation of the sample solution. The defects could be buffer solution based, biomolecule based or something related to how to handle the process. The sample surface shown in Figure 8.3 is prepared to study the heterotypic self-assembly of type-I and type-III collagen. The resulting structure showed two different network areas as seen in Figure 8.3.

Different populations seen on the surface might be only/mostly type-I or type-III collagen regions. Possible reason would be insufficient mixing of the sample aliquot,

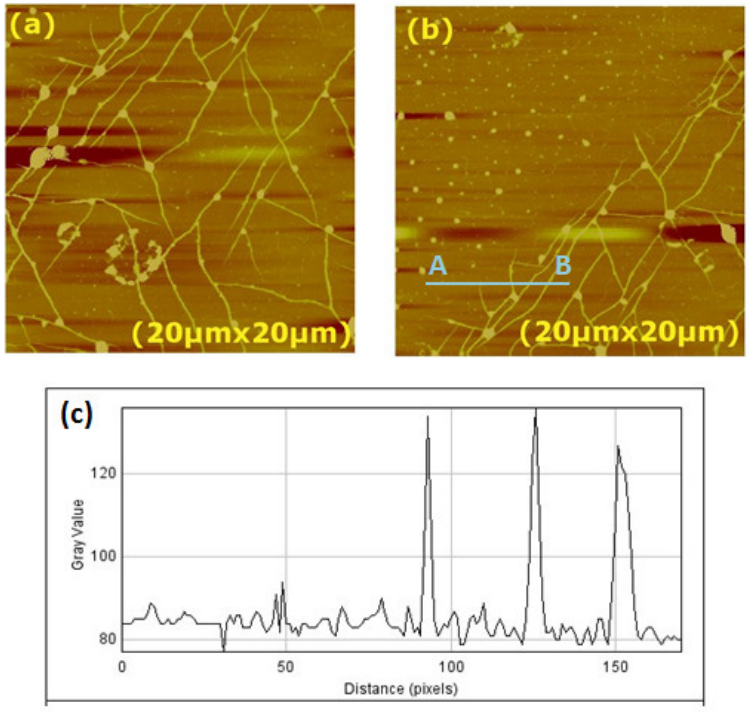

Figure 8.3: (a,b) Different area scans of 5 $\mu g/ml$ of the mixture(1:1) sample of type-I and type-III collagen deposited for 1 h in the presence of 200 mM KCl. Z-scale of the images are 30 nm. AFM Nanoscope IIIa was operated. c) Profile plot for the line from point A to point B taken from the panel b. The x-axis represents distance along the line and the y-axis is the vertically averaged pixel intensity.

as Section 6 showed that type-I and type-III collagen has a different lag phase. Thus, while one type of collagen is already nucleated and grows, the other type still may be in the lag phase. Therefore, in addition to pipetting, stirring and vortexing could solve the problem. However, the type-III sample which was prepared on the same day gave no assembly. That means that the type-III source used for the mixture sample may not be in a good condition. Reconstitution of a new type-III source may be the best.

How to deal with a biomolecule during the experiment and to be able to obtain consistent results takes a quite long time due to nano scale parameters of the systems.

For the self-assembly of type-III collagen, we found different and inconsistent patterns. Figure 8.4 shows an example. Mechanism for the observed pattern is unclear. Inhomogeneity of mica domain may be a reason. The orientational distribution of the Figure 8.4(b1) shows a wide range of angles meaning that there is not a preferred direction for the fibrils on the surface in this case.

8.1.3 Substrate related defects

Self-assembly of biomolecules in vitro may fail due to substrate related disorders. For mica, proper cleavage is important since the surface is supposed to be atomically clean before deposition of collagen. That could be obtained sometimes at the first try, but sometimes many cleavage trials should be performed untill a clean and unfolded/uncracked layer is obtained. Once the surface looks clean and smooth, the cleaved surface can be used for the deposition.

The assembly network of 5 $\mu g/ml$ of type-III collagen is shown in Figure 8.5. Although fibril formation occurs in a good condition, the overall distribution of the fibrils does not exhibit a consistent pattern. The fracture on the mica surface breaks the consistent pattern formation because different number of cleavage leads to a different orientation of surface electric dipole. Therefore, a thick layer of cleavage could be a possible solution. Two K layers modelled in Figure 6.5 are separated by (a) 9.98 $\mathring{A}$ and (b) 10.24 $\mathring{A}$ [4]. The color scale of the image shown in Figure 8.5b is 14.98 nm and the corresponding gray scale value is 140. The y-range difference on the line shown in the image which is 8 tells that that the inconsistency on the sample surface is due to the one K layer resulting from uneven cleavage of the mica surface. The plot profile was checked from various points on the cracked area and verified that difference between the two region approximately the same.

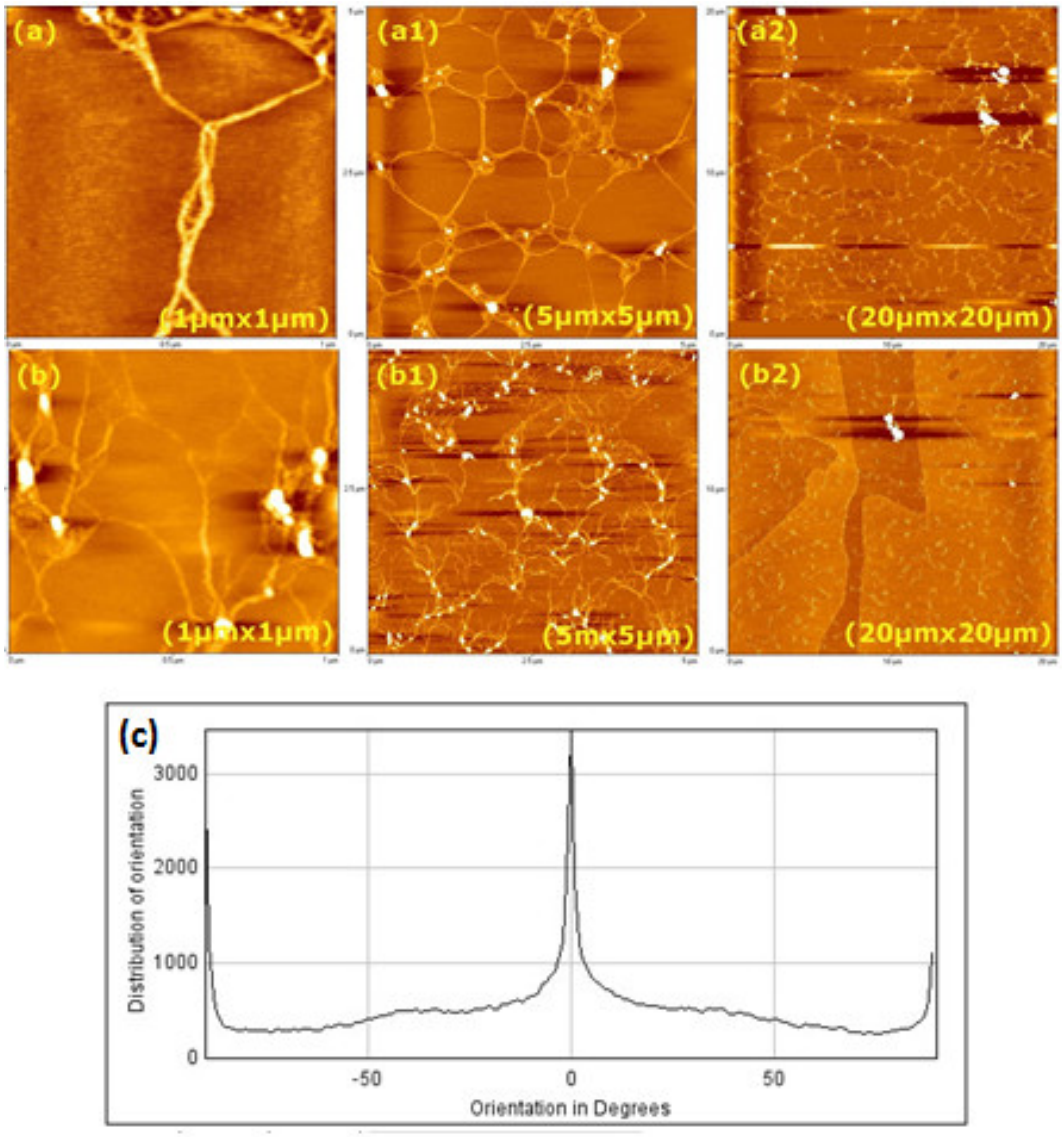

Figure 8.4: The network of 5 $\mu g/ml$ of type-III collagen deposited for 30 min (for the top row images) and 1 h (for the bottom row images) on phlogopite mice, after 10 sec centrifuge in the presence 150 mM KCl. AFM CP-II was operated The orientational distribution of the image (b1).

To stick the mica sheet to AFM mounting disk is as important as cleaving. If the metal disk is not smooth and/or clean enough, AFM scanning results in an enhanced surface roughness which makes the data analysis difficult. Even though

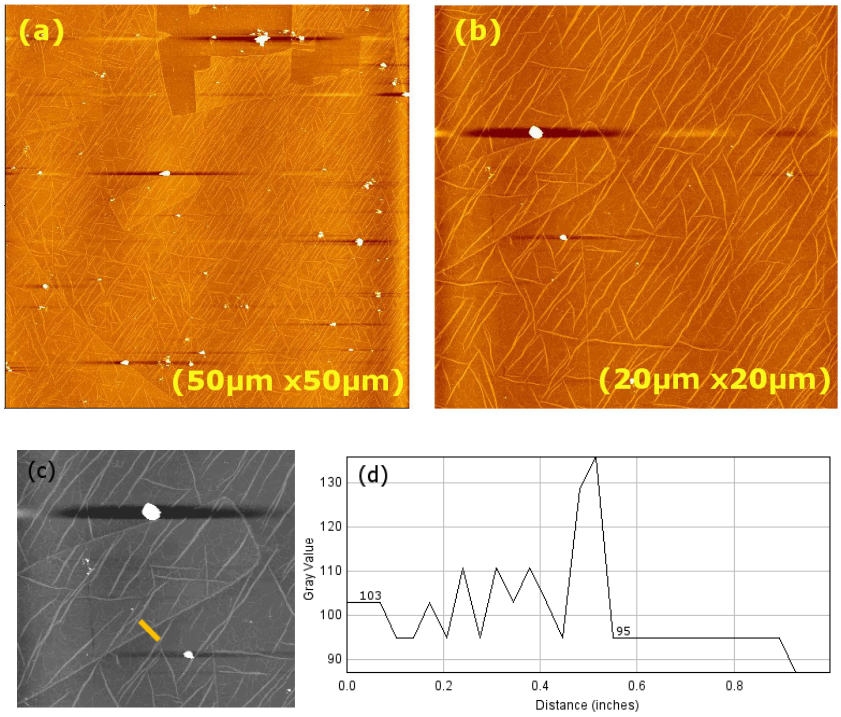

Figure 8.5: 5 $\mu g/ml$ of type-III collagen was deposited after 10 sec centrifuge on phlogopite mica for 37 min in the presence of 150 M KCl. The bad condition of mica breaks the consistent pattern formation. A thick layer of cleavage could be a possible solution. Z-scale is 20.57 nm (a) and 14.98 nm (b). AFM CP-II was operated. (c) 8-Bit version of the nonuniform part of panel (b). (d) The plot profile of the line shown in panel (c).

surface cleavage looks successful, due to the vavy stuck of the mica sheet, the resulting network is not preferential as optimized z scale upon flattening is not consistent on the overall substrate as shown in Figure 8.6.

The uneven distribution of collagen molecules are observed in the background of the small area image on the right in Figure 8.7. Another remarkable property is a curved growing of the fibrils. In these images, the fibrils are not straight aligned. We can explain this behaviour with a model shown in Figure 8.7. The case (c) represents the collagen fibrils grown on the freshly cleaved mica surface. Mica which

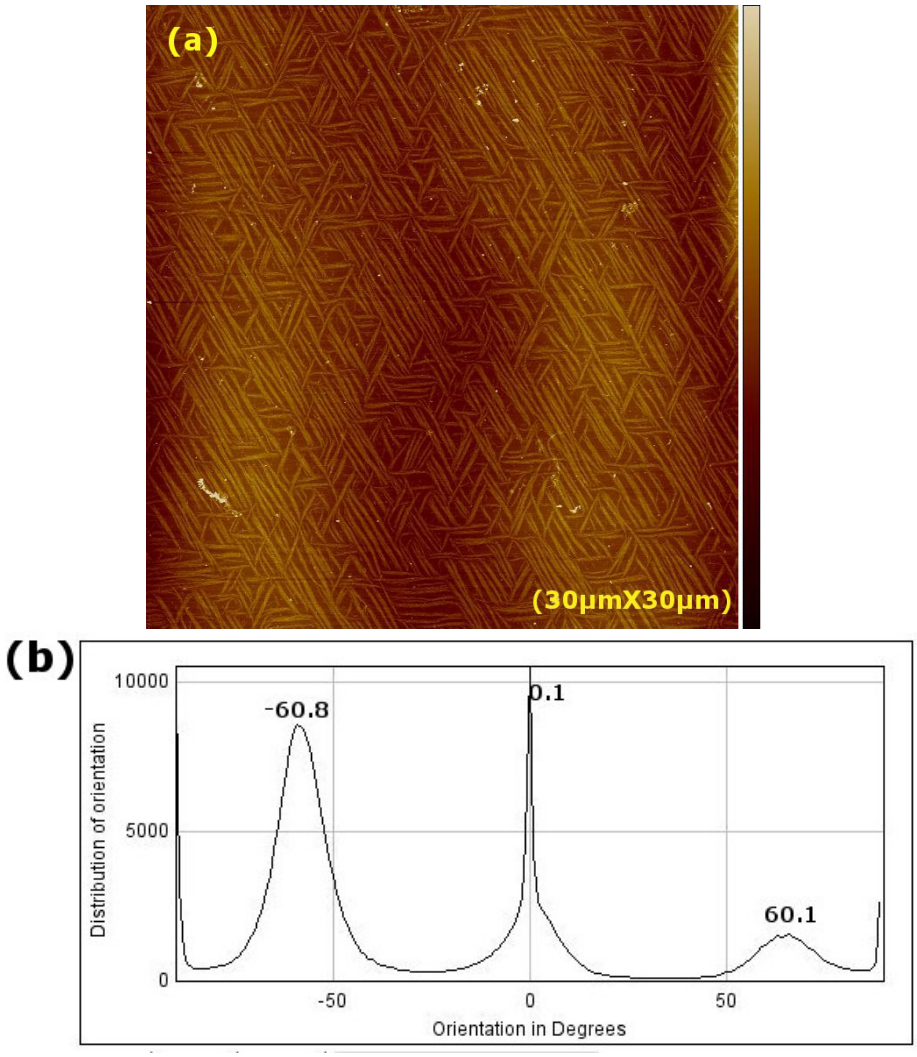

Figure 8.6: a)AFM Topography image of 5 $\mu g/ml$ concentration of mixture(1:3) sample deposited for 1 h on phlogopite mica in the presence of 200 mM KCl. The topography results showed a tilted structure of the surface which makes difficult to analyse fibrils on the surface. If additional cleavage does not solve the problem, the mica could be mounted on another metal disk. The color scale corresponds to 10 nm. Bruker Dimension Icon AFM was operated. b) The orientational distribution of image a) showing one dominant three direction of growth fibrils.

is negatively charged upon cleaving directly interacts with the collagen fibrils which are positively charged. The case (d) represents the situation that fibrils are formed on

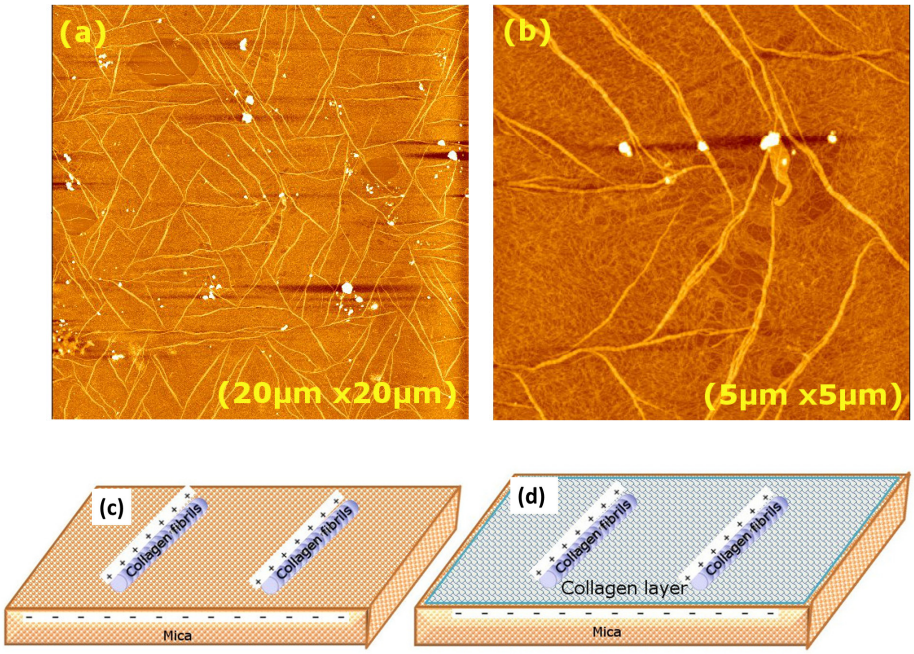

Figure 8.7: (a,b)5 $\mu g/ml$ of type-III collagen deposited for 3.15 h on phlogopite mica in the presence of 150 M KCl after 10 sec centrifuge. AFM CP-II was operated. (c) Model system to illustrate fibril formation on mica and fibril formation on a collagen layer onto mica (d).

the layer of collagen molecules distributed onto mica. The layer of collagen molecules between mica and fibrils diminish the effect of electrostatic attraction between the substrate and the collagen fibrils. The additional collagen layer in case (d) also leads to collagen-collagen repulsion force on the surface. By combination of the two forces, collagen fibrils feel the substrate effect less than the case (c). Therefore, fibrils grow in more independency. On the other hand, fibrils in case (d) grow under the strong substrate-collagen attractive force with less flexibility leading to more straight growing.

A good example of AFM image shown in Figure 8.8 was formed on phlogopite mica upon 5 h deposition of type-I collagen in the presence of 200 M KCl. The result-

ing network was analysed by 2 different techniques and compared. Both of analysis showed that collagen fibrils preferentially aligned into three directions which are determined by the combination of the surface symmetry of the underlying lattice and environmental condition such as the buffer condition [5, 4]. Unlike from the analysis performed by CAFE, image-j analysis of the network resulted in peaks repeating at every -90, 0 and +90 degrees. The high peaks observed at these points are numerical artifacts of Fast Fourier transform performed by image-j during the analysis.

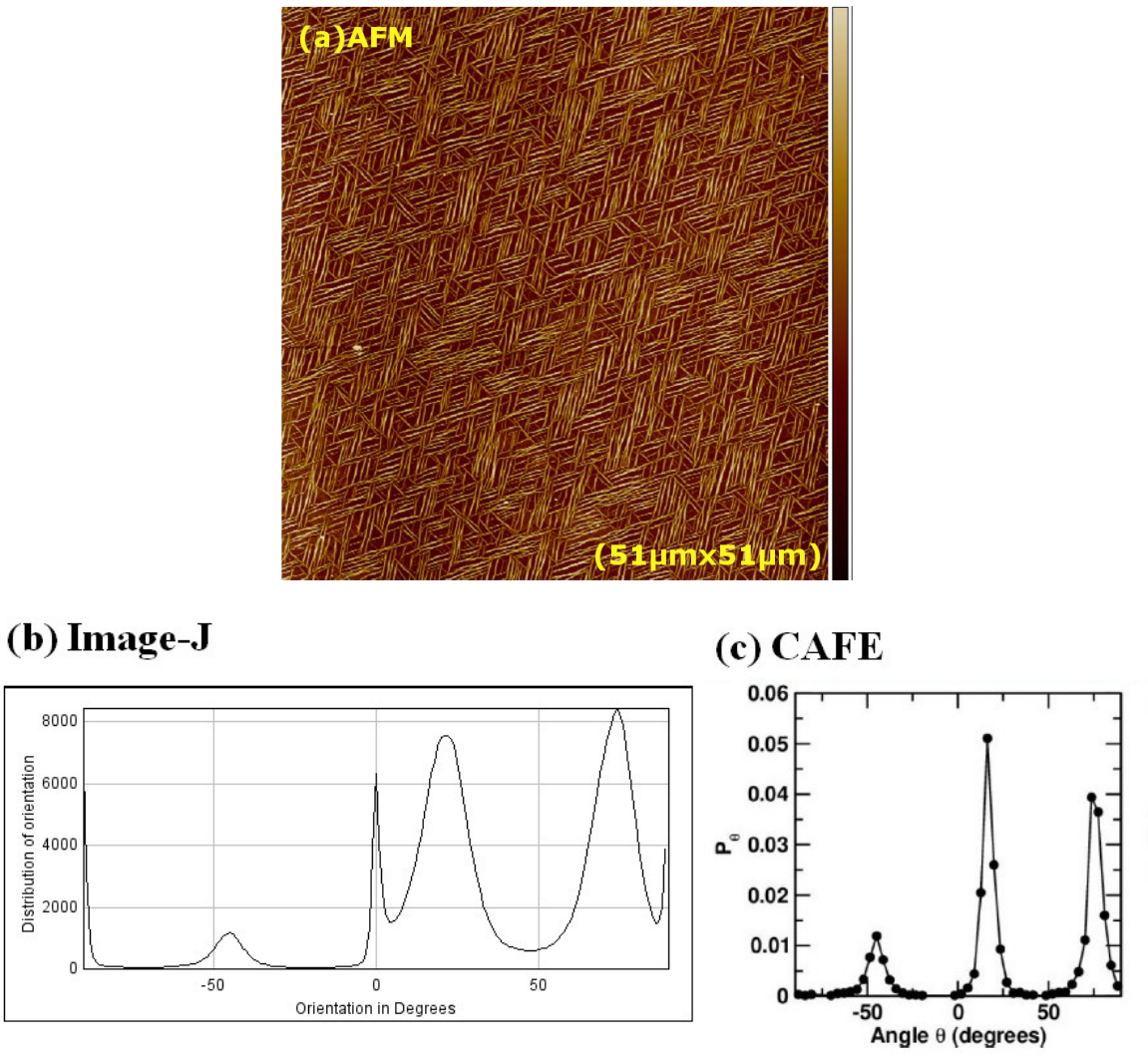

Figure 8.8: Analysis of collagen network formed at 2.5 $\mu g/ml$ concentration of type-I collagen. a) AFM image, z-scale is 12 nm. Bruker Dimension Icon AFM was operated. b) Orientational distribution of the network obtained by image-j and c) by CAFE [5].

8.2 Additional Experimental Observations

The type-I collagen network deposited for 30 min on muscovite mica after 10 sec centrifuge, in the presence of 50 mM glycine and 150 mM KCl are shown in Figure 8.10. Due to the aggregates on the surface, finding a clean area was almost impossible. The source of the aggregates could be an old buffer solution. To filter each of the electrolytes participating the buffer and to repeat the experiment could be a possible solution.

Although the aggregates and dirts on the surface, the orientational distribution of the network exhibits unidirectional alignment of fibrils on the surface. The peak at the center comes from the structural tensor that is used for the image analysis. As the bottom AFM image of Figure 8.10 contains more junks, the height of the peak decreases and the range of the orientation is widened. The orientational change of the fibrils observed in the images is also seen as $\sim 90^0$ from the data analysis.

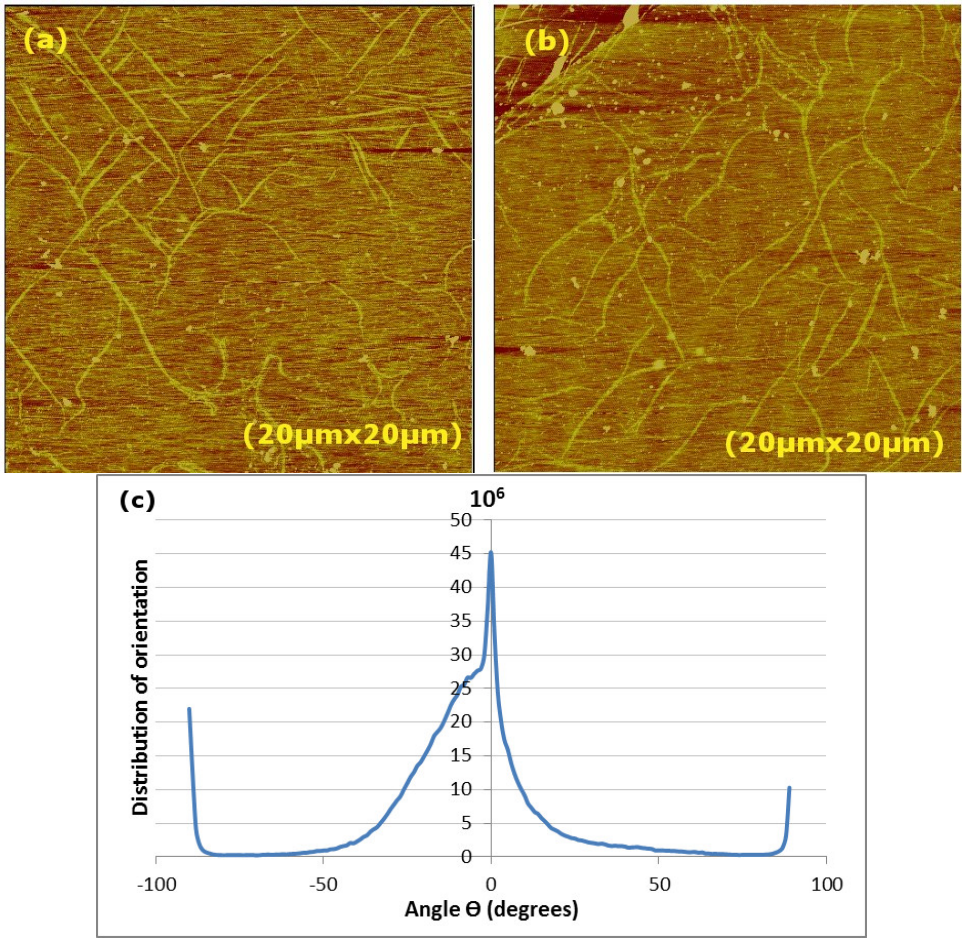

Figure 8.9: 5 $\mu g/ml$ concentration of type-III collagen was deposited for 30 min on phlogopite mica in the presence of 200 M KCl. Type-III collagen is in the process of assembly on the mica surface. At 2 h of the deposition, the growing was observed in an appropriate triangular shape. Z scale is 10 nm for panel(a), and 7 nm for panel(b). AFM Nanoscope IIIa was operated for the images.

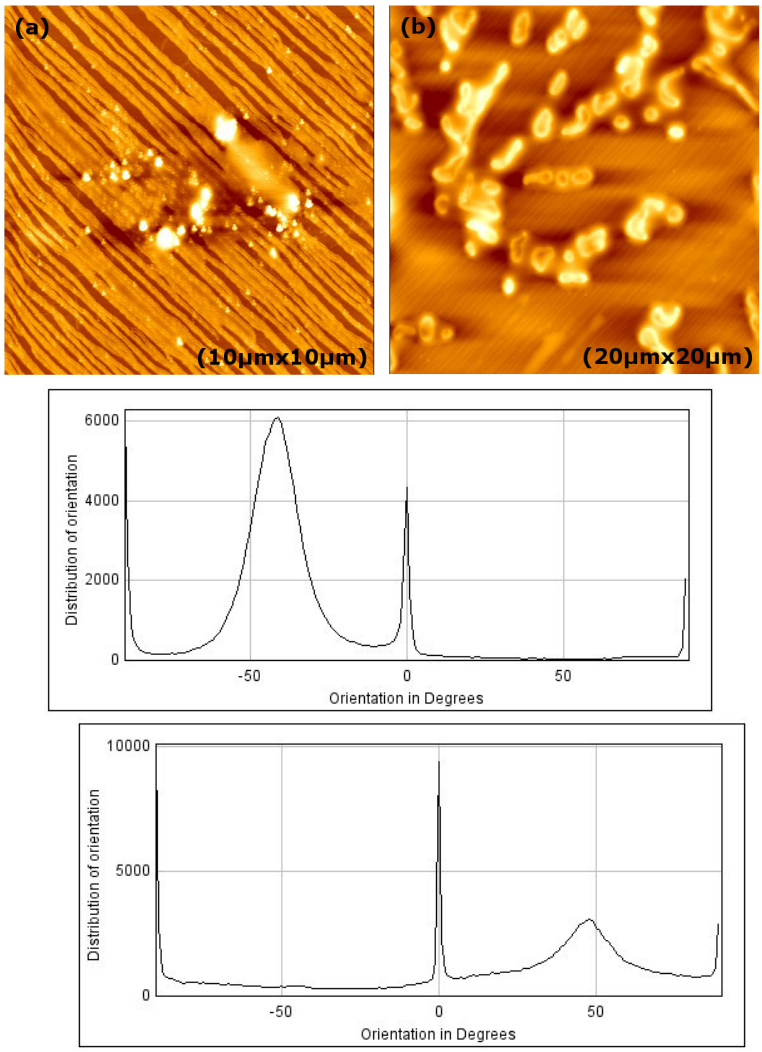

Figure 8.10: 5 $\mu g/ml$ type-I collagen deposited for 30 min. The corresponding orientational distribution of fibrils. Z-scale is 18.03 nm for panel(a), and 197.66 nm for panel(b). AFM CP-II was operated.

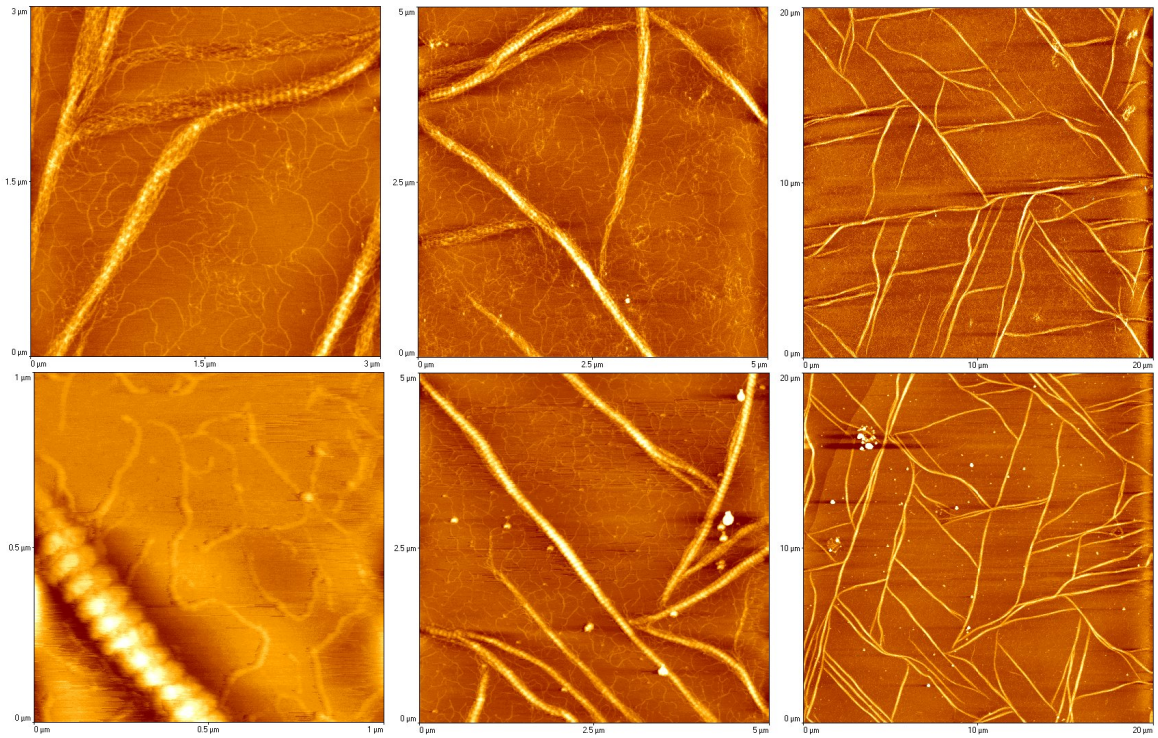

Figure 8.11: 5 $\mu g/ml$ of type-I collagen was deposited for 30 min for the upper images and 1 h for the bottom images on phlogopite mice after 10 sec centrifuge, in the presence of 50 mM glycine and 150 mM KCl. The fibril formation process is observed in details at 30 min of deposition and the characteristic d-periodic structure is shown in the bottom left image. AFM CP-II was operated.

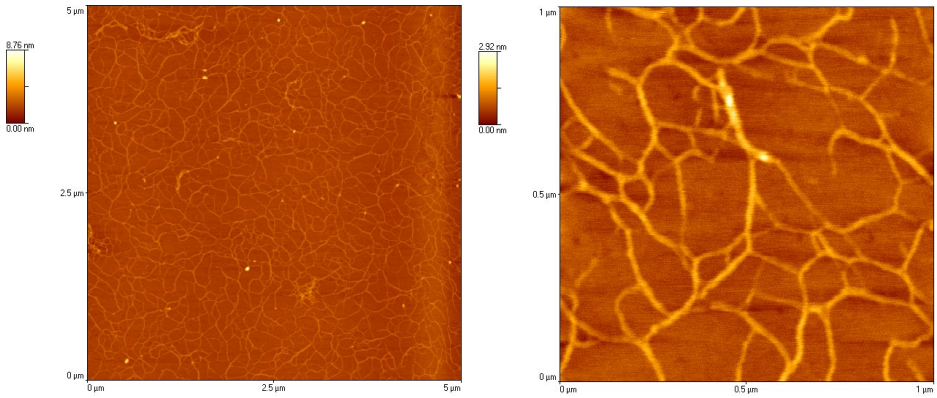

Figure 8.12: 5 $\mu g/ml$ of type-III collagen was deposited after 10 sec centrifuge on muscovite mica for 80 sec in the presence of 150 M KCl. AFM CP-II was operated.

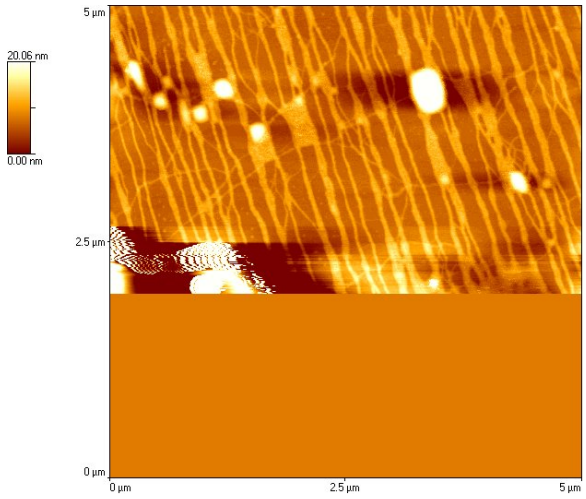

Figure 8.13: 5 $\mu g/ml$ of type-III collagen was deposited on muscovite mica for 1 h in the presence of 150 M KCl. High level of dirts and junks on the surface make impossible to find a clean area. The experiment should repeat with a higher level of protection from dirts like sealing of the sample right after deposition till scanning. AFM CP-II was operated.

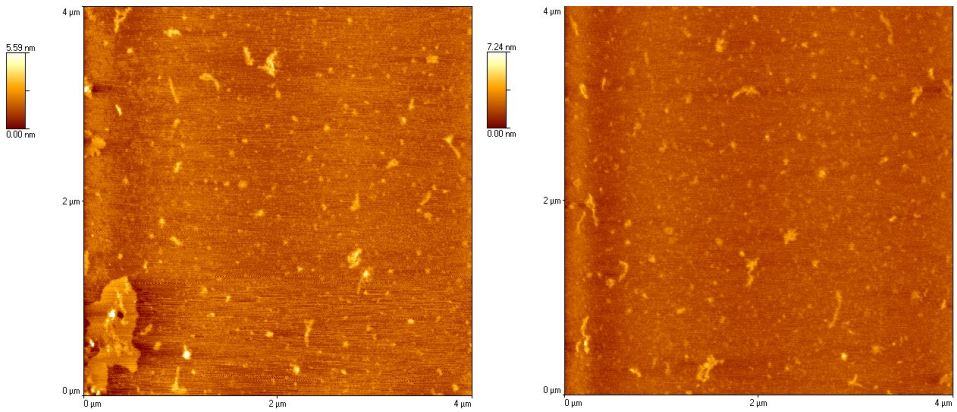

Figure 8.14: 0.1 $\mu g/ml$ of type-I collagen was deposited on muscovite mica for 2 min in the presence of 200 mM KCl. Too low concentration to observe the monomer molecules. AFM CP-II was operated.

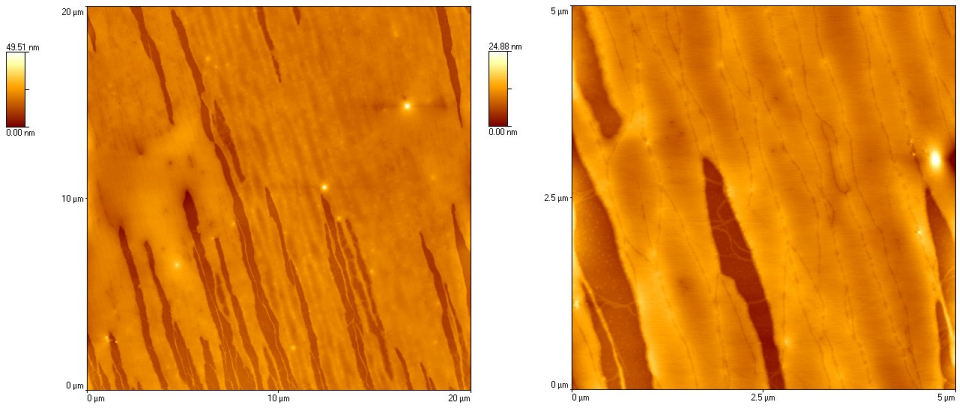

Figure 8.15: 5 $\mu g/ml$ of type-III collagen was deposited after 10 sec centrifuge on muscovite mica for 1 h in in the presence of 150 M KCl. The reason of the observed pattern is unclear. It could be a bad mica or old electrolyte or a composition of the two. We found that the electrolytes should be renewed at least once a month. AFM CP-II was operated.

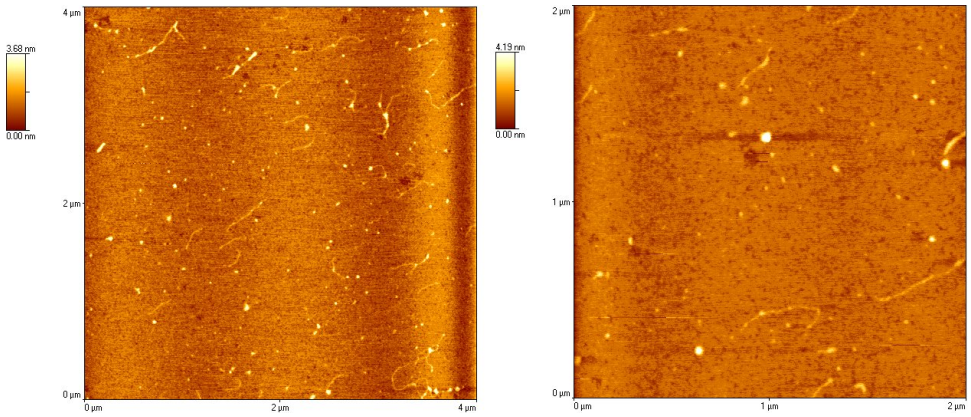

Figure 8.16: 0.1 $\mu g/ml$ concentration of type-III collagen was deposited on muscovite mica for 90 sec in the presence of 200 M KCl. The type-III molecules were quite dim. We reconstituted the type-III aliquot and obtained a better results. AFM CP-II was operated.

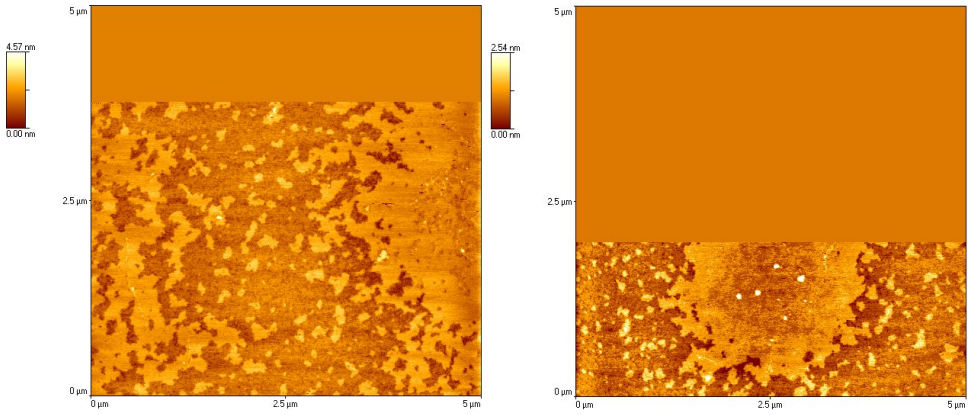

Figure 8.17: 0.4 $\mu g/ml$ concentration of type-III was deposited on muscovite mica for 90 sec in the presence of 200 M KCl. During the reconstitution process of type-III collagen, we used liquid nitrogen for some of the aliquots to figure out which method is the best to keep protein in its natural shape/properties. The observed structure of the sample showed that liquid nitrogen broke down the nature of the molecules and the sample surface was fully covered with the crystallized structure of type-III molecules. Thus, we eliminated this type of reconstitution of type-III collagen. AFM CP-II was operated.

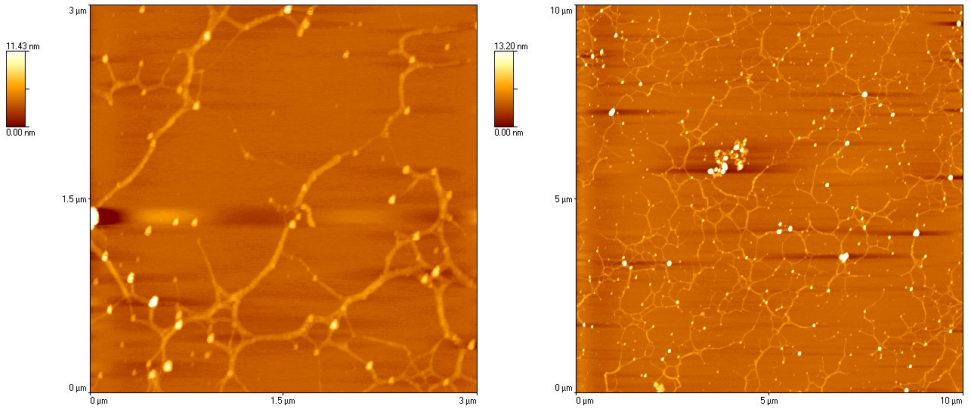

Figure 8.18: 5 $\mu g/ml$ concentration of type-III molecule was deposited on phlogopite mica for 20 min in the presence of 200 mM KCl. The sample surface was fully covered with collagen molecules without any fibrils yet. Type-III molecules are in the lag phase. The collagen network is observed as the one that is close to the early incubation at 1.30 min. AFM CP-II was operated.

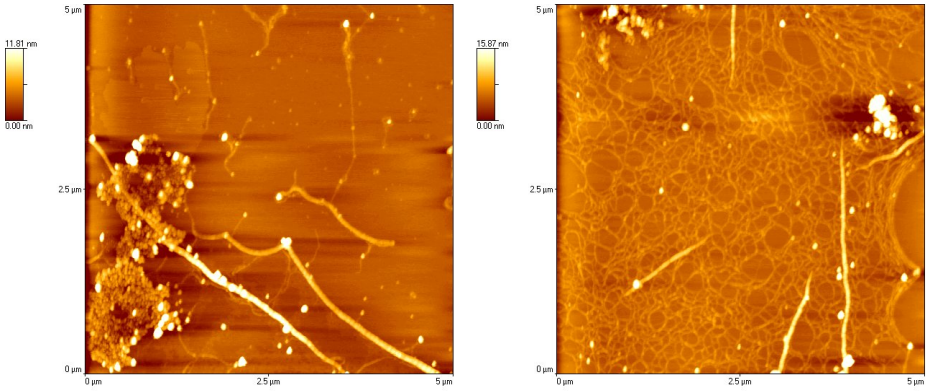

Figure 8.19: 5 $\mu g/ml$ concentration of type-III molecule was deposited for 3.45 h on phlogopite mica in the presence of 200 M KCl. Although the self-assembly of type-III molecules was observed on the surface, the resulting topography is not trustable, because the sample surface did not show an homogeneous appearance, which is probably due to the bad condition of mica. Some region among fibrils was found to be without collagen molecules as seen in the left image, some is full of type-III molecules as the right image. AFM CP-II was operated.

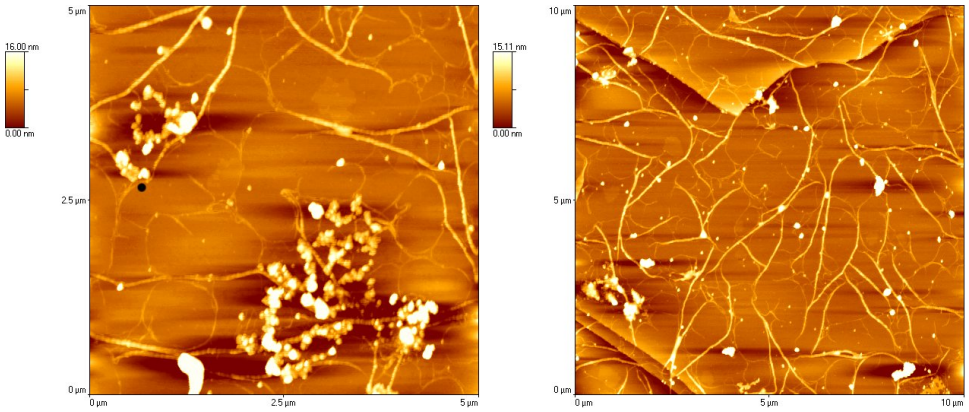

Figure 8.20: 5 $\mu g/ml$ concentration of type-I molecule was deposited for 30 min on phlogopite mica in the presence of 200 M KCl. Variety of problems are seen on the sample. Cracked surface of phlogopite mica is one of them. If the thickness of crack is about 10 $\mathring{A}$, further cleaving might solve the problem. The aggregates of small mass could be collagen molecules. We have found that type-I collagen has a shelf-life of 3 months at 4^0C. After reconstitution of type-I working solutionmolecules from the stock solution, we have obtain an expected pattern on phlogopite mica. AFM CP-II was operated.

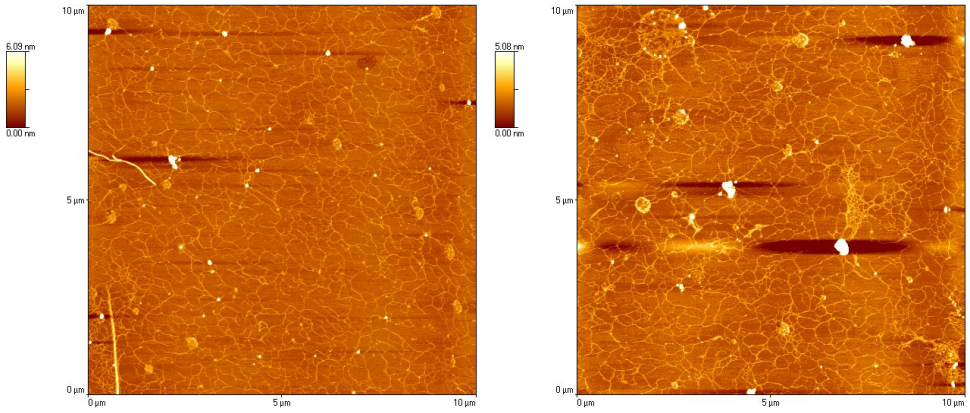

Figure 8.21: 5 $\mu g/ml$ concentration of type-I molecule was deposited for 30 min on phlogopite mica in the presence of 200 M KCl. The sample surface did not show almost any growing, but small collagen molecules did cover almost the entire surface. Even 2 h deposition did not result in an assembly. The sample solution might be not mixed well and uneven amount of electrolyte or collagen would be taken for deposition. The sample solution would be re-prepared. AFM CP-II was operated.

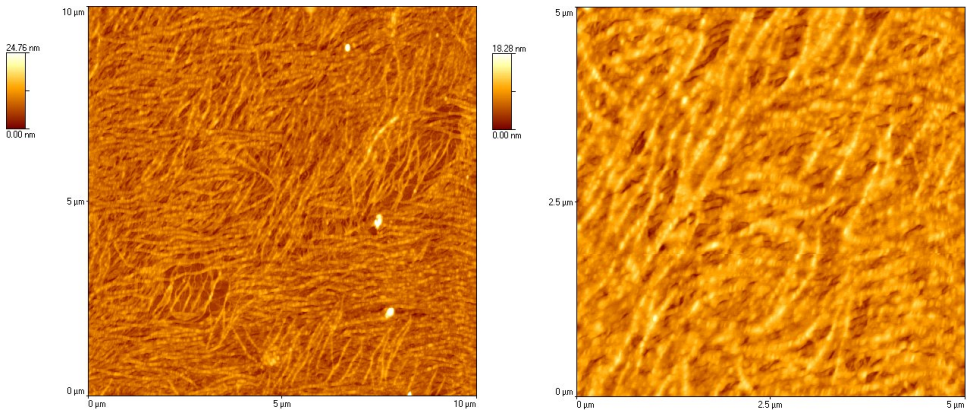

Figure 8.22: 5 $\mu g/ml$ concentration of type-I molecule was deposited for 2 h on phlogopite mica in the presence of 100 M KCl. Multiple layers of fibrils are observed on the substrate. AFM CP-II was operated.

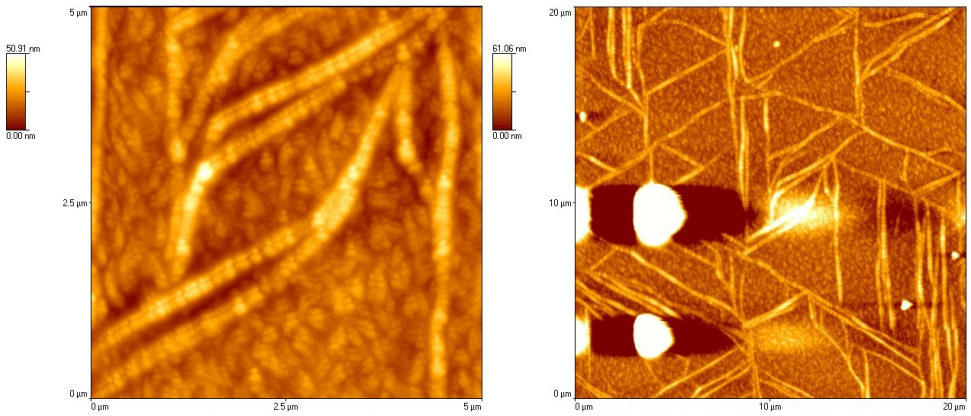

Figure 8.23: 5 $\mu g/ml$ type-I collagen was deposited after 10 sec centrifuge on phlogopite mice for 5 h, in the presence of 50 mM glycine and 150 mM KCl. At the end of 5 h deposition, we found no liquid on the mica surface, since the sample was left to the laboratory environment which caused the sample solution on the surface to evaporate. We figured out that for depositions more than 1 h, the sample should be protected in a moisture chamber, because the evaporation prevented the assembly process from its natural way. AFM CP-II was operated for the images.

9. SUMMARY AND OUTLOOK

The main goal of this research project is to study the heterotypic self-assembly of type-I and type-III collagen onto an atomically clean solid surface mica. For this, we used type-I collagen, which is most studied type on muscovite mica and created unidirectionally aligned collagen fibrils. We studied assembly on another substrate phlogopite mica to reproduce our previous results [4] and observed that under the appropriate condition of pH, electrolytes and K^+ ion, the self-assembly of collagen creates a triangular fibrillar network of collagen.

We explained self-assembly with two main non-covalent forces, which is called DLVO theory as a combination of attractive VDW and repulsive DL interaction. The concentration of KCl in the buffer solution was one of the significant parameters which affects the self-assembly. Adsorption of positively charged collagen molecules to negatively charged mica surface at pH 7 is sensitively dependent on the amount of K^+ due to the surface structure of mica. We have showed that by tuning the electrostatic interaction between collagen and mica with a varying concentration of KCl, the direction of the self-assembly can be controlled. Formation of long fibrils was prevented by high affinity of collagen to mica in the presence of insufficient K^+ ion in the buffer due to the highly charged mica surface. On the other hand, as the concentration of KCl increases, the size of fibrils such as diameter and length also increased indicating a lower affinity and higher surface diffusion of collagen due to the neutralization effect of K^+ ion on unoccupied binding pockets of mica surface. With a sensitive balance of KCl, we have managed the orientation of filaments and fabricated two patterns on different substrates as unidirectional and triangular collagen network on muscovite and phlogopite mica, respectively, to use as a template for our next

part of the research of the heterotypic assembly. With the inspiration of this filament growth guided by underlying substrate exhibiting in a variety of systems from bio- to non-bio, we have developed a computational and theoretical model to explain the template guided assembly of molecules in our previous study [5].

We performed a set of experiments to characterize the self-assembly of type-III collagen. We found that type-III collagen differs from type-I. At the nucleation level, we observed that type-III collagen has a longer lag phase than that of type-I . This observation raises a contradiction with the previous report on the type-III lag phase [78, 171, 73]. We consider that the interaction between collagen and mica affects the driving force of the assembly. Interaction with a solid surface is absent in the experimental set-up of the previous report. We showed that the interaction between molecules and mica is quite strong compared to the interaction between collagen-collagen with our simplified model. The longer lag phase of type-III could be understood in terms of its amino acid composition (Table 7.1). The higher number of polar amino acid in type-III collagen may suppress the nucleation events with repulsive hydrophilic effect that is lower on type-I collagen. Moreover, almost two-fold more non-polar amino acids on type-I compared to type-III should contribute to the attraction between collagen molecules leading a shorter time for molecules to aggregate, meaning a shorter lag phase observed in our homotypic self-assembly experiments.

After recognizing each type at the monomer and the nucleation level, we investigated the co-assembly of the two types that are the most abundant types in our body and we discovered an interesting influence of type-III collagen on the type-I assembly. When we investigated the mixture samples in terms of varying ratios of type-III to type-I, we found that upon an appropriate proportion of the mixture, the resulting morphology shows an enhanced number of nucleation even more than

that of type-I which was shown to have a shorter lag phase in our study of homotypic assembly. There is no previous study on the co-assembly of type-I and type-III collagen on the solid surface mica. Therefore, we have no information showing the reason of enhanced nucleation yet, but there are some speculations [185]. There are previous *in vivo* reports on type-III collagen suggesting that it is mostly found on the surface of the fibrillar tissue [78, 70, 179, 180, 181] which may be due to higher hydrophilic nature. We can explain the enhanced nucleation with this suggestion. Upon mixture, hydrophobic type-I molecules initiate nucleation with nascent base. Type-III molecules join the nascent form of nucleation and suppress the hydrophobic attraction with their higher hydrophilic structure by sitting on the surface. Therefore, remaining type-III molecules prefer to join another nascent base rather than to break hydrophilic repulsion with type-III coated new born fibrils. Thus, they prefer to attach a formed nuclei, resulting in an increased number of nucleation. We can not calculate the hydrophilic/hydrophobic effect precisely, since there is not a clear theoretical model yet. Its existence is known from experimental observation. We also calculated the DLVO force consisting of the two main interactions on the collagen-mica system and showed the necessity of a third force which we called water-mediated force. That is consistent with the previous simulation work from our group, finding the repulsive hydration force between collagen molecules [122].

Another striking effect of type-III collagen that we found is regarding its growing phase. We showed that with the addition of type-III collagen, the fibrillar network forms more regular, well-arranged, tight and shorter fibrils rather than long, wide-ranged distribution of fibrils. To use it as a regulatory element of the self-assembly of collagen could be a promising tool for both biological and material engineering applications as a controlled thin film generation.

To explain our system, we first applied the DLVO theory consisting of the elec-

trostatic and the wan der Waals forces to our simplified model collagen and mica. The calculations implied that there should be an additional repulsive force at contact which verifies the existence of repulsive hydration force at small separations, as reported in our previous study [122]. The theory remained insufficient to explain the assembly mechanism, since it is a continuum based theory. For example, we use a net/constant charge for each molecule. Instead, more local interaction of charges plays role in the fibril formation. Therefore, to understand the system better, a more detailed sequence level amino acid analysis are required. To do that, we used a scripting language, Python. With our one dimensional linear molecular model, we found the theoretical origin of the longer lag phase of type-III collagen molecules than that of type-I, as observed in our experiments (Fig. 7.2).Our program resulted in a stronger net force between type-I molecules. The higher interaction force must promote the aggregation between type-I molecules leading to a shorter lag phase. On the other hand, a smaller force requires more time for type-III molecules to nucleate and growth than type-I as shown in Fig. 4.3. Moreover, the heterotypic interaction score between type-I and type-III molecules resulted in an almost steady level of interaction at the locations from 0D to 3D. At a specific location, more interestingly, the hybrid assembly is more favorable than the type-I only and type-III only assembly, as pointing out our enhanced nucleation ratio between the two types. That most favorable case obtained at 2D location could be provided by a specific ratio of the two types as observed in our mixture(3:1) sample of the heterotypic assembly experiment (Fig.7.4).

Our method based on Python program opens a pathway to the field of proteins whose amino acid sequences are already known, but could not be benefited from them due to a large number of residues. They can not be handled without using a computer program. With this method, for given options of sequences of different proteins, the

most favorable structure that has the lowest energy (a native conformation) could be extracted. Even mutations in sequences imported manually could be tested and compared with existent experimental observations. This is perhaps one of the most effective methods to utilize the amino acid sequences provided by databases such as UniProt. This could be the most reliable means of comparing the effectiveness of interaction forces between protein molecules. We should note that, although our one dimensional model provides sufficiently effective method to be able to understand the intermolecular forces to some level, for more sophisticated analysis, three-dimensional structural information of molecules should be used for the programming. That will be our next focusing area in 3D.

To understand the co-assembly system of type-I and type-III collagen better, there are questions for future studies of the project. Studying the effect of pH is one of them. Although, it was studied for type-I assembly of higher concentration (0.1 mg/ml) [39], the influence of pH is not known on the heterotypic self-assembly. By decreasing pH, we expect to have a stronger electrostatic repulsive interaction between similar molecules and that might change the direction of the assembly. One of the reasons of choosing the two types of collagen is to understand the structure and functionality of ECM which has a structure of various types of collagen. The addition of other types and the observation of the difference on the resulting matrix could be interesting, as previous studies showed that morphology and composition of ECM has an important effect on responses of cells [186]. Therefore, how the co-assembly matrix reacts to the addition of cell could be also an important area. To understand the communication between cell and ECM better would be used to increase biological acceptance of implants.

REFERENCES

[1] D. Fan, A. Takawale, J. Lee, and Z. Kassiri. Cardiac fibroblasts, fibrosis and extracellular matrix remodeling in heart disease. *Fibrogenesis Tissue Repair*, 5(1):15–15, 2012.

[2] J. A. Petruska and A. J. Hodge. A subunit model for the tropocollagen macromolecule. *Proceedings of the National Academy of Sciences of the United States of America*, 51(5):871, 1964.

[3] Y. Li, A. Asadi, M. R. Monroe, and E. P. Douglas. pH effects on collagen fibrillogenesis *in vitro*: Electrostatic interactions and phosphate binding. *Materials Science and Engineering: C*, 29(5):1643–1649, 2009.

[4] W. W. Leow and W. Hwang. Epitaxially guided assembly of collagen layers on mica surfaces. *Langmuir*, 27(17):10907–10913, 2011.

[5] W. Hwang and E. Eryilmaz. Kinetic signature of fractal-like filament networks formed by orientational linear epitaxy. *Physical Review Letters*, 113(2):025502, 2014.

[6] M. R. Barnes, I. C. Gray, et al. *Bioinformatics for geneticists*, volume 1. Wiley Hoboken, NJ, 2003.

[7] K. Ito, K. Sumaru, and N. Ise. Elastic properties of colloidal crystals. *Physical Review B*, 46(5):3105, 1992.

[8] J. D. Joannopoulos, R. D. Meade, and J. N. Winn. Photonic crystals, 1995. *Princeton University, Princeton, NJ*, 2001.

[9] S. I. Stupp and P. V. Braun. Molecular manipulation of microstructures: biomaterials, ceramics, and semiconductors. *Science*, 277(5330):1242–1248, 1997.

[10] G. M. Whitesides, J. P. Mathias, and C. T. Seto. Molecular self-assembly and nanochemistry: a chemical strategy for the synthesis of nanostructures. Technical report, DTIC Document, 1991.

[11] B. A. Grzybowski, A. Winkleman, J. A. Wiles, Y. Brumer, and G. M. Whitesides. Electrostatic self-assembly of macroscopic crystals using contact electrification. *Nature materials*, 2(4):241–245, 2003.

[12] D. A. Cisneros, J. Friedrichs, A. Taubenberger, C. M. Franz, and D. J. Muller. Creating ultrathin nanoscopic collagen matrices for biological and biotechnological applications. *Small*, 3(6):956–963, 2007.

[13] K. Poole, K. Khairy, J. Friedrichs, C. Franz, D. A. Cisneros, J. Howard, and D. Mueller. Molecular-scale topographic cues induce the orientation and directional movement of fibroblasts on two-dimensional collagen surfaces. *Journal of molecular biology*, 349(2):380–386, 2005.

[14] A. G. A. Coombes, E. Verderio, B. Shaw, X. Li, M. Griffin, and S. Downes. Biocomposites of non-crosslinked natural and synthetic polymers. *Biomaterials*, 23(10):2113–2118, 2002.

[15] A. W. Lloyd. Interfacial bioengineering to enhance surface biocompatibility. *Medical device technology*, 13(1):18–21, 2001.

[16] S. Kumar, V. K. Aswal, and P. Callow. pH dependent interaction and resultant structures of silica nanoparticles and lysozyme protein. *Langmuir*, 2014.

[17] E. A. Cavalcanti-Adam, A. Micoulet, J. Blümmel, J. Auernheimer, H. Kessler, and J. P. Spatz. Lateral spacing of integrin ligands influences cell spreading and focal adhesion assembly. *European journal of cell biology*, 85(3):219–224, 2006.

[18] J. Engel and M. Chiquet. An overview of extracellular matrix structure and function. In *The extracellular matrix: an overview (R. P. Mecham, ed.)*, pages 1–39. Springer, Heidelberg, Germany, 2011.

[19] P. Bruckner. Suprastructures of extracellular matrices: paradigms of functions controlled by aggregates rather than molecules. *Cell and tissue research*, 339(1):7–18, 2010.

[20] J. K. Mouw, G. Ou, and V. M. Weaver. Extracellular matrix assembly: a multiscale deconstruction. *Nat. Rev. Molec. Cell Biol.*, 15(12):771–785, 2014.

[21] S. Bierbaum, R. Beutner, T. Hanke, D. Scharnweber, U. Hempel, and H. Worch. Modification of Ti6Al4V surfaces using collagen I, III, and fibronectin. I. biochemical and morphological characteristics of the adsorbed matrix. *Journal of Biomedical Materials Research Part A*, 67(2):421–430, 2003.

[22] K. Stuart and A. Panitch. Characterization of gels composed of blends of collagen I, collagen III, and chondroitin sulfate. *Biomacromolecules*, 10(1):25–31, 2008.

[23] M. P. Lutolf and J. A. Hubbell. Synthetic biomaterials as instructive extracellular microenvironments for morphogenesis in tissue engineering. *Nat. Biotechnol.*, 23(1):47–55, 2005.

[24] S. Heydarkhan-Hagvall, K. Schenke-Layland, A. P. Dhanasopon, F. Rofail, H. Smith, B. M. Wu, R. Shemin, R. E. Beygui, and W. R. MacLellan. Three-

dimensional electrospun ECM-based hybrid scaffolds for cardiovascular tissue engineering. *Biomaterials*, 29(19):2907–2914, 2008.

[25] N. Javid, S. Roy, M. Zelzer, Z. Yang, J. Sefcik, and R. V. Ulijn. Cooperative self-assembly of peptide gelators and proteins. *Biomacromolecules*, 14(12):4368–4376, 2013.

[26] S. Ricard-Blum. The collagen family. *Cold Spring Harbor perspectives in biology*, 3(1):a004978, 2011.

[27] M. K. Gordon and R. A. Hahn. Collagens. *Cell and tissue research*, 339(1):247–257, 2010.

[28] T. J. Wess. Collagen fibrillar structure and hierarchies. In *Collagen*, pages 49–80. Springer, 2008.

[29] I. K. Piechocka, A. S. G. van Oosten, R. G. M. Breuls, and G. H. Koenderink. Rheology of heterotypic collagen networks. *Biomacromolecules*, 12(7):2797–2805, 2011.

[30] H. Chanut-Delalande, A. Fichard, S. Bernocco, R. Garrone, D. J. S. Hulmes, and F. Ruggiero. Control of heterotypic fibril formation by collagen V is determined by chain stoichiometry. *J. Biol. Chem.*, 276(26):24352–24359, 2001.

[31] M. Dong, S. Xu, M. H. Bünger, H. Birkedal, and F. Besenbacher. Temporal assembly of collagen type II studied by atomic force microscopy. *Adv. Eng. Mater.*, 9(12):1129–1133, 2007.

[32] B. Salhi, F. Vaurette, B. Grandidier, D. Stiévenard, O. Melnyk, Y. Coffinier, and R. Boukherroub. The collagen assisted self-assembly of silicon nanowires. *Nanotechnology*, 20(23):235601, 2009.

[33] C. H. Lee, A. Singla, and Y. Lee. Biomedical applications of collagen. *International journal of pharmaceutics*, 221(1):1–22, 2001.

[34] J. Friedrichs, A. Taubenberger, C. M. Franz, and D. J. Muller. Cellular remodelling of individual collagen fibrils visualized by time-lapse afm. *Journal of molecular biology*, 372(3):594–607, 2007.

[35] M. R. Monroe, Y. Li, S. B. Ajinkya, L. B. Gower, and E. P. Douglas. Directed collagen patterning on gold-coated silicon substrates via micro-contact printing. *Materials Science and Engineering: C*, 29(8):2365–2369, 2009.

[36] B. Zhu, Q. Lu, J. Yin, J. Hu, and Z. Wang. Alignment of osteoblast-like cells and cell-produced collagen matrix induced by nanogrooves. *Tissue engineering*, 11(5-6):825–834, 2005.

[37] M. Papi, V. Palmieri, G. Maulucci, G. Arcovito, E. Greco, G. Quintiliani, M. Fraziano, and M. De Spirito. Controlled self assembly of collagen nanoparticle. *Journal of Nanoparticle Research*, 13(11):6141–6147, 2011.

[38] N. S. Murthy. Liquid crystallinity in collagen solutions and magnetic orientation of collagen fibrils. *Biopolymers*, 23(7):1261–1267, 1984.

[39] F. Jiang, H. Hörber, J. Howard, and D. J. Müller. Assembly of collagen into microribbons: effects of pH and electrolytes. *Journal of structural biology*, 148(3):268–278, 2004.

[40] D. L. Wilson, R. Martin, S. Hong, M. Cronin-Golomb, C. A. Mirkin, and D. L. Kaplan. Surface organization and nanopatterning of collagen by dip-pen nanolithography. *Proceedings of the National Academy of Sciences*, 98(24):13660–13664, 2001.

[41] S. Guido and R. T. Tranquillo. A methodology for the systematic and quantitative study of cell contact guidance in oriented collagen gels. correlation of fibroblast orientation and gel birefringence. *Journal of Cell Science*, 105(2):317–331, 1993.

[42] A. Gautieri, S. Vesentini, A. Redaelli, and M. J. Buehler. Hierarchical structure and nanomechanics of collagen microfibrils from the atomistic scale up. *Nano letters*, 11(2):757–766, 2011.

[43] H. Fernandes, A. Mentink, R. Bank, R. Stoop, C. van Blitterswijk, and J. de Boer. Endogenous collagen influences differentiation of human multipotent mesenchymal stromal cells. *Tissue Engineering Part A*, 16(5):1693–1702, 2010.

[44] T. Hoshiba, N. Kawazoe, and G. Chen. The balance of osteogenic and adipogenic differentiation in human mesenchymal stem cells by matrices that mimic stepwise tissue development. *Biomaterials*, 33(7):2025–2031, 2012.

[45] K. E. Kadler, C. Baldock, J. Bella, and R. P. Boot-Handford. Collagens at a glance. *Journal of cell science*, 120(12):1955–1958, 2007.

[46] R. O. Hynes. The extracellular matrix: not just pretty fibrils. *Science*, 326(5957):1216–1219, 2009.

[47] E. C. M. Mariman and P. Wang. Adipocyte extracellular matrix composition, dynamics and role in obesity. *Cellular and molecular life sciences*, 67(8):1277–1292, 2010.

[48] P. Lu, V. M. Weaver, and Z. Werb. The extracellular matrix: a dynamic niche in cancer progression. *The Journal of cell biology*, 196(4):395–406, 2012.

[49] D. Zangani, K. M. Darcy, P. A. Masso-Welch, E. S. Bellamy, M. S. Desole, and M. M. Ip. Multiple differentiation pathways of rat mammary stromal cells in

vitro: acquisition of a fibroblast, adipocyte or endothelial phenotype is dependent on hormonal and extracellular matrix stimulation. *Differentiation*, 64(2):91–101, 1999.

[50] N. S. Sharma, D. Nagrath, and M. L. Yarmush. Metabolic profiling based quantitative evaluation of hepatocellular metabolism in presence of adipocyte derived extracellular matrix. *PloS one*, 6(5):e20137, 2011.

[51] R. G. Thakar, F. Ho, N. F. Huang, D. Liepmann, and S. Li. Regulation of vascular smooth muscle cells by micropatterning. *Biochemical and biophysical research communications*, 307(4):883–890, 2003.

[52] E. Hohenester and J. Engel. Domain structure and organisation in extracellular matrix proteins. *Matrix biology*, 21(2):115–128, 2002.

[53] S. K. Akiyama, K. Nagata, and K. M. Yamada. Cell surface receptors for extracellular matrix components. *Biochimica et Biophysica Acta (BBA)-Reviews on Biomembranes*, 1031(1):91–110, 1990.

[54] F. Grinnell. Fibroblast biology in three-dimensional collagen matrices. *Trends in cell biology*, 13(5):264–269, 2003.

[55] S. Bierbaum, U. Hempel, U. Geißler, T. Hanke, D. Scharnweber, K.-W. Wenzel, and H. Worch. Modification of Ti6AL4V surfaces using collagen I, III, and fibronectin. II. influence on osteoblast responses. *Journal of Biomedical Materials Research Part A*, 67(2):431–438, 2003.

[56] D. P. Germain et al. Ehlers-Danlos syndrome type IV. *Orphanet J Rare Dis*, 2:32, 2007.

[57] F. M. Pope, G. R. Martin, J. R. Lichtenstein, R. Penttinen, B. Gerson, D. W. Rowe, and V. A. McKusick. Patients with ehlers-danlos syndrome type IV lack type III collagen. *Proceedings of the National Academy of Sciences*, 72(4):1314–1316, 1975.

[58] P. H. Byers, K. A. Holbrook, G. S. Barsh, L. T. Smith, and P. Bornstein. Altered secretion of type III procollagen in a form of type IV ehlers-danlos syndrome. biochemical studies in cultured fibroblasts. *Laboratory investigation; a journal of technical methods and pathology*, 44(4):336–341, 1981.

[59] G.-G. Zhu, J. Risteli, U. Puistola, A. Kauppila, and L. Risteli. Progressive ovarian carcinoma induces synthesis of type I and type III procollagens in the tumor tissue and peritoneal cavity. *Cancer research*, 53(20):5028–5032, 1993.

[60] S. Kauppila, J. Saarela, F. Stenbäck, J. Risteli, A. Kauppila, and L. Risteli. Expression of mRNAs for type I and type III procollagens in serous ovarian cystadenomas and cystadenocarcinomas. *The American journal of pathology*, 148(2):539, 1996.

[61] J. Turnay, N. Olmo, J. G. Gavilanes, and M. A. Lizarbe. Collagen metabolism in human colon adenocarcinoma. *Connective tissue research*, 23(4):251–260, 1989.

[62] K. Hamano, T. Kuga, M. Takahashi, K. Fujioka, T. Katoh, N. Zempo, Y. Fujimura, and K. Esato. The lack of type III collagen in a patient with aneurysms and an aortic dissection. *Journal of vascular surgery*, 28(6):1104–1106, 1998.

[63] S. B. Deak, J. J. Ricotia, T. J. Mariani, S. T. Deak, M. A. Zatina, J. W. Mackenzie, and C. D. Boyd. Abnormalities in the biosynthesis of type III procollagen in cultured skin fibroblasts from two patients with multiple aneurysms. *Matrix*, 12(2):92–100, 1992.

[64] C. J. Van Keulen, E. Van de Akker, G. Pals, and J. A. Rauwerda. The role of type III collagen in the development of familial abdominal aortic aneurysms. *European journal of vascular and endovascular surgery*, 18(1):65–70, 1999.

[65] I. Pucci-Minafra, M. Andriolo, L. Basirico, R. Alessandro, C. Luparello, C. Buccellato, R. Garbelli, and S. Minafra. Absence of regular alpha2 (I) collagen chains in colon carcinoma biopsy fragments. *Carcinogenesis*, 19(4):575–584, 1998.

[66] M. Pepin, U. Schwarze, A. Superti-Furga, and P. H. Byers. Clinical and genetic features of Ehlers–Danlos syndrome type IV, the vascular type. *New England Journal of Medicine*, 342(10):673–680, 2000.

[67] R. K. Freeman, J. Swegle, and M. J. Sise. The surgical complications of Ehlers-Danlos syndrome. *The American Surgeon*, 62(10):869–873, 1996.

[68] D. F. Cikrit, J. R. Glover, M. C. Dalsing, and D. Silver. The Ehlers-Danlos specter revisited. *Vascular and endovascular surgery*, 36(3):213–217, 2002.

[69] A. M. Peaceman and D. P. Cruikshank. Ehlers-danlos syndrome and pregnancy: association of type IV disease with maternal death. *Obstetrics and gynecology*, 69(3 Pt 2):428–431, 1987.

[70] R. Fleischmajer, R. Timpl, L. Tuderman, L. Raisher, M. Wiestner, J. S. Perlish, and P. N. Graves. Ultrastructural identification of extension aminopropeptides of type I and III collagens in human skin. *Proceedings of the National Academy of Sciences*, 78(12):7360–7364, 1981.

[71] Y. Maehata, S. Takamizawa, S. Ozawa, K. Izukuri, Y. Kato, S. Sato, A. Kimura, R.-I. Hata, et al. Type III collagen is essential for growth accelera-

tion of human osteoblastic cells by ascorbic acid 2-phosphate, a long-acting vitamin c derivative. *Matrix biology*, 26(5):371–381, 2007.

[72] Y. Maehata, S. Takamizawa, S. Ozawa, Y. Kato, S. Sato, E. Kubota, and R.-I. Hata. Both direct and collagen-mediated signals are required for active vitamin D 3-elicited differentiation of human osteoblastic cells: roles of osterix, an osteoblast-related transcription factor. *Matrix biology*, 25(1):47–58, 2006.

[73] M. L. Speranza, G. Valentini, and A. Calligaro. Influence of fibronectin on the fibrillogenesis of type I and type III collagen. *Collagen and related research*, 7(2):115–123, 1987.

[74] S. C. Cowin and S. B. Doty. *Tissue mechanics*. Springer, 2007.

[75] P. Fratzl. *Collagen: structure and mechanics*, volume 1. Springer New York:, 2008.

[76] F. Gobeaux, G. Mosser, A. Anglo, P. Panine, P. Davidson, M.-M. Giraud-Guille, and E. Belamie. Fibrillogenesis in dense collagen solutions: a physicochemical study. *Journal of molecular biology*, 376(5):1509–1522, 2008.

[77] L. D. Muiznieks and F. W. Keeley. Molecular assembly and mechanical properties of the extracellular matrix: A fibrous protein perspective. *Biochimica et Biophysica Acta (BBA)-Molecular Basis of Disease*, 1832(7):866–875, 2013.

[78] C. M. Lapiere, B. Nusgens, and G. E. Pierard. Interaction between collagen type I and type III in conditioning bundles organization. *Connective tissue research*, 5(1):21–29, 1977.

[79] A. M. Romanic, E. Adachi, K. E. Kadler, Y. Hojima, and D. J. Prockop. Copolymerization of pNcollagen III and collagen I. pNcollagen III decreases the rate

of incorporation of collagen I into fibrils, the amount of collagen I incorporated, and the diameter of the fibrils formed. *Journal of Biological Chemistry*, 266(19):12703–12709, 1991.

[80] F. H. Silver, J. W. Freeman, and G. P. Seehra. Collagen self-assembly and the development of tendon mechanical properties. *Journal of biomechanics*, 36(10):1529–1553, 2003.

[81] K. Gelse, E. Pöschl, and T. Aigner. Collagensstructure, function, and biosynthesis. *Advanced drug delivery reviews*, 55(12):1531–1546, 2003.

[82] M. Yamauchi, D. R. Young, G. S. Chandler, and G. L. Mechanic. Cross-linking and new bone collagen synthesis in immobilized and recovering primate osteoporosis. *Bone*, 9(6):415–418, 1988.

[83] C. M. Kielty and M. E. Grant. The collagen family: structure, assembly, and organization in the extracellular matrix. *Connective Tissue and Its Heritable Disorders: Molecular, Genetic, and Medical Aspects, Second Edition*, pages 159–221, 2003.

[84] J. D. Prockop. Collagens: molecular biology, diseases, and potentials for therapy. *Annual review of biochemistry*, 64(1):403–434, 1995.

[85] K. Kadler, D. Holmes, J. Trotter, and J. Chapman. Collagen fibril formation. *Biochem. J*, 316:1–11, 1996.

[86] S. C. Cowin. How is a tissue built? *Journal of biomechanical engineering*, 122(6):553–569, 2000.

[87] D. F. Holmes, C. J. Gilpin, C. Baldock, U. Ziese, A. J. Koster, and K. E. Kadler. Corneal collagen fibril structure in three dimensions: structural insights into

fibril assembly, mechanical properties, and tissue organization. *Proceedings of the National Academy of Sciences*, 98(13):7307–7312, 2001.

[88] F.-Z. Cui, Y. Li, and J. Ge. Self-assembly of mineralized collagen composites. *Materials Science and Engineering: R: Reports*, 57(1):1–27, 2007.

[89] C. C. Banos, A. H. Thomas, and C. K. Kuo. Collagen fibrillogenesis in tendon development: current models and regulation of fibril assembly. *Birth Defects Research Part C: Embryo Today: Reviews*, 84(3):228–244, 2008.

[90] L. Huang, K. Nagapudi, R. P. Apkarian, and E. L. Chaikof. Engineered collagen–PEO nanofibers and fabrics. *Journal of biomaterials science, Polymer edition*, 12(9):979–993, 2001.

[91] J. Engel. Versatile collagens in invertebrates. *Science*, 277(5333):1785–1786, 1997.

[92] S. J. Eppell, B. N. Smith, H. Kahn, and R. Ballarini. Nano measurements with micro-devices: mechanical properties of hydrated collagen fibrils. *Journal of the Royal Society Interface*, 3(6):117–121, 2006.

[93] J. A. J. van der Rijt, K. O. van der Werf, M. L. Bennink, P. J. Dijkstra, and J. Feijen. Micromechanical testing of individual collagen fibrils. *Macromolecular bioscience*, 6(9):697–702, 2006.

[94] L. Yang, K. O. Van der Werf, C. F. C. Fitié, M. L. Bennink, P. J. Dijkstra, and J. Feijen. Mechanical properties of native and cross-linked type I collagen fibrils. *Biophysical journal*, 94(6):2204–2211, 2008.

[95] L. Yang, K. O. Van der Werf, P. J. Dijkstra, J. Feijen, and M. L. Bennink. Micromechanical analysis of native and cross-linked collagen type I fibrils supports the

existence of microfibrils. *Journal of the mechanical behavior of biomedical materials*, 6:148–158, 2012.

[96] L. Yang, K. O. van der Werf, B. F. J. M. Koopman, V. Subramaniam, M. L. Bennink, P. J. Dijkstra, and J. Feijen. Micromechanical bending of single collagen fibrils using atomic force microscopy. *Journal of Biomedical Materials Research Part A*, 82(1):160–168, 2007.

[97] M. P. E. Wenger, L. Bozec, M. A. Horton, and P. Mesquida. Mechanical properties of collagen fibrils. *Biophysical journal*, 93(4):1255–1263, 2007.

[98] R. Fleischmajer, J. S. Perlish, R. E. Burgeson, F. Shaikh-Bahai, and R. Timpl. Type I and type III collagen interactions during fibrillogenesisa. *Annals of the New York Academy of Sciences*, 580(1):161–175, 1990.

[99] M. Raspanti, E. Binaghi, I. Gallo, and A. Manelli. A vision-based, 3D reconstruction technique for scanning electron microscopy: Direct comparison with atomic force microscopy. *Microscopy research and technique*, 67(1):1–7, 2005.

[100] G. J. Cameron, I. L. Alberts, J. H. Laing, and T. J. Wess. Structure of type I and type III heterotypic collagen fibrils: an X-ray diffraction study. *Journal of structural biology*, 137(1):15–22, 2002.

[101] L. Ala-Kokko, S. Kontusaari, C. T. Baldwin, H. Kuivaniemi, and D. J. Prockop. Structure of cDNA clones coding for the entire prepro alpha 1 (III) chain of human type III procollagen. differences in protein structure from type I procollagen and conservation of codon preferences. *Biochem. J*, 260:509–516, 1989.

[102] B. R. Williams, R. A. Gelman, D. C. Poppke, and K. A. Piez. Collagen fibril formation. *J. biol. Chem*, 253(18):6578–6585, 1978.

[103] R. A. Gelman, B. R. Williams, and K. A. Piez. Collagen fibril formation. evidence for a multistep process. *Journal of Biological Chemistry*, 254(1):180–186, 1979.

[104] K. E. Kadler, Y. Hojima, and D. J. Prockop. Collagen fibrils in vitro grow from pointed tips in the C-to N-terminal direction. *Biochem. j*, 268:339–343, 1990.

[105] S. Gay and E. J. Miller. *Collagen in the physiology and pathology of connective tissue*. Fischer, 1978.

[106] J. Gross and F. O. Schmitt. The structure of human skin collagen as studied with the electron microscope. *The Journal of experimental medicine*, 88(5):555, 1948.

[107] B. Erickson, M. Fang, J. M. Wallace, B. G. Orr, C. M. Les, and Mark M. Banaszak H. Nanoscale structure of type I collagen fibrils: Quantitative measurement of D-spacing. *Biotechnology journal*, 8(1):117–126, 2013.

[108] K. E. Kadler, Y. Hojima, and D. J. Prockop. Assembly of collagen fibrils de novo by cleavage of the type I pC-collagen with procollagen C-proteinase. assay of critical concentration demonstrates that collagen self-assembly is a classical example of an entropy-driven process. *Journal of Biological Chemistry*, 262(32):15696–15701, 1987.

[109] R. Usha and T. Ramasami. Influence of hydrogen bond, hydrophobic and electrovalent salt linkages on the transition temperature, enthalpy and activation energy in rat tail tendon (RTT) collagen fibre. *Thermochimica Acta*, 338(1):17–25, 1999.

[110] J. Schnell. Evidence for the existence of hydrophobic interactions as a stabilizing factor in collagen structure. *Archives of biochemistry and biophysics*, 127:496–502, 1968.

[111] G. C. Na, L. J. Phillips, and E. I. Freire. In vitro collagen fibril assembly: thermodynamic studies. *Biochemistry*, 28(18):7153–7161, 1989.

[112] D. J. S. Hulmes, A. Miller, D. A. D. Parry, K. A. Piez, and J. Woodhead-Galloway. Analysis of the primary structure of collagen for the origins of molecular packing. *Journal of molecular biology*, 79(1):137–148, 1973.

[113] H. K. Christenson. DLVO (Derjaguin–Landau–Verwey–Overbeek) theory and solvation forces between mica surfaces in polar and hydrogen-bonding liquids. *Journal of the Chemical Society, Faraday Transactions 1: Physical Chemistry in Condensed Phases*, 80(7):1933–1946, 1984.

[114] J. Marra and J. Israelachvili. Direct measurements of forces between phosphatidylcholine and phosphatidylethanolamine bilayers in aqueous electrolyte solutions. *Biochemistry*, 24(17):4608–4618, 1985.

[115] J. N. lsraelachvili. *Intermolecular and Surface Forces*. Academic Press, 1991.

[116] M. V. Maslova, L. G. Gerasimova, and W. Forsling. Surface properties of cleaved mica. *Colloid Journal*, 66(3):322–328, 2004.

[117] A. Faghihnejad and H. Zeng. Interaction mechanism between hydrophobic and hydrophilic surfaces: Using polystyrene and mica as a model system. *Langmuir*, 29(40):12443–12451, 2013.

[118] P. M. Claesson, P. C. Herder, C. E. Blom, and B. W. Ninham. Interactions between a positively charged hydrophobic surface and a negatively charged bare mica surface. *Journal of colloid and interface science*, 118(1):68–79, 1987.

[119] N. Mishchuk, J. Ralston, and D. Fornasiero. Influence of dissolved gas on van der Waals forces between bubbles and particles. *The Journal of Physical Chemistry A*, 106(4):689–696, 2002.

[120] J.-H. Lee and J. C. Meredith. Non-DLVO silica interaction forces in NMP–Water mixtures. II. an asymmetric system. *Langmuir*, 27(16):10000–10006, 2011.

[121] E. E. Meyer, Q. Lin, T. Hassenkam, E. Oroudjev, and J. N. Israelachvili. Origin of the long-range attraction between surfactant-coated surfaces. *Proceedings of the National Academy of Sciences of the United States of America*, 102(19):6839–6842, 2005.

[122] K. M. Ravikumar and W. Hwang. Role of hydration force in the self-assembly of collagens and amyloid steric zipper filaments. *Journal of the American Chemical Society*, 133(30):11766–11773, 2011.

[123] D. Henderson and M. Lozada-Cassou. A simple theory for the force between spheres immersed in a fluid. *Journal of colloid and interface science*, 114(1):180–183, 1986.

[124] D. Henderson and M. Lozada-Cassou. Does dielectric saturation provide a plausible explanation of the hydration solvation force? *Journal of colloid and interface science*, 162(2):508–509, 1994.

[125] N. A. M. Besseling. Theory of hydration forces between surfaces. *Langmuir*, 13(7):2113–2122, 1997.

[126] H .K. Christenson, P. M. Claesson, J. Berg, and P. C. Herder. Forces between fluorocarbon surfactant monolayers: Salt effects on the hydrophobic interaction. *The Journal of Physical Chemistry*, 93(4):1472–1478, 1989.

[127] H. K. Christenson, J. Fang, B. W. Ninham, and J. L. Parker. Effect of divalent electrolyte on the hydrophobic attraction. *Journal of Physical Chemistry*, 94(21):8004–8006, 1990.

[128] D. Leckband and J. Israelachvili. Intermolecular forces in biology. *Quarterly reviews of biophysics*, 34(02):105–267, 2001.

[129] M. Wasilewska and Z. Adamczyk. Fibrinogen adsorption on mica studied by AFM and in situ streaming potential measurements. *Langmuir*, 27(2):686–696, 2010.

[130] J. W. Pitera, M. Falta, and W. F. van Gunsteren. Dielectric properties of proteins from simulation: the effects of solvent, ligands, pH, and temperature. *Biophysical journal*, 80(6):2546–2555, 2001.

[131] S. Leikin, V. A. Parsegian, W.-H. Yang, and G. E. Walrafen. Raman spectral evidence for hydration forces between collagen triple helices. *Proceedings of the National Academy of Sciences*, 94(21):11312–11317, 1997.

[132] M. A. Osman, C. Moor, W. R. Caseri, and U. W. Suter. Alkali metals ion exchange on muscovite mica. *Journal of colloid and interface science*, 209(1):232–239, 1999.

[133] R. W. Loo and M. C. Goh. Potassium ion mediated collagen microfibril assembly on mica. *Langmuir*, 24(23):13276–13278, 2008.

[134] D. M. Czajkowsky and Z. Shao. Inhibition of protein adsorption to muscovite mica by monovalent cations. *Journal of microscopy*, 211(1):1–7, 2003.

[135] Guido Van Rossum and Fred L Drake Jr. *Python tutorial*. Centrum voor Wiskunde en Informatica, 1995.

[136] K Jarrod Millman and Michael Aivazis. Python for scientists and engineers. *Computing in Science & Engineering*, 13(2):9–12, 2011.

[137] K. A. Dill. Dominant forces in protein folding. *Biochemistry*, 29(31):7133–7155, 1990.

[138] G. Casari and M. J. Sippl. Structure-derived hydrophobic potential: hydrophobic potential derived from X-ray structures of globular proteins is able to identify native folds. *J. Mol. Biol.*, 224(3):725–732, 1992.

[139] E. S. Huang, S. Subbiah, and M. Levitt. Recognizing native folds by the arrangement of hydrophobic and polar residues. *J. Mol. Biol.*, 252(5):709–720, 1995.

[140] C. A. Schneider, W. S. Rasband, and K. W. Eliceiri. NIH Image to ImageJ: 25 years of image analysis. *Nature methods*, 9(7):671–675, 2012.

[141] G. Binnig, C. F. Quate, and C. Gerber. Atomic force microscope. *Physical review letters*, 56(9):930, 1986.

[142] H. K. Wickramasinghe. Scanned-probe microscopes. *Scientific American;(USA)*, 261(4), 1989.

[143] D. Rugar and P. Hansma. Atomic force microscopy. *Physics today*, 43(10):23–30, 1990.

[144] L. M. Demers, D. S. Ginger, S.-J. Park, Z. Li, S.-W. Chung, and C. A. Mirkin. Direct patterning of modified oligonucleotides on metals and insulators by dip-pen nanolithography. *Science*, 296(5574):1836–1838, 2002.

[145] K.-B. Lee, S.-J. Park, C. A. Mirkin, J. C. Smith, and M. Mrksich. Protein nanoarrays generated by dip-pen nanolithography. *Science*, 295(5560):1702–1705, 2002.

[146] M. C. Goh, M. F. Paige, M. A. Gale, I. Yadegari, M. Edirisinghe, and J. Strzelczyk. Fibril formation in collagen. *Physica A: Statistical Mechanics and its Applications*, 239(1):95–102, 1997.

[147] M. Fang, E. L. Goldstein, E. K. Matich, B. G. Orr, and Mark M. Banaszak H. Type I collagen self-assembly: the roles of substrate and concentration. *Langmuir*, 29(7):2330–2338, 2013.

[148] M. L. Schlegel, K. L. Nagy, P. Fenter, L. Cheng, N. C. Sturchio, and S. D. Jacobsen. Cation sorption on the muscovite (001) surface in chloride solutions using high-resolution X-ray reflectivity. *Geochimica et cosmochimica acta*, 70(14):3549–3565, 2006.

[149] J. Israelachvili and H. Wennerström. Role of hydration and water structure in biological and colloidal interactions. 1996.

[150] Y. Kuwahara. Comparison of the surface structure of the tetrahedral sheets of muscovite and phlogopite by AFM. *Physics and Chemistry of Minerals*, 28(1):1–8, 2001.

[151] Y. Kuwahara. Muscovite surface structure imaged by fluid contact mode AFM. *Physics and chemistry of minerals*, 26(3):198–205, 1999.

[152] F. Balzer, L. Kankate, H. Niehus, and H.-G. Rubahn. Epitaxy vs. dipole assisted growth for organic oligomer nanoaggregates. In *Optics & Photonics 2005*, pages 59250A–59250A. International Society for Optics and Photonics, 2005.

[153] C. Simbrunner, D. Nabok, G. Hernandez-Sosa, M. Oehzelt, T. Djuric, R. Resel, L. Romaner, P. Puschnig, C. Ambrosch-Draxl, I. Salzmann, et al. Epitaxy of rodlike organic molecules on sheet silicates- a growth model based on experiments and simulations. *Journal of the American Chemical Society*, 133(9):3056–3062, 2011.

[154] M. Sun, A. Stetco, and Merschrod S. E. F. Surface-templated formation of protein microfibril arrays. *Langmuir*, 24(10):5418–5421, 2008.

[155] Á. Karsai, Ü. Murvai, K. Soós, B. Penke, and M. Kellermayer. Oriented epitaxial growth of amyloid fibrils of the N27C mutant β25–35 peptide. *European Biophysics Journal*, 37(7):1133–1137, 2008.

[156] S.-G. Kang, H. Li, T. Huynh, F. Zhang, Z. Xia, Y. Zhang, and R. Zhou. Molecular mechanism of surface-assisted epitaxial self-assembly of amyloid-like peptides. *ACS nano*, 6(10):9276–9282, 2012.

[157] C. Simbrunner. Epitaxial growth of sexi-thiophene and para-hexaphenyl and its implications for the fabrication of self-assembled lasing nano-fibres. *Semiconductor Science and Technology*, 28(5):053001, 2013.

[158] D.-M. Smilgies, N. Boudet, B. Struth, Y. Yamada, and H. Yanagi. Highly oriented POPOP films grown on the KCl (001) surface. *Journal of crystal growth*, 220(1):88–95, 2000.

[159] K. Müller and C. C. Chang. Electric dipoles on clean mica surfaces. *Surface Science*, 14(1):39–51, 1969.

[160] N. Sánchez-Pastor, K. Aldushin, G. Jordan, and W. W. Schmahl. $k^+ - na^+$ exchange in phlogopite on the scale of a single layer. *Geochimica et Cosmochimica Acta*, 74(7):1954–1962, 2010.

[161] K. M. Ravikumar and W. Hwang. Region-specific role of water in collagen unwinding and assembly. *Proteins: Structure, Function, and Bioinformatics*, 72(4):1320–1332, 2008.

[162] A. J. Engler, S. Sen, H. L. Sweeney, and D. E. Discher. Matrix elasticity directs stem cell lineage specification. *Cell*, 126(4):677–689, 2006.

[163] G. D. Pins, D. L. Christiansen, R. Patel, and F. H. Silver. Self-assembly of collagen fibers. influence of fibrillar alignment and decorin on mechanical properties. *Biophysical Journal*, 73(4):2164–2172, 1997.

[164] J. P. R. O. Orgel, T. C. Irving, A. Miller, and T. J. Wess. Microfibrillar structure of type I collagen in situ. *Proceedings of the National Academy of Sciences*, 103(24):9001–9005, 2006.

[165] F. H. Silver and D. E. Birk. Molecular structure of collagen in solution: comparison of types I, II, III and V. *International Journal of Biological Macromolecules*, 6(3):125–132, 1984.

[166] D. L. Helseth and A. Veis. Collagen self-assembly in vitro. differentiating specific telopeptide-dependent interactions using selective enzyme modification and the addition of free amino telopeptide. *Journal of Biological Chemistry*, 256(14):7118–7128, 1981.

[167] F. H. Silver. A two step model for lateral growth of collagen fibrils. *Collagen and related research*, 3(3):167–179, 1983.

[168] F. H. Silver, I. Horvath, and D. J. Foran. Mechanical implications of the domain structure of fiber-forming collagens: Comparison of the molecular and fibrillar

flexibilities of the α1-chains found in types I–III collagen. *Journal of theoretical biology*, 216(2):243–254, 2002.

[169] M. G. Paterlini, G. Némethy, and H. A. Scheraga. The energy of formation of internal loops in triple-helical collagen polypeptides. *Biopolymers*, 35(6):607–619, 1995.

[170] S. F. Wotton and V. C. Duance. Type III collagen in normal human articular cartilage. *The Histochemical Journal*, 26(5):412–416, 1994.

[171] D. E. Birk and F. H. Silver. Collagen fibrillogenesis *in vitro*: Comparison of types I, II, and III. *Archives of biochemistry and biophysics*, 235(1):178–185, 1984.

[172] M. L. Fielden, R. A. Hayes, and J. Ralston. Surface and capillary forces affecting air bubble-particle interactions in aqueous electrolyte. *Langmuir*, 12(15):3721–3727, 1996.

[173] J.-H. Lee and J. C. Meredith. Non-DLVO silica interaction forces in NMP–Water mixtures. II. an asymmetric system. *Langmuir*, 27(16):10000–10006, 2011.

[174] M. Preuss and H.-J. Butt. Direct measurement of particle-bubble interactions in aqueous electrolyte: Dependence on surfactant. *Langmuir*, 14(12):3164–3174, 1998.

[175] H. Notbohm, S. Mosler, P. K. Müller, and J. Brinckmann. In vitro formation and aggregation of heterotypic collagen I and III fibrils. *International journal of biological macromolecules*, 15(5):299–304, 1993.

[176] K. Nakayasu, M. Tanaka, H. Konomi, and T. Hayashi. Distribution of types I, II, III, IV and V collagen in normal and keratoconus corneas. *Ophthalmic research*, 18(1):1–10, 1986.

[177] O. Schmut. The identification of type III collagen in calf and bovine cornea and sclera. *Experimental eye research*, 25(5):505–509, 1977.

[178] G. Papastavrou, S. Akari, and H. Möhwald. Interactions between hydrophilic and hydrophobic surfaces on microscopic scale and the influence of air bubbles as observed by scanning force microscopy in aqueous and alcoholic mediums. *EPL (Europhysics Letters)*, 52(5):551, 2000.

[179] R. Fleischmajer, B. R. Olsen, R. Timpl, J. S. Perlish, and O. Lovelace. Collagen fibril formation during embryogenesis. *Proceedings of the National Academy of Sciences*, 80(11):3354–3358, 1983.

[180] R. Fleischmajer, J. S. Perlish, R. Timpl, and B. R. Olsen. Procollagen intermediates during tendon fibrillogenesis. *Journal of Histochemistry & Cytochemistry*, 36(11):1425–1432, 1988.

[181] D. R. Keene, L. Y. Sakai, H. P. Bächinger, and R. E. Burgeson. Type III collagen can be present on banded collagen fibrils regardless of fibril diameter. *The Journal of cell biology*, 105(5):2393–2402, 1987.

[182] H. Yang and Z. Shu. The extraction of collagen protein from pigskin. *Journal of Chemical and Pharmaceutical Research*, 6(2):683–687, 2014.

[183] E. Ukraintsev, A. Kromka, H. Kozak, Z. Remeš, and B. Rezek. Artifacts in atomic force microscopy of biological samples.

[184] C. Yong. Elucidation and identification of double-tip effects in atomic force microscopy studies of biological structures. *Journal of Surface Engineered Materials and Advanced Technology*, 2012, 2012.

[185] E. Eryilmaz, W. Teizer, and Hwang W. Synergistic effect in the co-assembly of type-I and type-III collagens.

[186] J. C. Adams and F. M. Watt. Regulation of development and differentiation by the extracellular matrix. *Development-Cambrifge-*, 117:1183–1183, 1993.

APPENDIX A

PYTHON CODES

The codes counting the electrostatic interaction pairs between type-I molecules at the binding sites of 0D, 1D, 2D, 3D, and 4D as described in Fig. 4.2 are given from page 117 to 121. 'aa1' represents the amino acid sequence of type-I collagen. Note that the only a small part of the whole length is seen in the attached page. Each page is given to a specific binding location of the whole code. The part of our program which counts the electrostatic interaction between type-I molecules at 0D arrangement that means perfectly arrayed.

The codes counting the hydrophobic interaction pairs between type-I and type-III molecules at the binding sites of 0D, 1D, 2D, 3D, and 4D are given from page 122 to 124. 'aa3' represents the amino acid sequence of type-III collagen.

```
aa1='GPMGPSGPRGLPGPPGAPGPQGFQGPPGEPGEPGASGPMGPRGPPGPPGKNGDDGEAGKPGRPGERGPPGPQGAR
print(len(aa1))  #correct
aa11='GPMGPSGPRGLPGPPGAPGPQGFQGPPGEPGEPGASGPMGPRGPPGPPGKNGDDGEAGKPGRPGERGPPGPQGA

# Electrostatic interaction score between type-I molecules at 0D arrangement.
score0D=0
for i in range(len(aa1)):
    if (aa1[i]=='K' or aa1[i]=='R') and (aa11[i]=='E' or aa11[i]=='D'):
        score0D =score0D + 1
        print('Electrostatic score = ', score0D)
    elif (aa1[i]=='K' or aa1[i]=='R') and (aa11[i-1]=='E' or aa11[i-1]=='D'):
        score0D =score0D + 1
        print('Electrostatic score = ', score0D)
    elif (aa1[i]=='K' or aa1[i]=='R') and (aa11[i+1]=='E' or aa11[i+1]=='D'):
        score0D =score0D + 1
        print('Electrostatic score = ', score0D)
    elif (aa1[i]=='K' or aa1[i]=='R') and (aa11[i-2]=='E' or aa11[i-2]=='D'):
        score0D =score0D + 1
        print('Electrostatic score = ', score0D)
    elif (aa1[i]=='K' or aa1[i]=='R') and (aa11[i+2]=='E' or aa11[i+2]=='D'):
        score0D =score0D + 1
        print('Electrostatic score = ', score0D)
    elif (aa1[i]=='K' or aa1[i]=='R') and (aa11[i-3]=='E' or aa11[i-3]=='D'):
        score0D =score0D + 1
        print('Electrostatic score = ', score0D)
    elif (aa1[i]=='K' or aa1[i]=='R') and (aa11[i+3]=='E' or aa11[i+3]=='D'):
        score0D =score0D + 1
        print('Electrostatic score = ', score0D)

    elif (aa1[i]=='D' or aa1[i]=='E') and (aa11[i]=='K' or aa11[i]=='R'):
        score0D =score0D + 1
        print('Electrostatic score = ', score0D)
    elif (aa1[i]=='D' or aa1[i]=='E') and (aa11[i-1]=='K' or aa11[i-1]=='R'):
        score0D =score0D + 1
        print('Electrostatic score = ', score0D)
    elif (aa1[i]=='D' or aa1[i]=='E') and (aa11[i+1]=='K' or aa11[i+1]=='R'):
        score0D =score0D + 1
        print('Electrostatic score = ', score0D)
    elif (aa1[i]=='D' or aa1[i]=='E') and (aa11[i-2]=='K' or aa11[i-2]=='R'):
        score0D =score0D + 1
        print('Electrostatic score = ', score0D)
    elif (aa1[i]=='D' or aa1[i]=='E') and (aa11[i+2]=='K' or aa11[i+2]=='R'):
        score0D =score0D + 1
        print('Electrostatic score = ', score0D)
    elif (aa1[i]=='D' or aa1[i]=='E') and (aa11[i-3]=='K' or aa11[i-3]=='R'):
        score0D =score0D + 1
        print('Electrostatic score = ', score0D)
    elif (aa1[i]=='D' or aa1[i]=='E') and (aa11[i+3]=='K' or aa11[i+3]=='R'):
        score0D =score0D + 1
        print('Electrostatic score = ', score0D)
    #else:
     #   print ('Score does not change')
print ('Total Electrostatic score at 0D = ' , score0D)
```

```
# Electrostatic interaction score between type-I molecules at 1D arrangement.
D1=aa1[234:1015]
D11=aa11[0:781]

score1D=0
for i in range(len(D1)):
    if (D1[i]=='K' or D1[i]=='R') and (D11[i]=='E' or D11[i]=='D'):
        score1D =score1D + 1
        print('Electrostatic score = ', score1D)
    elif (D1[i]=='K' or D1[i]=='R') and (D11[i-1]=='E' or D11[i-1]=='D'):
        score1D =score1D + 1
        print('Electrostatic score = ', score1D)
    elif (D1[i]=='K' or D1[i]=='R') and (D11[i+1]=='E' or D11[i+1]=='D'):
        score1D =score1D + 1
        print('Electrostatic score = ', score1D)
    elif (D1[i]=='K' or D1[i]=='R') and (D11[i-2]=='E' or D11[i-2]=='D'):
        score1D =score1D + 1
        print('Electrostatic score = ', score1D)
    elif (D1[i]=='K' or D1[i]=='R') and (D11[i+2]=='E' or D11[i+2]=='D'):
        score1D =score1D + 1
        print('Electrostatic score = ', score1D)
    elif (D1[i]=='K' or D1[i]=='R') and (D11[i-3]=='E' or D11[i-3]=='D'):
        score1D =score1D + 1
        print('Electrostatic score = ', score1D)
    elif (D1[i]=='K' or D1[i]=='R') and (D11[i+3]=='E' or D11[i+3]=='D'):
        score1D =score1D + 1
        print('Electrostatic score = ', score1D)


    elif (D1[i]=='D' or D1[i]=='E') and (D11[i]=='K' or D11[i]=='R'):
        score1D =score1D + 1
        print('Electrostatic score = ', score1D)
    elif (D1[i]=='D' or D1[i]=='E') and (D11[i-1]=='K' or D11[i-1]=='R'):
        score1D =score1D + 1
        print('Electrostatic score = ', score1D)
    elif (D1[i]=='D' or D1[i]=='E') and (D11[i+1]=='K' or D11[i+1]=='R'):
        score1D =score1D + 1
        print('Electrostatic score = ', score1D)
    elif (D1[i]=='D' or D1[i]=='E') and (D11[i-2]=='K' or D11[i-2]=='R'):
        score1D =score1D + 1
        print('Electrostatic score = ', score1D)
    elif (D1[i]=='D' or D1[i]=='E') and (D11[i+2]=='K' or D11[i+2]=='R'):
        score1D =score1D + 1
        print('Electrostatic score = ', score1D)
    elif (D1[i]=='D' or D1[i]=='E') and (D11[i-3]=='K' or D11[i-3]=='R'):
        score1D =score1D + 1
        print('Electrostatic score = ', score1D)
    elif (D1[i]=='D' or D1[i]=='E') and (D11[i+3]=='K' or D11[i+3]=='R'):
        score1D =score1D + 1
        print('Electrostatic score = ', score1D)
    #else:
     #   print ('Score does not change')
print ('Total Electrostatic score at 1D = ' , score1D)
```

```
# Electrostatic interaction score between type-I molecules at 2D arrangement.
D2=aa1[468:1015]
D22=aa11[0:547]
score2D=0
for i in range(len(D2)):
    if (D2[i]=='K' or D2[i]=='R') and (D22[i]=='E' or D22[i]=='D'):
        score2D =score2D + 1
        print('Electrostatic score = ', score2D)
    elif (D2[i]=='K' or D2[i]=='R') and (D22[i-1]=='E' or D22[i-1]=='D'):
        score2D =score2D + 1
        print('Electrostatic score = ', score2D)
    elif (D2[i]=='K' or D2[i]=='R') and (D22[i+1]=='E' or D22[i+1]=='D'):
        score2D =score2D + 1
        print('Electrostatic score = ', score2D)
    elif (D2[i]=='K' or D2[i]=='R') and (D22[i-2]=='E' or D22[i-2]=='D'):
        score2D =score2D + 1
        print('Electrostatic score = ', score2D)
    elif (D2[i]=='K' or D2[i]=='R') and (D22[i+2]=='E' or D22[i+2]=='D'):
        score2D =score2D + 1
        print('Electrostatic score = ', score2D)
    elif (D2[i]=='K' or D2[i]=='R') and (D22[i-3]=='E' or D22[i-3]=='D'):
        score2D =score2D + 1
        print('Electrostatic score = ', score2D)
    elif (D2[i]=='K' or D2[i]=='R') and (D22[i+3]=='E' or D22[i+3]=='D'):
        score2D =score2D + 1
        print('Electrostatic score = ', score2D)


    elif (D2[i]=='D' or D2[i]=='E') and (D22[i]=='K' or D22[i]=='R'):
        score2D =score2D + 1
        print('Electrostatic score = ', score2D)
    elif (D2[i]=='D' or D2[i]=='E') and (D22[i-1]=='K' or D22[i-1]=='R'):
        score2D =score2D + 1
        print('Electrostatic score = ', score2D)
    elif (D2[i]=='D' or D2[i]=='E') and (D22[i+1]=='K' or D22[i+1]=='R'):
        score2D =score2D + 1
        print('Electrostatic score = ', score2D)
    elif (D2[i]=='D' or D2[i]=='E') and (D22[i-2]=='K' or D22[i-2]=='R'):
        score2D =score2D + 1
        print('Electrostatic score = ', score2D)
    elif (D2[i]=='D' or D2[i]=='E') and (D22[i+2]=='K' or D22[i+2]=='R'):
        score2D =score2D + 1
        print('Electrostatic score = ', score2D)
    elif (D2[i]=='D' or D2[i]=='E') and (D22[i-3]=='K' or D22[i-3]=='R'):
        score2D =score2D + 1
        print('Electrostatic score = ', score2D)
    elif (D2[i]=='D' or D2[i]=='E') and (D22[i+3]=='K' or D22[i+3]=='R'):
        score2D =score2D + 1
        print('Electrostatic score = ', score2D)
    #else:
     #   print ('Score does not change')
print ('Total Electrostatic score at 2D = ' , score2D)
```

```
# Electrostatic interaction score between type-I molecules at 3D arrangement.
D3=aa1[702:1015]
D33=aa11[0:313]
score3D=0
for i in range(len(D3)):
    if (D3[i]=='K' or D3[i]=='R') and (D33[i]=='E' or D33[i]=='D'):
        score3D =score3D + 1
        print('Electrostatic score = ', score3D)
    elif (D3[i]=='K' or D3[i]=='R') and (D33[i-1]=='E' or D33[i-1]=='D'):
        score3D =score3D + 1
        print('Electrostatic score = ', score3D)
    elif (D3[i]=='K' or D3[i]=='R') and (D33[i+1]=='E' or D33[i+1]=='D'):
        score3D =score3D + 1
        print('Electrostatic score = ', score3D)
    elif (D3[i]=='K' or D3[i]=='R') and (D33[i-2]=='E' or D33[i-2]=='D'):
        score3D =score3D + 1
        print('Electrostatic score = ', score3D)
    elif (D3[i]=='K' or D3[i]=='R') and (D33[i+2]=='E' or D33[i+2]=='D'):
        score3D =score3D + 1
        print('Electrostatic score = ', score3D)
    elif (D3[i]=='K' or D3[i]=='R') and (D33[i-3]=='E' or D33[i-3]=='D'):
        score3D =score3D + 1
        print('Electrostatic score = ', score3D)
    elif (D3[i]=='K' or D3[i]=='R') and (D33[i+3]=='E' or D33[i+3]=='D'):
        score3D =score3D + 1
        print('Electrostatic score = ', score3D)


    elif (D3[i]=='D' or D3[i]=='E') and (D33[i]=='K' or D33[i]=='R'):
        score3D =score3D + 1
        print('Electrostatic score = ', score3D)
    elif (D3[i]=='D' or D3[i]=='E') and (D33[i-1]=='K' or D33[i-1]=='R'):
        score3D =score3D + 1
        print('Electrostatic score = ', score3D)
    elif (D3[i]=='D' or D3[i]=='E') and (D33[i+1]=='K' or D33[i+1]=='R'):
        score3D =score3D + 1
        print('Electrostatic score = ', score3D)
    elif (D3[i]=='D' or D3[i]=='E') and (D33[i-2]=='K' or D33[i-2]=='R'):
        score3D =score3D + 1
        print('Electrostatic score = ', score3D)
    elif (D3[i]=='D' or D3[i]=='E') and (D33[i+2]=='K' or D33[i+2]=='R'):
        score3D =score3D + 1
        print('Electrostatic score = ', score3D)
    elif (D3[i]=='D' or D3[i]=='E') and (D33[i-3]=='K' or D33[i-3]=='R'):
        score3D =score3D + 1
        print('Electrostatic score = ', score3D)
    elif (D3[i]=='D' or D3[i]=='E') and (D33[i+3]=='K' or D33[i+3]=='R'):
        score3D =score3D + 1
        print('Electrostatic score = ', score3D)
    #else:
     #   print ('Score does not change')
print ('Total Electrostatic score at 3D = ' , score3D)
```

```
# Electrostatic interaction score between type-I molecules at 4D arrangement.
D4=aa1[936:1015]
D44=aa11[0:79]
score4D=0
for i in range(len(D4)):
    if (D4[i]=='K' or D4[i]=='R') and (D44[i]=='E' or D44[i]=='D'):
        score4D =score4D + 1
        print('Electrostatic score = ', score4D)
    elif (D4[i]=='K' or D4[i]=='R') and (D44[i-1]=='E' or D44[i-1]=='D'):
        score4D =score4D + 1
        print('Electrostatic score = ', score4D)
    elif (D4[i]=='K' or D4[i]=='R') and (D44[i+1]=='E' or D44[i+1]=='D'):
        score4D =score4D + 1
        print('Electrostatic score = ', score4D)
    elif (D4[i]=='K' or D4[i]=='R') and (D44[i-2]=='E' or D44[i-2]=='D'):
        score4D =score4D + 1
        print('Electrostatic score = ', score4D)
    elif (D4[i]=='K' or D4[i]=='R') and (D44[i+2]=='E' or D44[i+2]=='D'):
        score4D =score4D + 1
        print('Electrostatic score = ', score4D)
    elif (D4[i]=='K' or D4[i]=='R') and (D44[i-3]=='E' or D44[i-3]=='D'):
        score4D =score4D + 1
        print('Electrostatic score = ', score4D)
    elif (D4[i]=='K' or D4[i]=='R') and (D44[i+3]=='E' or D44[i+3]=='D'):
        score4D =score4D + 1
        print('Electrostatic score = ', score4D)

    elif (D4[i]=='D' or D4[i]=='E') and (D44[i]=='K' or D44[i]=='R'):
        score4D =score4D + 1
        print('Electrostatic score = ', score4D)
    elif (D4[i]=='D' or D4[i]=='E') and (D44[i-1]=='K' or D44[i-1]=='R'):
        score4D =score4D + 1
        print('Electrostatic score = ', score4D)
    elif (D4[i]=='D' or D4[i]=='E') and (D44[i+1]=='K' or D44[i+1]=='R'):
        score4D =score4D + 1
        print('Electrostatic score = ', score4D)
    elif (D4[i]=='D' or D4[i]=='E') and (D44[i-2]=='K' or D44[i-2]=='R'):
        score4D =score4D + 1
        print('Electrostatic score = ', score4D)
    elif (D4[i]=='D' or D4[i]=='E') and (D44[i+2]=='K' or D44[i+2]=='R'):
        score4D =score4D + 1
        print('Electrostatic score = ', score4D)
    elif (D4[i]=='D' or D4[i]=='E') and (D44[i-3]=='K' or D44[i-3]=='R'):
        score4D =score4D + 1
        print('Electrostatic score = ', score4D)
    elif (D4[i]=='D' or D4[i]=='E') and (D44[i+3]=='K' or D44[i+3]=='R'):
        score4D =score4D + 1
        print('Electrostatic score = ', score4D)
    #else:
     #   print ('Score does not change')
print ('Total Electrostatic score at 4D = ' , score4D)
print ('    Summary bet Typ-I&Typ-I     ')
print ('Elec score at 0D is ', score0D)
print ('Elec score at 1D is ', score1D)
print ('Elec score at 2D is ', score2D)
print ('Elec score at 3D is ', score3D)
print ('Elec score at 4D is ', score4D)
```

```
aa1='GPMGPSGPRGLPGPPGAPGPQGFQGPPGEPGEPGASGPMGPRGPPGPPGKNGDDGEAGKPGRPGERGPPGPQGARGLPGTAGLPGMK(
print(len(aa1))  #correct
aa3='GIAGYPGPAGPPGPPGPPGTSGHPGAPGAPGYQGPPGEPGQAGPAGPPGPPGAIGPSGKDGESGRPGRPGPRGFPGPPGMKGPAGMP(
print(len(aa3))    #correct

# Hydrophobic interaction score between type-I&III at 0D arrangement
score0D=0
for i in range(len(aa1)):
    if (aa1[i]=='V' or aa1[i]=='L' or aa1[i]=='I' or aa1[i]=='M' or aa1[i]=='F') and \
        (aa3[i]=='V' or aa3[i]=='L' or aa3[i]=='I' or aa3[i]=='M' or aa3[i]=='F'):
        score0D = score0D + 1
        print (i, 'Hydrophobic score is= ', score0D)
    elif (aa1[i]=='V' or aa1[i]=='L' or aa1[i]=='I' or aa1[i]=='M' or aa1[i]=='F') and \
        (aa3[i-1]=='V' or aa3[i-1]=='L' or aa3[i-1]=='I' or aa3[i-1]=='M' or aa3[i-1]=='F'):
        score0D = score0D + 1
        print (i, 'Hydrophobic score is= ', score0D)
    elif (aa1[i]=='V' or aa1[i]=='L' or aa1[i]=='I' or aa1[i]=='M' or aa1[i]=='F') and \
        (aa3[i+1]=='V' or aa3[i+1]=='L' or aa3[i+1]=='I' or aa3[i+1]=='M' or aa3[i+1]=='F'):
        score0D = score0D + 1
        print (i, 'Hydrophobic score is= ', score0D)

    elif (aa1[i]=='V' or aa1[i]=='L' or aa1[i]=='I' or aa1[i]=='M' or aa1[i]=='F') and \
        (aa3[i-2]=='V' or aa3[i-2]=='L' or aa3[i-2]=='I' or aa3[i-2]=='M' or aa3[i-2]=='F'):
        score0D = score0D + 1
        print (i, 'Hydrophobic score is= ', score0D)
    elif (aa1[i]=='V' or aa1[i]=='L' or aa1[i]=='I' or aa1[i]=='M' or aa1[i]=='F') and \
        (aa3[i+2]=='V' or aa3[i+2]=='L' or aa3[i+2]=='I' or aa3[i+2]=='M' or aa3[i+2]=='F'):
        score0D = score0D + 1
        print (i, 'Hydrophobic score is= ', score0D)

# Hydrophobic interaction score between type-I&III molecules at 1D arrangement.
D1=aa1[234:1015]
D11=aa3[0:793]

score1D=0
for i in range(len(D1)):
    if (D1[i]=='V' or D1[i]=='L' or D1[i]=='I' or D1[i]=='M' or D1[i]=='F') and \
        (D11[i]=='V' or D11[i]=='L' or D11[i]=='I' or D11[i]=='M' or D11[i]=='F'):
        score1D = score1D + 1
        print (i, 'Hydrophobic score is= ', score1D)
    elif (D1[i]=='V' or D1[i]=='L' or D1[i]=='I' or D1[i]=='M' or D1[i]=='F') and \
        (D11[i-1]=='V' or D11[i-1]=='L' or D11[i-1]=='I' or D11[i-1]=='M' or D11[i-1]=='F'):
        score1D = score1D + 1
        print (i, 'Hydrophobic score is= ', score1D)
    elif (D1[i]=='V' or D1[i]=='L' or D1[i]=='I' or D1[i]=='M' or D1[i]=='F') and \
        (D11[i+1]=='V' or D11[i+1]=='L' or D11[i+1]=='I' or D11[i+1]=='M' or D11[i+1]=='F'):
        score1D = score1D + 1
        print (i, 'Hydrophobic score is= ', score1D)
    elif (D1[i]=='V' or D1[i]=='L' or D1[i]=='I' or D1[i]=='M' or D1[i]=='F') and \
        (D11[i-2]=='V' or D11[i-2]=='L' or D11[i-2]=='I' or D11[i-2]=='M' or D11[i-2]=='F'):
        score1D = score1D + 1
        print (i, 'Hydrophobic score is= ', score1D)
    elif (D1[i]=='V' or D1[i]=='L' or D1[i]=='I' or D1[i]=='M' or D1[i]=='F') and \
        (D11[i+2]=='V' or D11[i+2]=='L' or D11[i+2]=='I' or D11[i+2]=='M' or D11[i+2]=='F'):
        score1D = score1D + 1
        print (i, 'Hydrophobic score is= ', score1D)

# Hydrophobic interaction score between type-I&III molecules at 2D arrangement.
D2=aa1[468:1015]
D22=aa3[0:559]

score2D=0
for i in range(len(D2)):
    if (D2[i]=='V' or D2[i]=='L' or D2[i]=='I' or D2[i]=='M' or D2[i]=='F') and \
        (D22[i]=='V' or D22[i]=='L' or D22[i]=='I' or D22[i]=='M' or D22[i]=='F'):
        score2D = score2D + 1
        print (i, 'Hydrophobic score is= ', score2D)
```

```
    elif (D2[i]=='V' or D2[i]=='L' or D2[i]=='I' or D2[i]=='M' or D2[i]=='F') and \
        (D22[i-1]=='V' or D22[i-1]=='L' or D22[i-1]=='I' or D22[i-1]=='M' or D22[i-1]=='F'):
        score2D = score2D + 1
        print (i, 'Hydrophobic score is= ', score2D)
    elif (D2[i]=='V' or D2[i]=='L' or D2[i]=='I' or D2[i]=='M' or D2[i]=='F') and \
        (D22[i+1]=='V' or D22[i+1]=='L' or D22[i+1]=='I' or D22[i+1]=='M' or D22[i+1]=='F'):
        score2D = score2D + 1
        print (i, 'Hydrophobic score is= ', score2D)
    elif (D2[i]=='V' or D2[i]=='L' or D2[i]=='I' or D2[i]=='M' or D2[i]=='F') and \
        (D22[i-2]=='V' or D22[i-2]=='L' or D22[i-2]=='I' or D22[i-2]=='M' or D22[i-2]=='F'):
        score2D = score2D + 1
        print (i, 'Hydrophobic score is= ', score2D)
    elif (D2[i]=='V' or D2[i]=='L' or D2[i]=='I' or D2[i]=='M' or D2[i]=='F') and \
        (D22[i+2]=='V' or D22[i+2]=='L' or D22[i+2]=='I' or D22[i+2]=='M' or D22[i+2]=='F'):
        score2D = score2D + 1
        print (i, 'Hydrophobic score is= ', score2D)

# Hydrophobic interaction score between type-I&III molecules at 3D arrangement.
D3=aa1[702:1015]
D33=aa3[0:325]

score3D=0
for i in range(len(D3)):
    if (D3[i]=='V' or D3[i]=='L' or D3[i]=='I' or D3[i]=='M' or D3[i]=='F') and \
        (D33[i]=='V' or D33[i]=='L' or D33[i]=='I' or D33[i]=='M' or D33[i]=='F'):
        score3D = score3D + 1
        print (i, 'Hydrophobic score is= ', score3D)
    elif (D3[i]=='V' or D3[i]=='L' or D3[i]=='I' or D3[i]=='M' or D3[i]=='F') and \
        (D33[i-1]=='V' or D33[i-1]=='L' or D33[i-1]=='I' or D33[i-1]=='M' or D33[i-1]=='F'):
        score3D = score3D + 1
        print (i, 'Hydrophobic score is= ', score3D)
    elif (D3[i]=='V' or D3[i]=='L' or D3[i]=='I' or D3[i]=='M' or D3[i]=='F') and \
        (D33[i+1]=='V' or D33[i+1]=='L' or D33[i+1]=='I' or D33[i+1]=='M' or D33[i+1]=='F'):
        score3D = score3D + 1
        print (i, 'Hydrophobic score is= ', score3D)
    elif (D3[i]=='V' or D3[i]=='L' or D3[i]=='I' or D3[i]=='M' or D3[i]=='F') and \
        (D33[i-2]=='V' or D33[i-2]=='L' or D33[i-2]=='I' or D33[i-2]=='M' or D33[i-2]=='F'):
        score3D = score3D + 1
        print (i, 'Hydrophobic score is= ', score3D)
    elif (D3[i]=='V' or D3[i]=='L' or D3[i]=='I' or D3[i]=='M' or D3[i]=='F') and \
        (D33[i+2]=='V' or D33[i+2]=='L' or D33[i+2]=='I' or D33[i+2]=='M' or D33[i+2]=='F'):
        score3D = score3D + 1
        print (i, 'Hydrophobic score is= ', score3D)
    #else:
        #print (i)

# Hydrophobic interaction score between type-I&III molecules at 4D arrangement.
D4=aa1[936:1015]
D44=aa3[0:91]

score4D=0
for i in range(len(D4)):
    if (D4[i]=='V' or D4[i]=='L' or D4[i]=='I' or D4[i]=='M' or D4[i]=='F') and \
        (D44[i]=='V' or D44[i]=='L' or D44[i]=='I' or D44[i]=='M' or D44[i]=='F'):
        score4D = score4D + 1
        print (i, 'Hydrophobic score is= ', score4D)
    elif (D4[i]=='V' or D4[i]=='L' or D4[i]=='I' or D4[i]=='M' or D4[i]=='F') and \
        (D44[i-1]=='V' or D44[i-1]=='L' or D44[i-1]=='I' or D44[i-1]=='M' or D44[i-1]=='F'):
        score4D = score4D + 1
        print (i, 'Hydrophobic score is= ', score4D)
    elif (D4[i]=='V' or D4[i]=='L' or D4[i]=='I' or D4[i]=='M' or D4[i]=='F') and \
        (D44[i+1]=='V' or D44[i+1]=='L' or D44[i+1]=='I' or D44[i+1]=='M' or D44[i+1]=='F'):
        score4D = score4D + 1
        print (i, 'Hydrophobic score is= ', score4D)
```

```
    elif (D4[i]=='V' or D4[i]=='L' or D4[i]=='I' or D4[i]=='M' or D4[i]=='F') and \
        (D44[i+1]=='V' or D44[i+1]=='L' or D44[i+1]=='I' or D44[i+1]=='M' or D44[i+1]=='F'):
        score4D = score4D + 1
        print (i, 'Hydrophobic score is= ', score4D)
    elif (D4[i]=='V' or D4[i]=='L' or D4[i]=='I' or D4[i]=='M' or D4[i]=='F') and \
        (D44[i-2]=='V' or D44[i-2]=='L' or D44[i-2]=='I' or D44[i-2]=='M' or D44[i-2]=='F'):
        score4D = score4D + 1
        print (i, 'Hydrophobic score is= ', score4D)
    elif (D4[i]=='V' or D4[i]=='L' or D4[i]=='I' or D4[i]=='M' or D4[i]=='F') and \
        (D44[i+2]=='V' or D44[i+2]=='L' or D44[i+2]=='I' or D44[i+2]=='M' or D44[i+2]=='F'):
        score4D = score4D + 1
        print (i, 'Hydrophobic score is= ', score4D)
    #else:
        #print (i)

print ('   Hydrophobic Summary bet Typ-I&Typ-III     ')
print ('Hydrop score at 0D is ', score0D)
print ('Hydrop score at 1D is ', score1D)
print ('Hydrop score at 2D is ', score2D)
print ('Hydrop score at 3D is ', score3D)
print ('Hydrop score at 4D is ', score4D)
```